Spindle assembly and the control of microtubule nucleation through NEDD1 phosphorylation

Krystal Timón Pérez

TESI DOCTORAL UPF / 2018

Thesis supervisor:

Dr. Isabelle Vernos

Cell and Developmental Biology Programme

Center for Genomic Regulation (CRG)

upf. Universitat Pompeu Fabra Barcelona

CRG Centre de Regulació Genòmica

"Me enseñaron que el camino del progreso

no era rápido ni fácil"

Marie Curie

A mis padres,
Enrique y Carmen

Agradecimientos / Acknowledgments

Hace exactamente 4 años, 8 meses y 8 días que empecé esta aventura llamada doctorado y la primera persona a la que tengo que agradecérselo es a Isabelle. Gracias por haberme dado la oportunidad de hacer mi tesis doctoral en tu laboratorio. Las dos sabemos que no ha sido un camino fácil pero siempre me he sentido reconfortada por tener tu apoyo en todos los ámbitos, tanto a nivel científico como personal. He aprendido muchísimo contigo y quiero agradecerte sobretodo las largas discusiones en nuestras reuniones interminables y las "brain stormings" siempre interrumpidas por alguna carcajada! Has sido una jefa fantástica y has dejado el listón muy alto para los próximos que vengan, gracias de corazón por todo, Isabelle.

En segundo lugar, quiero agradecer a Mónica, mi "supervisor en la sombra": para mi has sido más que una compañera de laboratorio, más que una amiga, casi como una segunda madre! Has tenido toda la paciencia del mundo conmigo, y nunca olvidaré tus míticos: "piensa", en momentos clave! Gracias a ti he crecido como científica y ha sido un placer compartir horarios intempestivos en el laboratorio, porque nosotras somos así, nocturnas ☺

Núria, tu has sido otro de mis pilares en el laboratorio. Gracias por haberme acompañado en esta experiencia, con amigas como tu los resultados negativos sientan un poco "menos mal". Estoy muy contenta de haber podido contar contigo, gracias por tu ayuda en el labo, pero sobretodo, gracias por tu amistad!

Gracias a todos los miembros (pasados y presentes) del Vernos Lab: Sylvain, Nathalie, Jacopo, Tommaso, Jacobo, Miquel, Claudia, Aitor, Georgina, Farners, Alejandra, Iván, Álvaro. Ha sido un placer trabajar con vosotros durante estos años y también compartir experiencias fuera del laboratorio. Sé que los que os quedais allí me echaréis de menos ;)

Gerard, gracias por todo, más allá de nuestras conversaciones científicas en cultivos, los coffee-breaks, y nuestros "dancing moments" en los retreats del departamento, te has convertido en un gran amigo. Además contigo tengo 2x1, gracias por presentarme a Miri porque ella también ha tenido su parte en esta tesis! Miri: sigo tus pasos, espérame!

Bogu, you know that these almost 5 years wouldn't have been the same without you. You were one of my first friends at the CRG and I am so happy to have had your support

during this time. I wanted to thank you for all the good times spent together and for the so necessary “non-scientific” breaks, you made much easier the lab life. Luci, gracias por el apoyo y por sacarnos del laboratorio cuando era necesario, de igual manera has contribuído a mantener el equilibrio en esta vida tan estresada que hemos llevado muchas veces.

Mari, you came to the CRG in a complicated moment of my PhD thesis and I am very happy to have met you. Thanks for all the scientific advice you gave me, for helping me with the formatting of the thesis but, more importantly, for being such a good friend ;)

Rocío, quería agradecerte la oportunidad que me diste para hacer mi tesis de master en tu laboratorio del EMBL. Para mi fue una experiencia fantástica y recuerdo con mucho cariño el año que pasé con vosotros y mi trabajo con los ratones (lo eché mucho de menos cuando llegué a Barcelona). Gracias por haberme preparado para el doctorado y por haberme motivado para continuar mi carrera en el laboratorio de Isabelle, me aconsejaste muy bien ;)

Tina, you were my first mentor at EMBL but in a few weeks you became one of my best friends in Monterotondo, it’s incredible how fast the time has passed but now you have a PhD degree and I am about to submit my thesis! Thanks for all the lessons you gave me, for teaching me how to do the best surgeries in mice, for the endless hours in front of the confocal microscope looking for mitosis, for all the scientific support but, overall, thanks for your friendship! I learnt many important things in life from you and I couldn’t be more grateful.

I wanted to acknowledge the members of my thesis committee: Jens, Pedro and Juan. Your comments and advice were essential to keep the project on the right path. In addition, I would like to thank the members of my PhD thesis defense board: Jens, Joan, Jerome, Sara and Elvan for their critical reading and evaluation of my work.

Quiero agradecer a mi familia “biotec”: con vosotros empezó todo! Desde aquella primera noche de novatadas en la Hurtado en 2005 hasta hoy han cambiado muchas cosas, pero nunca nuestra amistad! Pibe, Ander, Antón: gracias por toda una carrera juntos, durante esta tesis he recordado muchas veces las noches de estudio en la Central pero también los cortos en el Húmedo. Que nuestras quedadas “biotec” se mantengan durante muchos años! Chemi: gracias por todo, sabes que Luengo estaría orgulloso de nosotras si leyera

estas líneas (y nuestras tesis!). Irene: solo las dos sabemos por todo lo que hemos pasado y sabes que eres demasiado importante para mi, gracias por apoyarme en todo. Has estado conmigo antes, durante y después de nuestras tesis y para mi eres como una hermana (que se lo digan a Carmen!). Haber escogido biotecnología como carrera me ha permitido llegar hasta donde estoy, vivir experiencias muy enriquecedoras a nivel laboral en varios países y haber conocido personas maravillosas sin las que no podría imaginar mi vida hoy: gracias a todos los que habéis formado parte de mi etapa universitaria.

Adri,Víctor y Aída: habéis sido mi familia en Alemania y también vosotros sois un poco responsables de que hoy esté aquí terminando mi tesis. Al acabar la carrera empezamos juntos nuestra andadura científica en dos laboratorios contiguos de una pequeña ciudad alemana: Heidelberg, y desde entonces nuestros caminos se han mantenido siempre cruzados. Gracias por haberme acompañado en todo el proceso de aprendizaje y por hacer que mi estancia en HD fuera inolvidable.

Quiero agradecer a mi familia por haberme apoyado incondicionalmente en todas las decisiones que he tomado y por haber entendido todos los momentos difíciles que a veces han aparecido durante la tesis. Me gustaría agradecer de forma especial a mi padre, sé que estaría orgullo de haberme visto seguir sus pasos y convertirme en una doctora como él. Acordarme de ti me ha dado fuerzas en muchos momentos duros y por eso esta tesis va dedicada a ti, al mejor de los padres, a la luz que nunca me abandona: Enrique.

Finalmente, dedico esta tesis también a la persona más importante de mi vida, a una gran mujer: mi madre Carmen. Gracias por estar siempre a mi lado, por confiar en mi, por apoyarme en los momentos difíciles y por haberme cuidado tanto a lo largo de estos años de doctorado. De ti aprendí que en esta vida todo se consigue con esfuerzo y superación y eres el mejor modelo a seguir que puedo tener. Estoy muy orgullosa de ser hija tuya y quiero que sepas que esta tesis doctoral no habría visto la luz sin ti, **GRACIAS**.

Abstract

During mitosis, the microtubules organize a bipolar spindle that segregates the chromosomes. In higher eukaryotes, these microtubules are nucleated through three different pathways involving the centrosomes (centrosomal pathway), the chromatin (Ran-GTP pathway), and pre-existing microtubules (Augmin-dependent pathway).

These three pathways rely on the γ-tubulin ring complex (γ-TuRC) and its adaptor NEDD1. During mitosis, NEDD1 phosphorylation determines its role in microtubule nucleation through the three pathways: Nek9-dependent Ser377 for centrosomal nucleation, AuroraA-dependent Ser405 for the Ran-GTP dependent pathway and Cdk1-dependent Ser411 for the Augmin-dependent microtubule amplification.

To define the specific contribution of these microtubule nucleation pathways in spindle assembly, we established several inducible stable cell lines to express phosphorylation variants of NEDD1 on Ser377, Ser405 and Ser411 individually or in combination upon NEDD1 silencing.

Our data show that, in agreement with previous results, the three sites are important for spindle assembly. Moreover, they suggest that phosphorylation at Ser411 is responsible for NEDD1 mobility shift in mitosis and plays a major role in NEDD1 function in mitosis.

Resumen

Durante la mitosis, los microtúbulos se organizan en un huso mitótico que segrega los cromosomas. En organismos eucariotas, estos microtúbulos se nuclean a través de tres vías diferentes que involucran los centrosomas (vía centrosomal), la cromatina (vía dependiente de Ran-GTP/vía cromosomal) y microtúbulos pre-existentes (vía dependiente del complejo proteico Augmin).

Estas tres vías dependen de un complejo de nucleación llamado γ-TuRC y la proteína adaptadora NEDD1. Durante la mitosis, la fosforilación de NEDD1 determina su papel en la nucleación de microtúbulos a través de las tres vías: la fosforilación en la Ser377 dependiente de la kinasa Nek9 controla la nucleación centrosomal, la fosforilación en la Ser405 dependiente de la kinasa AuroraA regula la nucleación chromosomal y la fosforilación en la Ser411 dependiente de la kinasa Cdk1 gobierna la nucleación sobre los microtúbulos.

Para definir la contribución específica de estas vías de nucleación en el ensamblaje del huso, generamos varias líneas celulares inducibles para expresar mutantes de fosforilación de NEDD1 en Ser377, Ser405 y Ser411 individualmente o en combinación tras silenciar NEDD1 endógena.

Nuestros datos muestran que, de acuerdo con resultados previos, los tres sitios de fosforilación son importantes para el ensamblaje del huso. Además sugieren que la fosforilación en Ser411 es responsable del cambio de mobilidad de NEDD1 en mitosis y juega un papel importante en la función de NEDD1 en mitosis.

Preface

The work presented in this thesis was carried out in the Cell and Developmental Biology Program at the Center for Genomic Regulation (CRG), under the supervision of Dr. Isabelle Vernos.

Cell division is a fundamental process for the propagation of life, organism development and the maintenance and regeneration of tissues in adult organisms. Problems in cell division may lead to spontaneous abortion, genetic diseases (i.e trisomies) and the formation of tumours.

In order to properly divide and segregate the chromosomes to the daughter cell, the cell needs to build a macromolecular machine made of microtubules known as the bipolar spindle. Spindle assembly involves three different pathways of microtubule nucleation: the centrosomal, Augmin-mediated and the chromosomal pathways, the last one being specific to dividing cells. Therefore, studying how the three pathways work together in the dividing cell may help understanding pathologies associated with cell division defects.

In the last years, our knowledge about the mechanisms regulating the three microtubule nucleation pathways has substantially increased. However, the question of how the three pathways are specifically integrated for the spatial and temporal control of microtubule nucleation during mitosis is not well understood yet.

To address this question, we have established an optimized experimental system that allowed us to investigate the relative contribution of the three microtubule nucleation pathways to the assembly of a mitotic spindle.

The results presented in this thesis provide novel insights into the role of NEDD1 phosphorylation in controlling the centrosomal and chromosomal pathways for spindle assembly. In addition, the data support a possible re-interpretation of previous conclusions on reported phenotypes specifically associated to the Augmin pathway in mitosis.

Abbreviations list

A: Alanine

AA: Amino acid

APC: Anaphase Promoting Complex

ATP: Adenosin Triphosphate

ATPases: Adenosine Triphosphatase

Augmin: Protein complex required for centrosome-independent microtubule organization

AurA: Mitotic kinase Aurora-A

AurB: Mitotic kinase Aurora-B

AurC: Mitotic kinase Aurora-C

CAMSAP: Calmodulin-regulated spectrin-associated protein

Cdc2: Cell division cycle protein 2

Cdc25: Cell division cycle protein 25

Cdk1: Cyclin-dependent kinase 1

cDNA: Complementary DNA

CLAPs: Cytoplasmic linker associated proteins

CLIPs: Cytoplasmic linker proteins

CRM1: Chromosome-region maintenance protein-1

D: Aspartic acid

DMEM: Dulbecco's Modified Eagle's Medium

DMSO: Dimethyl sulfoxide

DNA: Deoxyribonucleic Acid

E: Glutamic acid

EB: End Binding protein

Eg5: Kinesin family member 11

EM: Electron microscopy

FAM29A: Family with sequence similitary 29, member A

FBS: Fetal Bovine Serum

Fcat: Frequency of catastrophes

Fres: Frequency of rescues

G0: Gap phase 0

G1: Gap phase 1

G2: Gap phase 2

G2/M: DNA damage checkpoint

GCPx: Gamma-tubulin complex protein x

GDP: Guanosine diphosphate

GEF: Guanine nucleotide exchange factor

GMPCPP: Guanosine-5´[(α, β)-methyleno] triphosphate

GTP: Guanosine triphosphate

HAUS: Human Augmin complex

HICE1: Hec-interacting and centrosome-associated protein 1

HMMR: Hyaluronan-mediated motility receptor

IF: immunofluorescence

IP: Immunoprecipitation

K-fiber: Kinetochore fiber

kDa: kilodalton

Kip3 Kinesin-like protein KIP3

KNSL: KAT8-associated nonspecific lethal

L: average length

M phase: Mitotic phase

MAPs: Microtubule Associated Proteins

MARK: Microtubule-affinity regulating kinase

MCAK: Mitotic centromere associated kinesin

MCRS1: Microspherule protein 1

MDa: MegaDalton

MOZART: Mitotic Spindle Organizing Protein Associated with the Ring of γ-tubulin

MPF: Maturation promoting factor

mRNA: Messenger ribonucleic acid

MTOC: Microtubule organizing center

MTs: Microtubules

Myt1: Membrane-associated tyrosine-and threonine-specific cdc2-inhibitory kinase

NE: Nuclear envelop

NEBD: Nuclear envelope breakdown

NEDD1: Neural precursor cell expressed developmentally down-regulated protein 1

NES: Nuclear export signal

NIMA: Never in mitosis A

NLS: Nuclear localization signal

Nm: nanometer

NPC: Nuclear pore complex

Ntf2: Nuclear transport factor 2

NuMA: Nuclear mitotic apparatus

PBS: Phosphate-Buffered Saline

PCM: Pericentriolar material

Pf: protofilament

Plk1: Polo-like kinase 1

Plk3: Polo-like kinase 3

Plk4: Polo-like kinase 4

PP1: Protein phosphatase 1

PTMs: Post-translational modifications

Ran-BP1: Ran-binding protein 1

Ran-BP2: Ran-binding protein 2

Ran-GAP1: Ran GTPase activating protein 1

Ran-GTP: Ras-related nuclear protein-GTP

RCC1: Regulator of chromosome condensation

RHAMM: Hyaluronan-mediated motility receptor

RNAi: Interfering RNA

S phase: Synthesis phase

SAC: spindle assembly checkpoint

SAFs: Spindle assembly factors

SAS-6: Spindle assembly abnormal protein 6 homolog

SDS-PAGE: Sodium Dodecyl Sulfate Polyacrylamide Gel Electrophoresis

Ser: Serine

siRNA: Small interfering RNA

T: Threonine

TBS-T: Tris-Buffered Saline with Tween

TBS: Tris-Buffered Saline

TEM: Transmission electron microscopy

Thr: Threonine

TPX2: Targeting protein for Xenopus kinesin-like protein 2

Vg: velocity of growth

Vs: velocity of shrinkage

WB: Western Blot

xKCM1: *Xenopus* kinesin catastrophe modulator-1

xKLP2: *Xenopus* kinesin like protein 2

xMAP215: *Xenopus* microtubule-associated protein 215 kDa

Y: Tyrosine

γ-TuRC: Gamma-tubulin Ring Complex

γ-TuSC: Gamma-tubulin Small Complex

Table of contents

List of figures

List of tables

INTRODUCTION

I-The microtubule cytoskeleton

Microtubules (MTs) are one of the three main cytoskeleton building blocks of the cell, together with actin and intermediate filaments (Figure 1). They are found in all dividing eukaryotic cells and in most differentiated cell types, being involved in many important functions for the cell as for example: intracellular transport, organelle positioning, motility, signalling and cell division (Alberts et al 2007; Kollman et al. 2011).

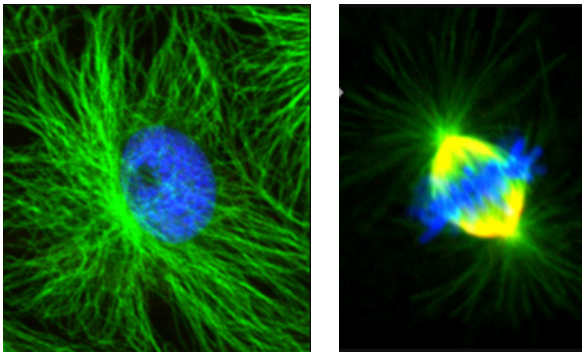

Figure 1: Microtubule organization during interphase and mitosis.
Single confocal microscopy images of XL177 *Xenopus laevis* cells fixed and stained with antibodies against α-tubulin (in green) to visualize the microtubules and Hoechst 33258 (in blue) to label the DNA. The picture in the left shows the radial cytoplasmic microtubule array of a cell in interphase while the picture in the right shows a cell in mitosis forming a bipolar spindle. Adapted from (Wittmann et al., 2000).

Microtubules were visualized for the first time in the early 1950's by transmission electron microscopy (TEM) imaging in spermatozoids of *Sphagnum* and in ciliated epithelia from metazoan (Fawcett and Porter, 1954; Manton and Clarke, 1952). However, it was not until 1963 when the term "microtubule" was formulated by Ledbetter and Porter, who obtained electron microscopy (EM) images of microtubules in plant cells, both in interphase and mitosis (Ledbetter and Porter, 1963), (Figure 2).

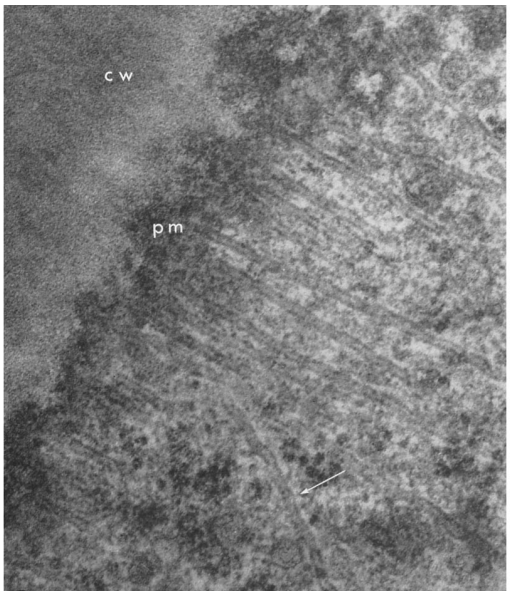

Figure 2: Electron microscopy images of microtubules.

EM images from a *Phleum* root tip cell in mitosis. Most of the microtubules appear parallel-oriented while the microtubules marked with an arrow are disposed at a ≈30º degree angle with respect to the others. Cell wall: cw, plasma membrane: pm. Adapted from (Ledbetter and Porter, 1963).

From these early observations to date, extensive knowledge about microtubule structure and function has been gained, although it continues to be an exciting field of study as many important aspects of microtubules and its relevance for life are still under investigation.

In this introduction I will start by explaining the main basic properties of the microtubules. Second, I will focus on microtubule nucleation, the main microtubule nucleator in the cell and its connection with the cell cycle. I will continue with a brief introduction to cell division and the mitotic spindle as a macromolecular machine essential for mitosis. I will then summarize the general principles for the regulation of microtubule dynamics and microtubule organization. I will finish with the mechanism of spindle assembly and the regulation of microtubule nucleation in mitosis which are particularly relevant for this thesis.

The microtubules: basic properties

Microtubules are polymers made of α- and β-tubulin heterodimers that bind head-to-tail to form polarized protofilaments. In mammals, the number of protofilaments per microtubule is 13. In other organisms this number can vary and *in vitro* microtubules have been reported to have between 12 to 17 protofilaments (Chrétien and Wade, 1991). Microtubules composed of 13 protofilaments that interact laterally and in the same

orientation to form a hollow tube about 25 nm in diameter (Chretien et al., 1992; Downing and Nogales, 1998). This tube has a marked polarity with a plus-end where the β-tubulin is exposed and a minus-end where the α-tubulin is exposed (Nogales et al., 1998, 1999). The polarity of the tube provides specific dynamic characteristics to the ends where different polymerization and depolymerization reactions occur.

In the microtubule lattice α-tubulins interact laterally with α-tubulins and β-tubulins interact laterally with β-tubulins, but the helical symmetry of the microtubules also generates a different kind of lateral contact between two protofilaments where the α-tubulins interact with β-tubulins. this unique contact within the microtubule structure is known as the "seam" (Akhmanova and Steinmetz, 2008; McIntosh et al., 2009), (Figure 3).

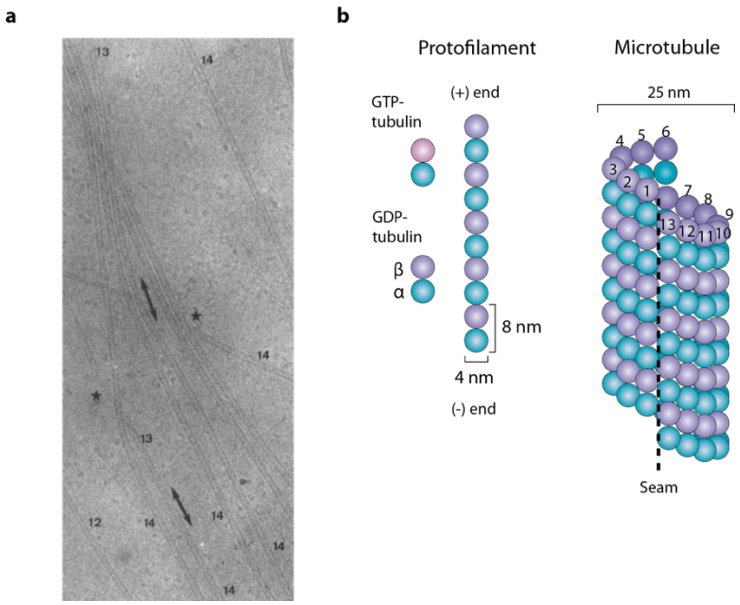

Figure 3: Microtubule structure.

a) Micrograph showing a typical view of vitrified microtubules which have characteristic contrasts for the indicated numbers of protofilaments (pf). Transition regions from one type of image contrast to another within the same microtubule are marked by double arrows. The different contrasts indicate that the protofilament number changes within the microtubule. The contrast associated with flattened microtubules can be seen at some cross-over regions marked by stars. Adapted from (Chretien et al, 1992). **b)** Organization of tubulins into a 13-pf MT. The tubulin dimers associate longitudinally to form a protofilament with an intrinsic polarity with the α-tubulin at the minus-end and the β-tubulin at the plus-end. The lateral interaction of 13 protofilaments generates a MT of 25nm in diameter. Within the protofilament, the α-tubulins interacts with α-tubulins from the next protofilament, except at the seam, where α-tubulins interact with the β-tubulins from the next protofilament. Adapted from (Akhmanova and Steinmetz, 2008).

α- and β-tubulins are proteins of 55 kDa that share 40% identity in amino acid sequence and can be bound to GDP or GTP. During polymerization, GTP bound to β-tubulin (at the exchangeable or E-site) is hydrolyzed; the resulting GDP cannot exchange contributing to the formation of the microtubule lattice composed by GDP-β-tubulin. Only upon depolymerization the GDP is exchanged by GTP at the E site of β-tubulin, promoting a new polimeryzation cycle. α-tubulins can also bind GTP although this binding is to the non-exchangeable site or N-site, so GTP is not hydrolyzed during polymerization (Desai and Mitchison, 1997). The mechanism of GTP hydrolysis results in a conformational change of the tubulin dimer that generates instability within the microtubule lattice. GTP-tubulin "caps" the plus-end of the growing microtubule conferring stability (Alushin et al., 2014; Vale et al., 1994), (Figure 4).

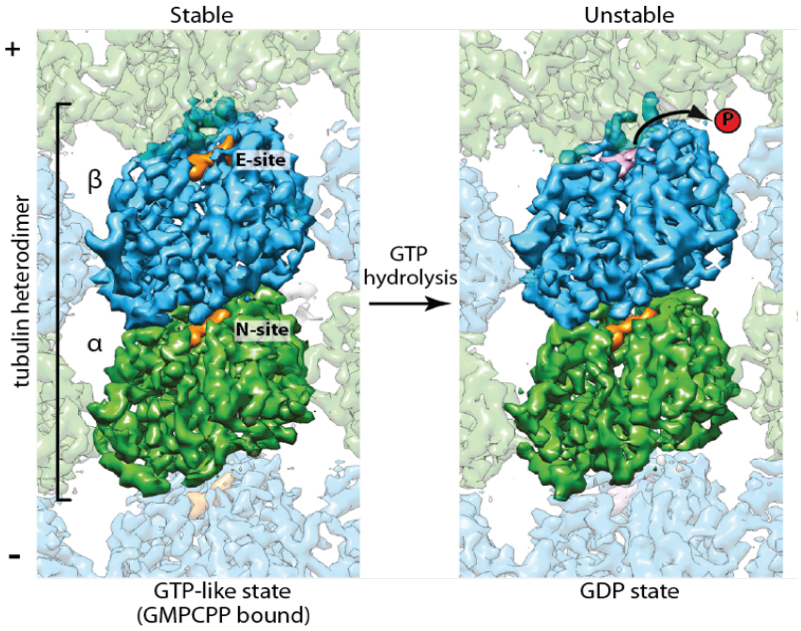

Figure 4: High resolution cryo-EM structures of dynamic and stabilized microtubules.
The cryo-EM map shows the tubulin heterodimer in two distinct nucleotides states: a GTP-like state (bound to a non hydrolyzable analog of GTP: GMPCPP) is shown in the left panel, with a resolution of 4,7Å. A GDP bound state (corresponding to dynamic microtubules in which GTP is hydrolyzed during assembly) is shown in the right panel with a resolution of 4,9Å. α-tubulin, green; β-tubulin, blue; GMPCPP/GTP, orange; GDP, pink. Adapted from (Alushin et al., 2014).

Microtubules are dynamic filaments that may be growing (mainly at the plus-end) or shrinking. They can switch between these two states in a behaviour known as dynamic instability (Mitchison & Kirschner 1984b). The transition between growth and shrinkage

is defined as “catastrophe”, while the switch from shrinkage to growth is called “rescue” (Figure 5). Dynamic instability can occur at both minus and plus-ends of the microtubules, however the plus-ends are more dynamic while minus-ends grow much slower and undergo catastrophe less frequently than plus-ends (Desai and Mitchison, 1997). The difference in the rates of growth at the two ends is explained by changes in the conformation of tubulin dimers as they are being incorporated into the polymer. GTP-β-tubulin produces straight protofilaments that contact with each other laterally and strongly. But GTP to GDP hydrolysis produces a conformational change in the protein that induces the curving of the protofilament. As mentioned before, the GTP cap prevents the curvature of the protofilaments, keeping microtubule ends straight. However, the loss of the GTP cap through GTP hydrolysis eliminates the protection at the plus-ends, leading to depolymerization of the curved protofilaments, (Alberts, 2007; Carlier, 1989).

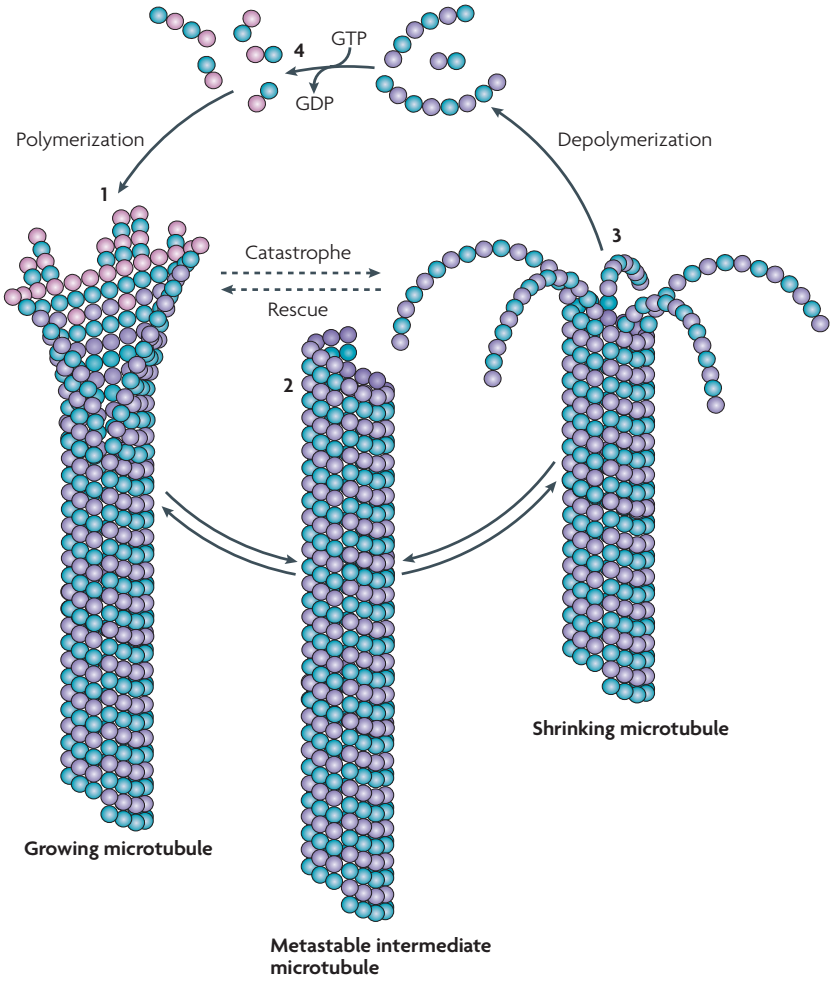

Figure 5: Dynamic instability.

1) Growing microtubules are assembled from a pool of α-β-tubulins. The heterodimers form tubulin sheets that adopt a closed conformation in order to assemble the hollow structure of 25 nm diameter. Growing microtubule sheets maintain a GTP-tubulin cap that protects the microtubule from depolymerization. **2)** Metastable intermediate microtubules present blunt ends and they might pause, undergo further growth (rescue) or switch to the depolymerization phase (catastrophe). **3)** Shrinking microtubules are unstable polymers with curved protofilaments that "peel-off" from the microtubule lattice like a banana. **4)** Free GDP-tubulin dimers exchange GDP for GTP at the β-tubulin subunit, allowing a new polymerization cycle. Adapted from (Akhmanova and Steinmetz, 2008).

This polymerization model is known as the allosteric model and it posits, as explained above, that unpolymerized α-β-tubulin adopts a more polymerization-competent conformation after its binding to GTP. Recently, a different model regarding the actual cause of the conformational change in tubulin dimers has been proposed. This model is known as the lattice model and it claims that conformational changes occur only upon recruitment into the growing lattice (Rice et al., 2008).

During the process of dynamic instability four parameters can be measured: the velocity of growth (Vg), the velocity of shrinkage (Vs), the frequency of rescues (Fres), and the frequency of catastrophes (Fcat), (Verde et al., 1992). These parameters can determine the average length (L) of a given microtubule population by using the next formula:

$$L = (VgFres – VsFcat) / (Fcat + Fres)$$

In vitro, microtubules can spontaneously polymerize over a certain tubulin concentration that is above physiological levels (Figure 6). Microtubule growth *in vitro* happens in two sequential phases. A first slow phase involves the polymerization of small intermediates that are unstable. In a second rapid phase the pre-formed oligomers continue to grow by the continuous addition of tubulin heterodimers. During the first steps of growth the disassembly is energetically favored over assembly (explaining the slow reaction of initial growth) but once an oligomer large enough is formed, assembly becomes energetically favored and elongation proceeds fast (Kollman et al., 2011).

In vivo, tubulin concentration is not sufficient to promote spontaneous growth events. Therefore, cells have evolved additional mechanisms involving specific nucleator complexes that compensate or bypass the early, slower growth phase observed during spontaneous growth. In the next section, I will describe the microtubule nucleation process and the known microtubule nucleation complexes.

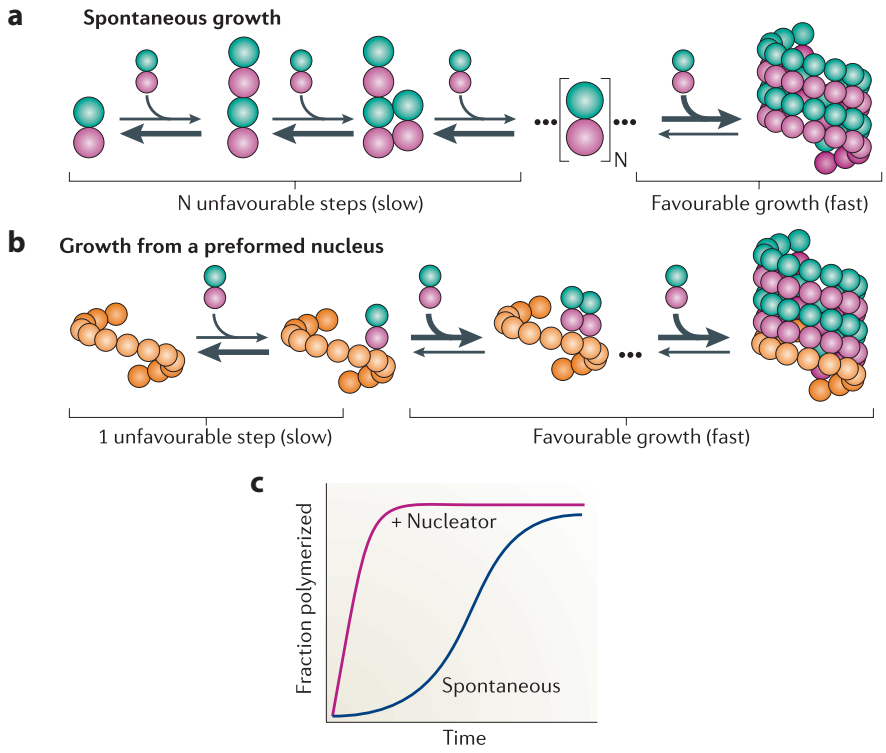

Figure 6: Microtubule nucleation.

a) Spontaneous microtubule growth *in vitro* occurs in two stages: a relatively slow phase through unstable early assembly intermediates, and a rapid elongation phase. In early steps, the assembly energetics favors disassembly over assembly but, after a sufficiently large oligomer is formed by a variable number of steps (denoted by N), assembly is energetically favored and elongation proceeds rapidly. Whether disassembly or assembly is favored by the assembly energetics is indicated by a bold arrow. **b)** *In vivo*, preformed nuclei allow microtubule growth to bypass the slow phase, providing spatial and temporal control over new microtubule growth. **c)** Graphic representation comparing spontaneous microtubule polymerization and microtubule growth with a nucleator. The presence of a nucleator promotes rapid microtubule polymerization, bypassing the lag phase observed during spontaneous growth. Adapted from (Kollman et al., 2011).

II-Microtubule nucleation

As mentioned before, living cells need to promote microtubule nucleation from tubulin concentrations much lower than *in vitro* conditions. Mammalian cells keep their tubulin concentration around 25µM by different mechanisms involving regulation at mRNA and protein levels. In order to initiate nucleation, cells make use of specific nucleation complexes that bypass the initial unstable intermediates and at the same time provide spatial and temporal control of microtubule nucleation.

The very first described microtubule nucleator is γ-tubulin, a member of the tubulin

superfamily. γ-tubulin was identified in a study through a screen for β-tubulin mutation suppressors in *Aspergillus nidulans* (Weil et al., 1986). The molecular weight of γ-tubulin is about 50 kDa and it shares around 33% identity with α- and β-tubulin (Oakley and Oakley, 1989). γ-tubulin is found nearly ubiquitously in all eukaryotes and it is essential for microtubule nucleation and cell division. It localizes to all the microtubule organizing centers in the cell (MTOCs), reviewed in (Joshi, 1994; Pereira and Schiebel, 1997), although it is also involved in nucleation from non-MTOC sites, suggesting a critical role in the initiation of all new microtubules within the cell (Kollman et al., 2011).

The resolution of a 2.7 Å crystal structure of γ-tubulin bound to GTP-γS (a non-hydrolysable GTP analoge) revealed a curved conformation for γ-tubulin- GTP-γS, similar to that observed for the unpolymerized α-β-heterodimers bound to GDP (Aldaz et al., 2005). This study also proposed that γ-tubulins can associate laterally in the same way as the α- and β-tubulin heterodimers interact in the microtubule lattice, providing a template that favors microtubule nucleation *in vivo*.

In the 90', electron microscopy analyses of a γ-tubulin complex isolated from *Xenopus laevis* egg extract revealed that γ-tubulin is associated with several proteins to form an open ring-shaped complex of 25 nm diameter (Zheng et al., 1995) . On the same year, electron microscopy studies on *Drosophila melanogaster* purified centrosomes revealed several rings of γ-tubulin with identical diameter as *Xenopus laevis* shaped-ring structures (Moritz et al., 1995). Later in that decade, biochemical analysis identified at least seven proteins co-purifying with γ-tubulin in mammalian cells (Murphy et al. 1998). These proteins are known as γ-tubulin complex proteins or GCPs (GCP2-6). All of them share high homology on two short motifs: grip-1 and grip-2 (from γ-tubulin ring protein motif). One molecule of GCP2, one molecule of GCP3 and two molecules of γ-tubulin constitute a γ-tubulin small complex or γ-TuSC (Oegema et al., 1999). The γ-TuSC is a small subunit of a bigger complex that Oegama and colleagues named γ-tubulin ring complex or γ-TuRC (Figure 7). They characterized both complexes by using sucrose gradients from *Drosophila* embryo extracts, defining a size of ≈ 280kDa for the γ-TuSC and a size of ≈ 2,2 MDa for the γ-TuRC. γ-TuSCs show microtubule nucleation activity *in vitro* although they are less active than intact γ-TuRCs, suggesting that the assembly into a larger

complex favors the nucleation activity (Oegema et al., 1999). In addition to its nucleating activity, the γ-TuRCs can also act as a minus-end capping complex, therefore stabilizing microtubules (Anders and Sawin, 2011; Wiese and Zheng, 2000). Further studies on the γ-TuRC composition and its stoichiometry revealed that it is composed of ≈ 14 copies of γ-tubulin, 12 copies of GCP2/3, 2-3 copies of GCP4, 1 copy of CGP5 and less than one copy of GCP6 (Choi et al., 2010). This quantification should be taken with caution as the unexpected low presence of GCP6 could imply the possibility of heterogeneity in the sample.

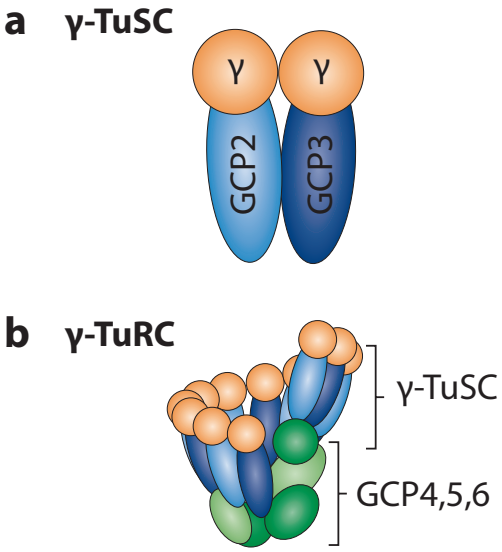

Figure 7: Schematic representation of γ-TuSC and γ-TuRC.

The γ-tubulin small complex (γ-TuSC) is the conserved, essential core of the microtubule nucleating machinery, and it is found in nearly all eukaryotes. **a)** The γ-TuSC has two copies of γ-tubulin and one each of γ-tubulin complex protein 2 (GCP2) and GCP3. **b)** In many eukaryotes, multiple γ-TuSCs assemble with GCP4, GCP5 and GCP6 into the γ-tubulin ring complex (γ-TuRC). Adapted from (Kollman et al., 2011).

Regarding the three-dimensional structure of the whole γ-TuRC complex, several advances have been recently made. Using budding yeast as a model organism, Kollman and colleagues studied the structure of the minimal ring structure or γ-TuSC (Kollman et al. 2008; Kollman et al. 2010) (Figure 8). By performing Cryo-electron microscopy on γ-TuSC assembled into a filament, they showed a structural ring composition of 13 γ-tubulins per turn, matching microtubule symmetry. Since each γ-tubulin plus-end is fully exposed in the filament, a model in which γ-tubulin makes longitudinal contacts with the minus-ends of α-β-tubulin was favored. This observation, together with the 13-fold γ-tubulin symmetry, provides a strong evidence to support a γ-tubulin template mechanism for microtubule nucleation (Kollman et al. 2010).

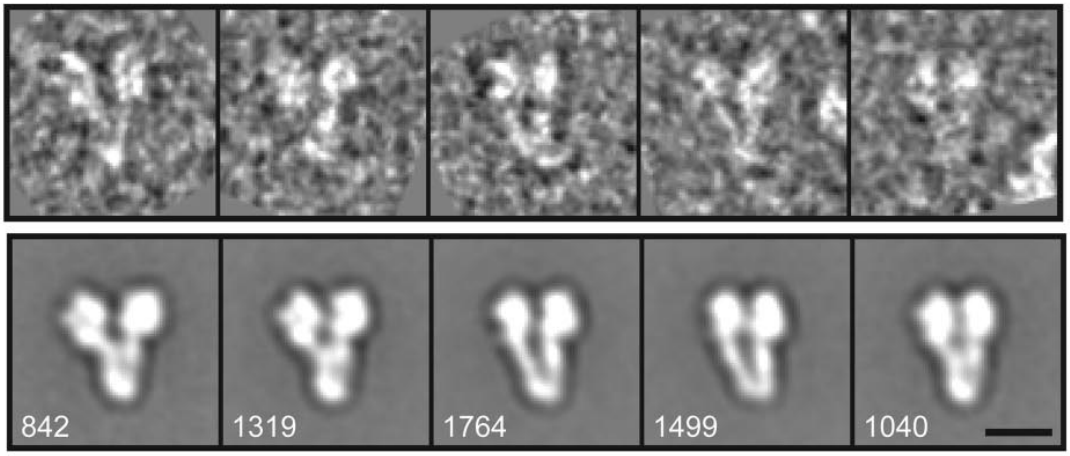

Figure 8: Negative stain images of Saccharomyces γ-TuSC.

The upper panel shows individual Y-shaped γ-TuSC complexes selected for reconstruction. The lower panel shows the reconstruction of the corresponding complexes, indicating the number of particles in each class of structures found, which vary in the branching angle between the arms of the Y-shaped particle. Bar, 10 nm. Adapted from (Kollman et al., 2008).

However, it is important to mention that, to date, two models have been proposed to explain the mechanism of γ-tubulin-dependent microtubule nucleation. The first model is known as the "protofilament model" and it postulates that, due to the flexible structure of the γ-TuRC, it may potentially unfurls to present a single protofilament of γ-tubulins that laterally attach to α-β-tubulin dimers to promote nucleation (Erickson and Stoffler, 1996). A second model, currently known as the "template model" but initially described as "seeded nucleation model" suggests that the γ-tubulins in the γ-TuRC act as a template for microtubule nucleation, making lateral contacts with each other around the ring and longitudinal contacts with α-β-tubulin dimers (Zheng et al., 1995) (Figure 9).

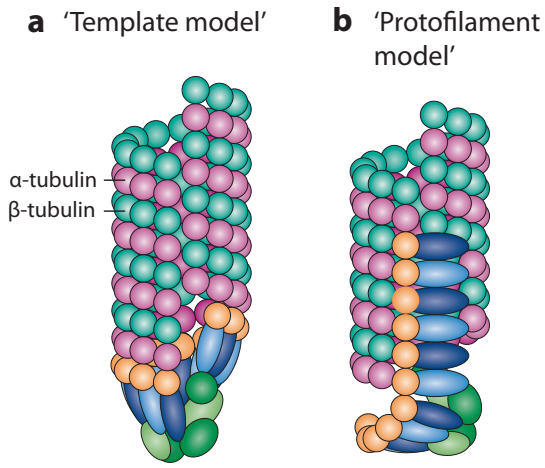

Figure 9: Schematic representation of two distinct models of γ-TuRC assembly.

a) The most widely accepted model for the mechanism of γ-TuRC-based nucleation, the 'template model', suggests that the γ-TuRC acts as a template, presenting a ring of γ-tubulins that make longitudinal contacts with α-tubulin–β-tubulin (α-β-tubulin). **b)** By contrast, the 'protofilament model' suggests that the γ-TuRC unfurls to present a γ-tubulin protofilament, which would nucleate through lateral contacts with α-β-tubulin. Adapted from (Kollman et al., 2011).

New data on the γ-TuRC components, as for example the GCP4 crystal structure (Guillet et al., 2011), together with initial observations of γ-tubulin being bound to the ends of microtubules (Meads and Schroer, 1995; Moudjou et al., 1996; Stearns and Kirschner, 1994) and the more recent analysis by electron and light microscopy of the γ-TuRC and its interaction with the microtubule minus-end *in vitro*, have provided more evidence for the template model, which is nowadays widely accepted (Kollman et al., 2010b, 2011, 2015; Moritz et al., 2000; Wiese and Zheng, 2000). Indeed, recent work from Kollman and colleagues suggested that the activation of the γ-TuRC complex involves a conformational change of GCP3 that straightens at his hinge point, adjusting the position of γ-tubulins in the γ-TuSC to better match the symmetry of the microtubules in the lattice (Kollman et al., 2011) (Figure 10). Moreover, they recently showed that a conformational change switch in the complex involving the transition from an open to a closed state can provide the perfect matching of the γ-tubulin molecules in the γ-TuSC with the microtubule minus-end, enhancing microtubule nucleation activity (Kollman et al., 2015).

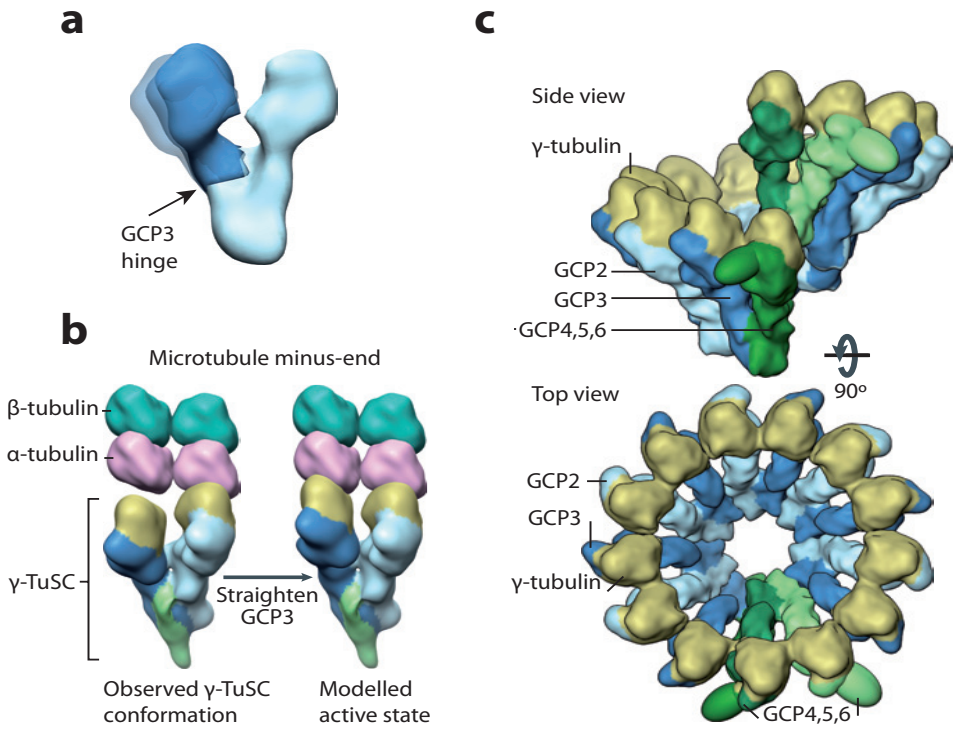

Figure 10: A model for γ-TuSC activation and γ-TuRC assembly.

a) The negative-stain electron microscopy reconstruction of free γ-TuSC revealed flexibility at a hinge point in γ-tubulin complex protein 3 (GCP3). **b)** A model for the conformational activation of the γ-TuSC through the straightening of GCP3. In the observed conformation, the two γ-tubulins are held apart so that they cannot both be making contacts with the microtubule. However, straightening at the GCP3 hinge point by 23° would close the intra-γ-TuSC γ-tubulin gaps, bringing all of the γ-tubulins in the ring to microtubule lattice-like spacing. **c)** A revised model of γ-TuRC assembly. Through conserved lateral interactions, GCP4, GCP5 and GCP6 could be directly incorporated into the ring structure, as opposed to forming a cap structure as in previous models mentioned in Figure 9. Although GCP4, GCP5 and GCP6 might incorporate at any position within the ring, it is plausible to think of them interacting at the ends where they might function to initiate or terminate ring formation and to stabilize the ring at the overlap. Adapted from (Kollman et al., 2011).

The γ-TuRC is not only composed of γ-tubulin and GCP proteins. More components that do not belong to the GCP protein family have been identified. These are MOZART1 (Hutchins et al., 2010) and GCP8/MOZART2 (Teixido-Travesa et al., 2010).

MOZART1 stands for "mitotic-spindle organizing protein with a ring of γ-tubulin" and it is a small protein of only 8,5 kDa that was first described as a member of the human γ-TuRC (Hutchins et al., 2010; Teixido-Travesa et al., 2010). MOZART1 has been shown to be required for the targeting of γ-TuRC to microtubule nucleation sites (Dhani et al., 2013; Hutchins et al., 2010; Janski et al., 2012; Masuda et al., 2013; Nakamura et al., 2012) and very recently, its mechanism of action has been revealed (Cota et al., 2017).

MOZART1 has not only an essential function in γ-TuRC assembly but it also binds specifically to fully assembled γ-TuRCs to allow interaction with γ-TuRC targeting factors, regulating in this way microtubule nucleation (Cota et al., 2017).

MOZART2 was identified in both interphase and mitotic γ-TuRCs and it was shown not to be required for γ-TuRC assembly but important for γ-TuRC recruitment and microtubule nucleation at interphase centrosomes (Teixido-Travesa et al., 2010).

There are other proteins associated to the γ-TuRC and the best characterized one is CGP-WD/NEDD1 (from now on referred as NEDD1) (Haren et al., 2006; Lüders et al., 2006). NEDD1 stands for "neural precursor cell expressed developmentally down-regulated protein 1" and it was originally discovered in a cDNA subtraction screen to identify genes responsible for the development of the central nervous system (Kumar et al., 1992). NEDD1 is conserved through evolution with homologues in all vertebrates as well in *Drosophila melanogaster*. Mouse and human NEDD1 genes encode a 71 kDa protein with 660 amino acids (Kumar et al., 1994). The different NEDD1 homologues share a WD40 domain in the N-terminal half of the protein and a C-terminal domain with 100 amino acids encoding a coiled-coil structure. Mammalian NEDD1 contains seven WD40 repeats at the N-terminus; this region is required for centrosomal localization while the C-terminal region is crucial for its interaction with γ-tubulin (Haren et al., 2006; Lüders et al., 2006) (Figure 11).

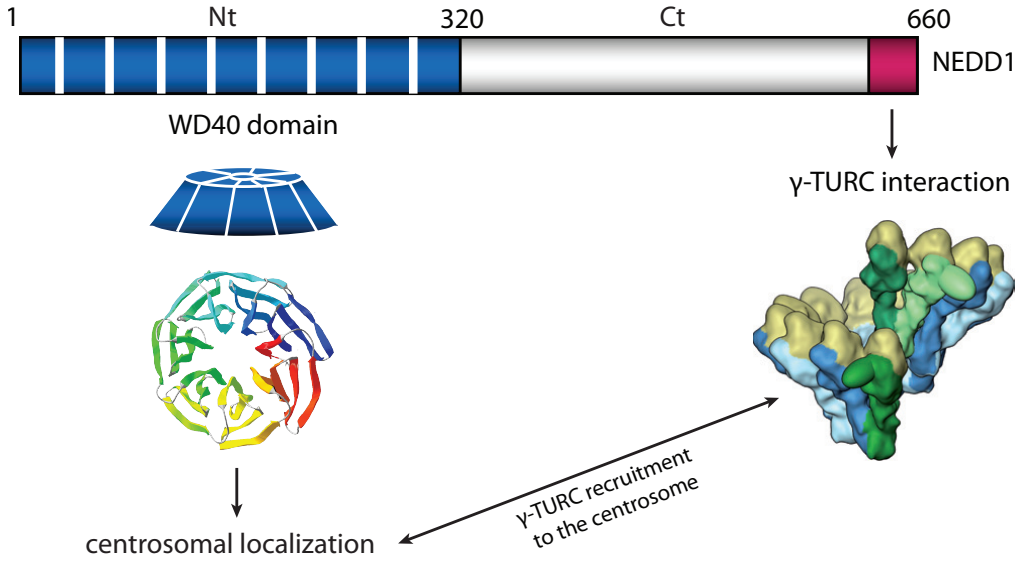

Figure 11: Schematic representation of NEDD1 functional domains

The conserved WD40 domain (blue color) is in the N-terminal part of the protein. The predicted three-dimensional structure of the NEDD1 WD-repeat domain led to the proposal of a β propeller structure composed of seven blades shown here in different colors (adapted from (Haren et al., 2009)). The WD40 domain is necessary for NEDD1 localization to the centrosomes. The C-terminal domain of NEDD1 (red color) is responsible for its interaction with γ-tubulin. γ-TuRC reconstruction taken from (Kollman et al., 2011).

Over the last years different groups have studied NEDD1 function in mitosis. NEDD1 localizes to the centrosome and spindle microtubules, colocalizing as well with γ-tubulin. NEDD1 depletion by siRNA in mammalian cells leads to almost a complete loss of γ-tubulin from the centrosome and the spindle, impairing microtubule nucleation. The phenotype of NEDD1 depleted cells is characterized by a mitotic arrest, with an accumulation of aberrant spindles with poorly separated poles and microtubules arranged in a monoastral pattern, also known as monopolar structures (Haren et al., 2006; Lüders et al., 2006). NEDD1 has also been shown to be necessary for daughter centriole assembly during duplication or for centriole maturation, as NEDD1 depletion leads to only once centriole at each pole (Haren et al., 2006). Interestingly, a proportion of NEDD1 has been found in low molecular weight fractions not associated with γ-tubulin (Lüders et al., 2006), raising the possibility of a putative NEDD1 function independent from its interaction with γ-tubulin.

NEDD1 is the main γ-TuRC-targeting factor although is not required for γ-TuRC

assembly and it can localize to centrosomes independently of the γ-TuRC, as shown in human cells, *Xenopus laevis* and *Drosophila melanogaster* (Haren et al., 2006; Liu and Wiese, 2008; Lüders et al., 2006; Vérollet et al., 2006). The targeting of the γ-TuRC is regulated by phosphorylation of NEDD1 at specific residues (Gomez-Ferreria et al., 2012b; Johmura et al., 2011; Lüders et al., 2006; Pinyol et al., 2013; Sdelci et al., 2012; Zhang et al., 2009). The regulation of γ-TuRC targeting by NEDD1 phosphorylation is very important for spindle assembly as it controls the spatial and temporal regulation of microtubule nucleation at different sites in the cell. I will explain the molecular basis and the main players important for this regulation in the section VIII of this introduction.

III- The centrosome as the main MTOC in animal cells

The main MTOC in animal cells is the centrosome. In the late 1880s, Edouard van Beneden and Theodor Boveri independently observed for the first time the centrosome while studying fertilization and the first embryonic divisions (Wunderlich, 2002). Beneden named it as *corpuscule central* while Boveri called it *centrosome*, because of its location at the center of the cell (Scheer, 2014).

The centrosome is composed of two centrioles (the mother and the daughter) surrounded by pericentriolar material (PCM) (Chrétien et al., 1997; Ibrahim et al., 2009; Paintrand et al., 1992; Vorobjev and Chentsov, 1982). The PCM is an electro-dense material composed of many different proteins forming a mesh. Initially the PCM was thought to be randomly organized although recent data revealed the position of different proteins within the PCM, suggesting a highly ordered structure organized as radial layers of proteins surrounding the centrioles (Lawo et al., 2012; Mennella et al., 2012). Centrioles are cylindrical structures of 250 nm diameter and a length ranging from 150 to 500 nm, depending on the cell type (Winey and O'Toole, 2014). Centrioles are typically composed of 9 microtubule triplets organized with a clockwise radial symmetry around a cartwheel structure. The cartwheel has been proposed to be formed by an oligomer of the conserved coiled-coil spindle assembly abnormal protein SAS-6 (Kitagawa et al., 2011; Nigg and Stearns, 2011). Some organisms present singlets or doublets of microtubules instead of triplets (Carvalho-Santos et al., 2011). The microtubules of a triplet are named A-tubule (the most internal one), B-tubule (in the middle) and C-tubule (the most external one).

Whereas A is a complete microtubule of 13 protofilaments, B and C have 10 protofilaments each and share 3 protofilaments with the preceding tubule to make complete, 13 protofilament microtubules (Winey and O'Toole, 2014). Centrioles are polarized structures: each centriole is formed by microtubule doublets (A and B) at its distal part and microtubule triplets (A, B and C) at its proximal part. At the basal side of the mother centriole there are protein linkers that tether the daughter centriole forming a 90º angle with respect of the mother centriole. At the apical side of the mother centriole there are distal and subdistal appendages that dock cytoplasmic microtubules and might anchor centrioles to the cellular membrane to form the basal body of cilia and flagella (reviewed in (Bettencourt-Dias and Glover, 2007; Winey and O'Toole, 2014)). Although the centrioles are ancestral structures present in all eukaryotic groups (Carvalho-Santos et al., 2010), the structure of the centrosomes is not conserved in all organisms (Carvalho-Santos et al., 2011).

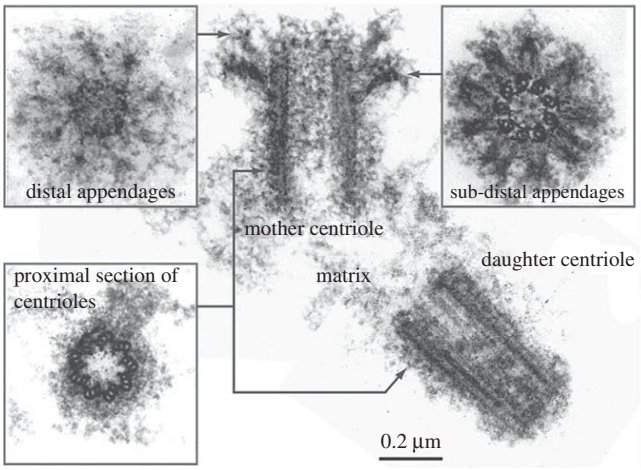

Figure 12: Centriole structure.
Electron micrographs of centrioles in isolated centrosomes shown in longitudinal and cross sections. In the mother centriole two types of appendages can be appreciated: the distal and the sub-distal appendages. The latter are very proximal to the distal appendages and often appear as distinct triangular structures attached laterally to the sides of the microtubule scaffold. From (Winey and O'Toole, 2014).

The centrosome is important for many functions during the cell cycle. In differentiated cells arrested in G0 as well as in sperm cells, the centrosome forms the basal body of cilia and flagella. In cycling cells, the centrosome is the primary MTOC of the cells during interphase and in mitosis it is the main microtubule nucleator and it is important for many other functions as for example defining the two poles of the mitotic spindle and helping in spindle positioning and asymmetric division.

The centrosome duplicates once per cell cycle during S-phase in a process coordinated with DNA replication. Centrosome duplication consists of several steps during cell cycle.

In early G1, the mother and daughter centrioles separate in a process known as centriole disengagement. Disengagement requires the activity of Plk1, an important mitotic kinase (Tsou et al., 2009), as well as separase, the protease that separates sister chromatids at the metaphase to anaphase transition (Uhlmann et al., 2000). In S phase, synthesis of a daughter centriole occurs in the vicinity of each preexisting centriole. This event is called procentriole formation and it is under the regulation of the kinase Plk4 that controls the recruitment of several components to the cartwheel as for example SAS-6 (Nigg and Stearns, 2011). In G2 phase, the procentrioles first elongate to complete the duplication process and once they are duplicated a maturation step occurs. During this maturation process in late G2 phase, the duplicated centrosomes recruit several components to the PCM, including γ-tubulin, that triplicates its amount (Khodjakov and Rieder, 1999). As a consequence, the centrosomes increase the PCM mass and thus microtubule nucleation activity by 5-7 folds (Piehl et al., 2004; Wiese and Zheng, 2006). The centrosomes also increase in size and separate to allow the formation of a bipolar spindle. In M phase, the mother and daughter centrioles detach from each other in a process known as centrosome disjunction.

The centrosome is a critical organelle for the G2/M checkpoint. Centrosome separation starts at G2 phase and it is completed in M phase. Several key proteins involved in controlling G2/M checkpoint are recruited to the centrosome. The most important one is Cdk1 and its regulator cyclin B, which is the kinase master regulator of cell cycle. I will describe these two important players of the cell cycle in the next section.

IV- The cell cycle

Prokaryotes and eukaryotes present common strategies for cell division. Although the cell organization is much different, in both cases cells first grow and duplicate the DNA in each chromosome, then chromosomes are segregated in equal number to each daughter cell and finally the cell divides.

Cell division is much simpler in prokaryotes, where cells contain only a single circular chromosome and replication and segregation are often coupled. Chromosomes are bound to the cell membrane and after division each daughter cell will inherit the new chromosome in a process called binary fission (reviewed in Reyes-Lamothe et al. 2012).

In contrast, cell division in eukaryotes is much more complex and in this case replication and segregation are separated in time. Indeed, several different phases can be distinguished: S phase (synthesis), when the DNA replication occurs and the centrosome duplicates, a mitotic phase (M), when chromosome segregation takes places, and three GAP phases that precede and follow S phase. The first GAP phase or G1 (Gap phase 1) is important for cell growth and mRNA, protein and ribosome synthesis. In G2 (Gap phase 2) cells grow more, continue making proteins and organelles and begin to reorganize their content in preparation for mitosis. G1, S, and G2 together are called interphase. G0 (Gap phase 0) is a resting phase where the cell has left the cycle and has stopped dividing. Cells can also enter this quiescent state under growth inhibiting conditions as for example lack of nutrients or high cell density.

Cell cycle is generally described to last 24 hours, but its duration can vary a lot depending on the system and the cell type. Considering a 24-hour cycle, G1 lasts approximately 12 hours, S-phase 6 hours, G2 6 hours, and mitosis 30 minutes. The mitotic phase is the shorter phase of the cell cycle and it is divided into five steps: prophase, prometaphase, metaphase, anaphase and telophase.

The molecular basis of the cell cycle

The kinase Cdk1 (previously known as Cdc2) and its regulator cyclin B were first identified from a meiotic cytoplasm containing a maturation promoting factor (MPF) that was able to mediate mitotic entry (Masui and Markert, 1971; Schorderet-Slatkine and Drury, 1973). This MPF was later found to be a protein complex containing both Cdk1 and cyclin B and this discovery was a major breakthrough for the molecular understanding of the cell cycle machinery (Dunphy et al., 1988; Labbe et al., 1989). Cyclin B is part of the family of proteins called cyclins whose name is due to its oscillatory behavior through the cell cycle. Cyclins are synthetized and destroyed depending on regulated transcription and degradation cycles (Evans et al., 1983).

There are different cyclin-Cdk complexes playing specific functions in each phase of the cell cycle. Cyclin D-Cdk4/6 promotes progression in G1 phase. Cyclin E-Cdk2 is responsible for the entry into S phase. Cyclin A-Cdk2 is essential for the S phase main events. Cyclin A-Cdk1 is responsible for G2. Cyclin B-Cdk1 triggers the entry into

mitosis and its inactivation triggers anaphase and mitotic exit (Figure 13). I will describe more in detail the cyclin B-Cdk1 complex as it is the one driving mitosis entry.

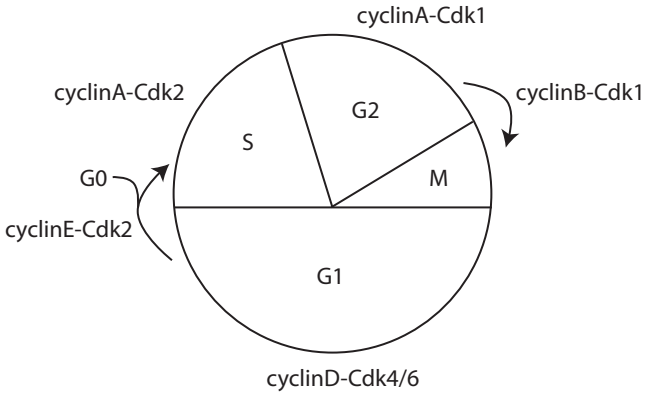

Figure 13: Schematic drawing of the cell cycle phases and their regulation by cyclins.

The cell cycle is divided in different phases: the interphase, constituted by two gap phases (G1 and G2) and one synthesis phase (S), and mitosis (M). G0 is a quiescent state in which cells enter upon prolonged block in G1, upon the correct stimuli, a cell can resume the cell cycle. The main Cyclin-Cdk complexes are indicated for each phase. Arrows represent the cell cycle transitions, characterized by synthesis and degradation of cyclins.

Several feedback loops regulate cyclin B-Cdk1 activity. A negative loop occurs between Cdk1 and the kinases Myt1 and Wee1; both kinases phosphorylate Cdk1 on T14 and Y15, thereby inhibiting cyclin B-Cdk1 activity. The T14 and Y15 phosphorylations are removed by phosphatases of the Cdc25 familiy which are in a positive feedback loop with Cdk1. Once activated, cyclin B-Cdk1 activity inhibits Wee1 and Myt1 and activates the Cdc25 phosphatases.

A second loop involves the kinase Plk1 that activates cyclin B-Cdk1 at different levels: first, by activating Cdc25 (Qian et al., 2001). Second, by binding to the AurA adaptor Bora. Plk1-Bora binding is promoted upon Bora phosphorylation by Cdk1; Bora then associates with AurA that in turn, activates Plk1.

AurA can also stimulate cyclin B-Cdk1 activation through activation of Cdc25 and regulation of centrosome maturation. Cdc25 is recruited to the centrosomes during their maturation, enhancing the local concentration of cyclin B-Cdk1. In addition, several proteins in the mitotic entry network are targeted to the centrosomes, enhancing as well the local concentration of cyclin B-Cdk1 activators (reviewed in (Lindqvist et al., 2009)). In this way, AurA and Plk1 temporally connect the activation of cyclin B-Cdk1 and mitosis entry with centrosome maturation.

In summary, there are several feedback loops controlling cyclin B-Cdk1 activity to ensure

commitment to mitosis once the decision to enter mitosis has been made but a certain degree of redundancy is also present, as defects in some of the network players do not completely block mitosis entry (Lindqvist et al., 2009).

In fact, the cyclin-dependent kinase Cdk1 coordinates mitotic events through the regulation of multiple proteins either directly or in collaboration with a number of kinases that include Polo, Aurora and NIMA family members (reviewed in (Nigg, 2001)). In the next paragraphs I briefly summarize some of the main mitotic functions related to these kinase families because they are important regulators of NEDD1 (see section IX).

Aurora kinases

There are three human and murine homologues of Aurora kinases named as Aur-A, -B, and -C.

Aurora kinases are involved in multiple functions including centrosome duplication, maturation and separation, spindle assembly and stability, chromosome condensation and segregation, and cytokinesis (Carmena and Earnshaw, 2003; Katayama et al., 2003). Aurora kinases have a catalytic domain that is highly conserved and an N-terminal domain that varies both in sequence and length. Aur-A has been the kinase most intensively studied; it localizes to centrosomes and is essential for mitotic progression. In late G1/early S phase, AurA is found in the PCM of centrosomes and its level of expression rises through the cell cycle (Stenoien et al., 2003). During prophase, AurA keeps its localization at the centrosomes and later in metaphase it localizes to both centrosomes and spindle microtubules. In mitosis, TPX2 binds AurA at the centrosome and targets it to the microtubules proximal to the spindle pole, whereby, at metaphase, it regulates chromosome alignment/segregation (Katayama et al., 2003). TPX2 also regulates AurA kinase activity by inhibiting the activity of the phosphatase PP1 and promoting AurA autophosphorylation at Thr 288. As mitosis progresses, an increasing number of proteins associate with AurA and one of its known substrates is NEDD1.

Polo-like kinases

The family of mammalian Plk consist of 4 members: Plk1, Plk2 (snk, serum-inducible), Plk3 (Fnk/Prk, FGF-inducible/ proliferation-related), and Plk4 (Sak) (Takai et al., 2005). These kinases have a highly conserved N-terminus domain and a C-terminal domain containing highly conserved sequences of 30 amino acids called polo-boxe. This polo-box domain mediates the subcellular distribution of Plk to mitotic structures and substrate specificity interactions. Plk play important roles in bipolar spindle assembly, centrosome maturation and separation in late G2 phase, chromosome segregation, Cdk1/cyclin B1 activation, and cytokinesis. In mitosis, Plk associates with spindle poles and kinetochores and in late anaphase, Plk is distributed along the midzone of the mitotic spindle. It has been reported that Plk1 is involved in the recruitment of γ-tubulin to the centrosomes (Barr et al., 2004; Lane and Nigg, 1996) but also to the microtubules of the mitotic spindle (Zhu et al., 2009). Plk1, together with CDK1, activates the NIMA family member Nek9 early in mitosis controlling centrosomes separation through Nek6/7 and Eg5 (Bertran et al., 2011) (see NIMA family description below).

Nek (NIMA) kinases

The Nek (NIMA, never in mitosis A) related kinase family contains 11 members (Nek1-11) (Belham et al., 2003; Bowers and Boylan, 2004; Hayward et al., 2004). However, the collective location and function of this mitotic kinase family is not well understood. Human Nek kinases share substantial homology at the amino terminal domain but exhibit variable homology at the carboxyl region. Different Neks have been involved in the control of the centrosome and microtubule cytoskeleton (Quarmby and Mahjoub, 2005). For example, Nek2 regulates premitotic centrosome disjunction, while Nek9 (also known as Nercc1) and Nek6 and Nek7 are involved in the control of spindle structure and function (O'Regan et al., 2007). Nek9 is activated at centrosomes during early mitosis, interacts with both Nek6 and Nek7 and, in turn, activates them by phosphorylation (Belham et al., 2003; Roig et al., 2002, 2005). Nek9 was later shown to be activated in early mitosis by a two-step mechanism that involves Nek9 sequential phosphorylation by Cdk1 and Plk1. Downstream of Plk1, Nek9 and Nek6/7 mediate centrosome separation

during prophase through the control of Eg5 recruitment to centrosomes (Bertran et al., 2011).

V- Cell division and the mitotic spindle

Mitosis entry does not only involve changes at the molecular level. At the cellular level, the DNA and the microtubule cytoskeleton undergo morphological changes during the different mitotic phases described below:

1) Prophase: the DNA condensates into chromosomes, the microtubules become short and dynamic, the duplicated centrosomes separate and move to opposite sides of the nucleus.

2) Prometaphase: the nuclear envelope (the physical barrier that encloses the nucleus) breaks down and the chromosomes are released from the nucleus. The chromosomes consist of sister chromatids bound to each other along their length and at the center trough the sister kinetochores, a multiprotein structure assembled at the centromeres that captures microtubules plus-ends to form the kinetochore fibers (K-fibers).

3) Metaphase: microtubules organize a bipolar spindle and chromosomes are aligned at the center of this structure forming the metaphase plate.

4) Anaphase: sister chromatids are separated and pulled to opposite poles of the cell, ensuring in this way that each daughter cell receives an equal set of chromosomes.

5) Telophase: the nuclear envelope re-forms around each set of chromosomes, separating the nuclear DNA from the cytoplasm, and the chromosomes begin to decondense.

The final step of cell division is cytokinesis, characterized by the separation of the parental cytoplasm following the generation of a cleavage furrow by invagination of the plasma membrane, so that each daughter cell inherits one of the two nuclei (Alberts, 2007).

An essential process that takes place from prophase to metaphase is the assembly of the mitotic spindle. The mitotic spindle is a complex macromolecular machine made of centrosomes, chromosomes, microtubules and microtubule associated proteins, as for

example microtubule motors. This structure and its correct function is essential for the proper segregation of chromosomes to the two daughter cells and therefore, the cell has developed mechanisms to ensure the lack of errors during this process. The spindle assembly checkpoint or SAC is the main protection mechanism that the cell uses to block the progression of mitosis until all chromosomes are properly aligned and attached to the spindle microtubules.

Different pathways contribute to spindle assembly as well as different classes of microtubules compose the mitotic spindle. In the next section I provide an overview on the structure of the mitotic spindle while the different pathways that cooperate to assemble a functional bipolar spindle will be explained in the section number VIII.

Three different populations of microtubules are present within the spindle: the astral microtubules, the interpolar microtubules and the kinetochore fibers (designated as K-fibers from now on) (Figure 14). Astral and interpolar microtubules are individual microtubules that have similar similar dynamic properties with a half-life time of about 30 seconds to 1 minute (Mitchison et al., 1986). Astral microtubules emanate from the two centrosomes in a radial pattern to reach the cell cortex, playing a role in centrosome separation during prophase and spindle positioning (Rosenblatt, 2005). They are also important in the processes of asymmetric and polarized cell division (reviewed in (Knoblich, 2010)). However, mitosis can occur without astral microtubules, indicating that their function is not essential for cell division (Khodjakov et al., 2000b; Mahoney et al., 2006). The interpolar microtubules are the most abundant class of microtubules although they are very heterogeneous, some can emanate from the centrosomes across the whole spindle while others can be very short as well (Mastronarde et al., 1993) and not all of them need to be connected to the spindle poles. Interpolar microtubules have many functions, including the establishment and maintenance of spindle bipolarity and helping in the process of chromosome congression trough their interaction with chromokinesins (reviewed in (Vanneste et al., 2011)) or through lateral attachments to the kinetochores (Cai et al., 2009; Magidson et al., 2011; Wignall and Villeneuve, 2009). The last class of spindle microtubules are the K-fibers, bundles of 20-40 parallel microtubules (McEwen et al., 1997; Rieder, 1981) directly connected to the kinetochores. This kind of microtubules are much more stable than astral and interpolar microtubules, with a half-life time of about 4 to 8 minutes (Bakhoum et al., 2009; Zhai et al., 1995),

being therefore more resistant to depolymerizing agents like cold or nocodazole. The main function of the K-fibers is to attach the chromosomes to the two spindle poles and to segregate the sister chromatids into the daughter cells. During metaphase, K-fibers attached to the kinetochores generate pulling forces and tension between the sister kinetochores that are crucial to trigger chromosome segregation. In fact, there is a dramatic change in the dynamics as the microtubules of the K-fibers constantly depolymerize at the minus-ends and polymerize at the plus-ends, generating a poleward tubulin flux that will create tensions responsible for the fast shortening of the K-fibers in anaphase and further chromosome segregation (Mitchison et al., 1986; Sawin and Mitchison, 1991).

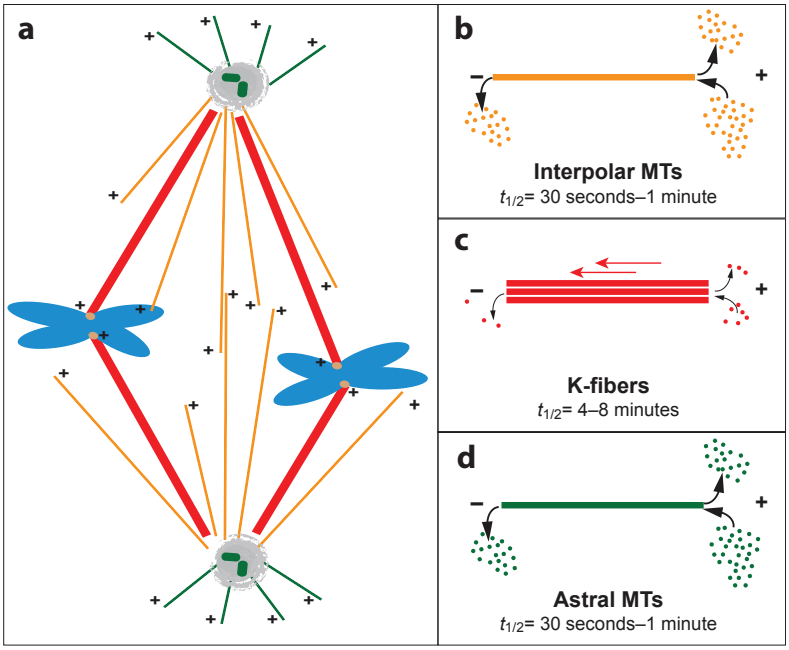

Figure 14: The three subclasses of spindle MTs.

a) Schematic drawing of a metaphase spindle, showing its three different MT subclasses: interpolar MTs (orange), K-fibers (red) and astral MTs (green). The '+' indicates the plus-ends of the MTs. **(b–d)** Representation of the three kinds of spindle MTs and their dynamic properties. Astral MTs have dynamic properties that are similar to those of the interpolar MTs (Mitchison et al., 1986). K- fibers are less dynamic and undergo a constant polewards tubulin flux (indicated by arrows). Adapted from (Meunier and Vernos, 2012).

VI- Microtubule dynamics in dividing cells

When a cell enters into mitosis the interphase microtubule network disassembles as a consequence of a radical change in microtubule dynamics. In interphase, microtubules

are relatively long and stable as they undergo few catastrophes. When the cell enters into mitosis, microtubule dynamics increases exponentially. The increase of catastrophe over rescue events leads to the formation of short and unstable microtubules (Verde et al., 1992). These rapid changes in microtubule dynamics are regulated by the activity of different MAPs (reviewed in (Akhmanova and Steinmetz, 2015)). Microtubule dynamics is defined by a balance of activities exerted by different MAPs that are regulated through different mechanisms, including post-translational modifications (PTMs). A beautiful example of the control of microtubule dynamics was shown *in vitro* using *Xenopus* egg extracts where xMAP215 antagonized the activity of xKCM1, indicating a balance of activities between a stabilizing protein, xMAP215, and a destabilizing factor, xKCM1 (Tournebize et al., 2000).

MAPs are post-translationally regulated by phosphorylation and other PTMs that can affect their affinity for microtubules, cellular localization or overall function. Many kinases are involved in this regulation as for example AurA and Plk1 that phosphorylate MAP9 controlling its localization to the spindle and its function in spindle assembly and mitosis progression (Ramkumar et al., 2018). Another example are MARK kinases that phosphorylate Tau, MAP2 and MAP4 on their microtubule binding domain, causing their dissociation from microtubules and increased microtubule dynamics (Drewes et al., 1997).

Some MAPs bind to the whole microtubule lattice while others are specific for the plus or the minus ends. A general classification of the MAPs includes two main categories: MAPs whose effect promotes microtubule depolymerization or severing and MAPs that promote microtubule polymerization.

MT depolymerization is mainly promoted by few members of the kinesin protein family.

Kinesins are a superfamily of microtubule associated ATPases characterized by the presence of a highly conserved catalytic or “motor” head domain containing microtubule and ATP-binding sites (reviewed in (Goldstein and Philp, 1999)). Most kinesins are processive motors, generating force and movement along microtubules but there are some kinesins that work as microtubule depolymerases, as for example the kinesin-13 family members, which were the first described as nonmotile kinesins with microtubule depolymerase activity (Desai et al., 1999). The member of the kinesin-13 family MCAK

(standing for "mitotic centromere-associated kinesin"), binds and acts at both ends of the microtubules using the energy from ATP hydrolysis to remove the tubulin dimers from the microtubule ends. When this type of kinesin depolymerases act on the microtubule structure, they reduce the length of the microtubule plus-end GTP-cap triggering catastrophe and therefore microtubule instability (Asenjo et al., 2013; Desai et al., 1999; Hunter et al., 2003). Kinesin-8 family members, as for example Kip3, act as depolymerases but with a plus-end specificity (Varga et al., 2006, 2009). A different class of plus-end associated proteins are the EB (End Binding) proteins that *in vitro* promote microtubule catastrophe while *in vivo* they favor microtubule elongation maybe by competing with other depolymerases (reviewed in (Akhmanova and Steinmetz, 2015)). In addition to depolymerase activities, another class of proteins acts promoting microtubule destabilization. Examples of this class of proteins are katanin, fidgetin and spastin, also known as microtubule severing enzymes. These enzymes cut the microtubule lattice or remove tubulin subunits directly from the end, thus generating unprotected microtubule tips that can behave differently depending on the cellular components that associate with the microtubule ends: they can become stabilized, grow or shrink in absence of stabilizing proteins (Sharp and Ross, 2012).

Microtubule polymerization can also be catalyzed by the protein XMAP215 (ch-TOG in humans). XMAP215 was initially identified in *Xenopus laevis* (Gard and Kirschner, 1987) but it was not till much later when its mechanism of action was revealed. XMAP215 acts as a processive polymerase, associating with the microtubules plus-ends and catalyzing multiple rounds of tubulin dimers addition (Brouhard et al., 2008).

There are other MAPs that promote microtubule polymerization by stabilizing microtubules. These microtubule stabilizing factors may play different roles as for example preventing the activity of microtubule depolymerizing factors or promoting microtubule rescue events. Regarding to the latter category, CLIPs (Cytoplasmic Linker Proteins) and CLASPs (Cytoplasmic Linker Associated Proteins) are examples of proteins that promote microtubule rescue. CLIP proteins regulate microtubule dynamics by increasing rescue events *in vivo* (Komarova et al., 2002) while *in vitro* studies with purified CLASP proteins have shown that these proteins can promote microtubule rescue and suppress catastrophe by recruiting tubulin dimers to the microtubule lattice (Al-Bassam et al., 2010). On the other hand, some microtubule stabilizing factors exert their

function by competing with microtubule depolymerizers. In this regard we can find many examples of this kind of proteins that act specifically at the minus ends of the microtubules.

Microtubule dynamics at the minus ends

The regulation of the plus-ends of the microtubules has been extensively studied while not so much is known about the dynamics at the minus-ends. Microtubule nucleation occurs at the minus-ends which are protected by the capping activity of the γ-TuRC. The γ-TuRC is not only acting as the main microtubule nucleator in the cell but it has a different role in regulating the microtubule dynamics at the minus-ends by blocking both its growth and shrinkage; the minus-end capping by the γ-TuRC is then important for microtubule stability (Anders and Sawin, 2011; Wiese and Zheng, 2000).

On the other hand, there are microtubules without a γ-TuRC, probably due to the activity of severing enzymes. The minus-ends of these microtubules are highly dynamic and this dynamicity is regulated by different factors; several proteins can stabilize the minus-ends but in mitosis the only protein that exerts this function is MCRS1. MCRS1 was identified as minus-end specific protein that associates with non-centrosomal microtubules and, more specifically, to a particular type of microtubules known as K-fibers. The role of MCRS1 is to protect the minus-ends from MCAK depolymerization (Meunier and Vernos, 2011). Few years later, new data about MCRS1 function during mitosis were revealed. In fact, MCRS1 was shown to be a novel substrate of the kinase Aurora A and its phosphorylation at specific residues was crucial to control K-fiber dynamics at their minus-ends (Meunier et al., 2016). The latter publication was the result of the two first years of my PhD work together with the post-doc Sylvain Meunier and I am attaching the manuscript in the annex I of this thesis. Further studies demonstrated that MCRS1 was interacting with a big complex composed of seven subunits known as the KNSL (KAT8-associated nonspecific lethal) complex, which is an important chromatin modifier in higher animals. It was shown that the members of the complex KANSL1 and KANSL3 together with MCRS1 constituted a mitosis-specific microtubule minus-end-associated complex essential for chromosomal microtubule assembly and correct K-fiber dynamics (Meunier et al., 2015).

Another example of microtubules minus-ends protecting factors is the CAMSAP (calmodulin-regulated spectrin-associated protein) protein family. Members of this family bind and stabilize microtubules minus-ends. Different studies have shown that CAMSAPs proteins can counteract the depolymerase activity of MCAK and stabilize free growing minus-ends of preexisting microtubules (Hendershott and Vale, 2014; Jiang et al., 2014).

VII- Microtubule organization

During mitosis microtubules need to reorganize in order to assemble a bipolar spindle, which is a dynamic molecular machine that allows the segregation of chromosomes between the two daughter cells. There are two families of proteins that play essential roles in microtubule organization: kinesins and dyneins. Proteins belonging to both families are molecular motors that interact with the microtubules using the energy derived from ATP hydrolysis to walk along the microtubule lattice.

Dyneis can be classified in axonemal dynein, which was first identified in cilia (Gibbons and Rowe, 1965) and cytoplasmic dynein, characterized in *Clamydomonas* axonemes (Vallee et al., 1988). Dyneins are MDa complexes that walk along the microtubules in minus-end direction. During mitosis, Dynein localizes to different structures performing a wide variety of functions. Dynein interacts with several proteins that are crucial for adapting the motor to is cellular function; these proteins are known as adaptors. Dynein has been shown to be important in spindle positioning and orientation, spindle pole focusing and organization and chromosome movement, between others (reviewed in (Kardon and Vale, 2009)).

The second family of molecular motors is composed of kinesin proteins. Kinesin superfamily proteins are molecular motors that transport cargos in a bidirectional way along microtubules. The first kinesin was identified from squid giant axons (Vale et al., 1985) and was shown to move along microtubules towards their plus end. Today we know that kinesin superfamily is composed of 15 families and 45 members have been identified in human (Hirokawa et al., 2009). Over the years there has been a bit of inconsistency or confusion regarding kinesins classifications; there are several ways of classifying the kinesins families, for example sorting them according to their sequence similarities and

functions (Lawrence et al., 2004). All kinesins are highly similar in their motor domain, but three main subgroups can be defined depending on the location of their motor domain. N-kinesins have the motor domain at their N-terminus and walk towards the microtubule plus-end (kinesins-1 to 12). C-kinesins have the motor domain at their C-terminus and are generally minus-end directed (kinesin-14). M-kinesins have instead a central motor domain and they are particular kinesins that depolymerize microtubules (kinesin-8 and kinesin-13 families). During mitosis, kinesins are involved in many important processes as for example: centrosome separation and spindle bipolarization, spindle pole focusing, chromosome capture and congression, chromosome segregation and microtubule dynamics regulation (reviewed in (Vicente and Wordeman, 2015)).

Apart from its role in microtubule organization, kinesins and dyneins are also important for the transport of cellular cargoes (vesicles, complexes, organelles, mRNA granules) along the microtubules towards a specific destination, an example of this would be the axonemal transport.

VIII- Mechanisms of spindle assembly

The mitotic spindle is a complex machinery that requires the contribution of different assembly mechanisms. In mitosis, microtubules are nucleated through three main microtubule assembly pathways: the centrosomal, the chromosomal and the Augmin-mediated microtubule assembly pathways.

VIII.A- The search and capture model

The discovery of microtubule dynamic instability (Mitchison and Kirschner, 1984) was a starting point for the authors to propose two years later the “search and capture” model for spindle assembly (Kirschner & Mitchison 1986). This model postulated that dynamic and unstable centrosomal microtubules grow and shrink exploring the cellular space until they are captured and stabilized when they do contact a kinetochore. Capture of microtubules by the kinetochores progressively connects chromosomes to the bipolar spindle.

As explained in section III, the centrosome is the primary MTOC in animal cells.

For a long time, centrosomes have been described to have a dominant role in spindle asembly. However, the formation of mitotic spindles in systems lacking centrosomes as plants was reported earlier in the 80's by using the immuno-gold staining method (Mey et al., 1982). Another example of acentrosomal cell divisions are animal oocytes and early embryos of some species (reviewed in (Manandhar et al., 2005)). Later on, different groups performed experimental ablation of centrosomes as well as disruption of centrosome function and showed that mitotic spindles could still form (Khodjakov et al., 2000b; Mahoney et al., 2006; Megraw et al., 1999, 2001). Moreover, using *Drosophila melanogaster* as a model organism, it was shown that an entire organism can form without centrosomes (Basto et al., 2006). Additional lines of evidence pointed out that cells may use other mechanisms for spindle assembly. For example, a computer simulation predicted that in human cells the "search and capture" model would require many hours to attach all the microtubules to the kinetochores instead of the 20 minutes duration in physiological conditions (Wollman et al., 2005). In addition, K-fibers formation in animal cells without centrosomes and K-fibers growth without direct connection to centrosomes in animal cells was reported (Khodjakov et al., 2003, 2000b; Maiato et al., 2004). Finally, a Ran-GTP dependent microtubule nucleation pathway essential for spindle assembly was identified and characterized (Carazo-Salas et al., 1999, 2001; Kalab et al., 1999; Nachury et al., 2001; Ohba et al., 1999; Wilde and Zheng, 1999; Zhang et al., 1999).

Altogether, the previous data supported the idea that spindle assembly and mitosis can occur in the absence of centrosomes, suggesting the existence of additional acentrosomal sources of microtubules having a role in spindle formation and chromosome segregation.

VIII.B- The Ran-GTP pathway

The first evidence of a chromatin dependent pathway for spindle assembly was observed by Karsenti and colleagues when they injected lambda DNA into metaphase arrested *Xenopus laevis* eggs and they saw that the plasmid DNA was sufficient to drive microtubule assembly (Karsenti et al. 1984b). Some years later it was shown that beads coated with plasmid-DNA could promote spindle assembly in *Xenopus laevis* egg extracts (Heald et al., 1996). But only 15 years later from the initial observations, the molecular mechanism of Ran-GTP mediated microtubule nucleation from chromatin was

discovered by five independent studies (Carazo-Salas et al., 1999; Kalab et al., 1999; Ohba et al., 1999; Wilde and Zheng, 1999; Zhang et al., 1999). Before describing how the Ran-GTP pathway promotes microtubule assembly around the chromosomes, I will briefly explain the nucleo-cytoplasmatic transport driven by Ran-GTPase.

VIII.B1- The nucleo-cytoplasmatic transport

Ran is a small GTPase member of the Ras-GTPase superfamily (Drivas et al., 1990) that drives nucleo-cytoplasmic transport trough the nuclear pore complex (NPC) (Melchior et al., 1993; Moore and Blobel, 1993). This transport is rapid for small cargos (<40kDa) while bigger proteins or macromolecules diffuse inefficiently through the NPC and need the help of the receptors named β-karyopherins. β-karyopherins consist of importins, if they import cargos into the nucleus, and exportins, if they export cargos outside the nucleus. The interaction between β-karyopherins and cargo proteins is regulated by Ran (Gorlich et al., 1996). Ran binds to β-karyopherins when it is in the GTP state (Ran-GTP) and dissociates when it is in the GDP state (Ran-GDP). The cycle of Ran-GTP/Ran-GDP within the cell depends on the presence of several proteins such as the Ran guanosine-exchange factor (GEF) RCC1 (Bischoff and Ponstingl, 1991a, 1991b, Ohtsubo et al., 1987, 1989; Renault et al., 2001), RanGAP1 (Ran-GTPase activating protein) (Becker et al., 1995; Bischoff et al., 1994; Seewald et al., 2002), RanBP1(Ran-binding protein-1) (Bischoff et al., 1995; Coutavas et al., 1993) and RanBP2 (Ran-binding protein-2) (Yokoyama et al., 1995). In interphase, RCC1 is bound to the chromatin favoring the accumulation of Ran-GTP in the nucleus while Ran-GAP1 and its co-activators RanBP1 and RanBP2 are in the cytoplasm, favoring the presence of Ran-GDP there. This different localization of GEFs and GAPs and the existence of the nuclear envelop (NE) promotes a gradient of Ran-GTP to Ran-GDP in which the GTP form is much more concentrated in the nucleus of the cell (Kaláb et al., 2006). During protein transport, β-karyopherins recognize the cargoes by specific amino acid sequences named nuclear localization signal (NLS) or nuclear export signal (NES). NLSs are sequences usually rich in basic amino acids such as lysines and arginines (Kalderon et al., 1984; Lanford et al., 1986; Robbins et al., 1991), while NES are rich in hydrophobic residues such as leucines (Fischer et al., 1995; Wen et al., 1995). Both exportins and importins bind to Ran-GTP. In the nucleus, Ran-GTP interacts with exportins stabilizing its binding to the cargo. A Ran-GTP-

exportin-cargo(NES) complex is formed and translocated to the cytoplasm through the NPC. Once in the cytoplasm, the GTP hydrolysis mediated by RanGAP1, promotes the dissociation of the complex and the release of the NES-containing cargo. The small protein Ntf2 (Nuclear transport factor 2) helps Ran-GDP to enter back into the nucleus where the Ran guanosin-exchange factor RCC1 exchange the GDP to GTP. Conversely, an importin-cargo(NLS) complex is formed in the cytoplasm. After translocation to the nucleus, the import complex is dissociated by Ran-GTP, which binds to importins and releases the NLS-containing cargo. By keeping high concentrations of Ran-GTP in the nucleus and of Ran-GDP in the cytoplasm, the cell controls the directionality of the transport through the NPC (reviewed in (Clarke and Zhang, 2008a)) (Figure 15).

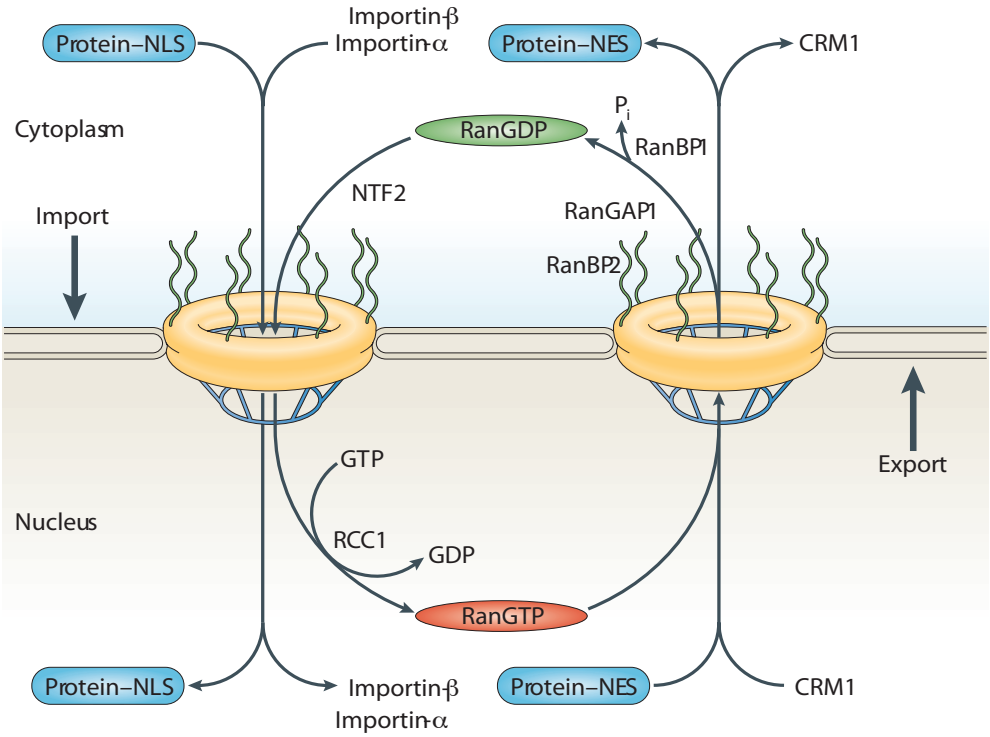

Figure 15: Ran directs nucleocytoplasmic transport.

Ran shuttles across the nuclear envelope through nuclear pores, but is concentrated in the nucleus because of nuclear transport factor-2 (NTF2)-mediated active import. In the nucleus, a high concentration of Ran-GTP is generated by nucleotide exchange. This is catalyzed by chromatin-bound RCC1. Ran-GTP causes the dissociation of imported complexes, which contain proteins that carry a nuclear localization signal (NLS), by binding to importin-β and ejecting the cargo. Conversely, binding of Ran-GTP to chromosome-region maintenance protein-1 (CRM1) promotes the assembly of export complexes containing proteins with a nuclear export signal (NES). In the cytoplasm, Ran-GTP meets Ran-GAP1 and RanBP1 or Ran-BP2, which stimulates GTP hydrolysis and the export complexes dissociate. The importins and exportins are recycled by transport back across the pore (not shown). In addition to this basic mechanism, other members of the importin family mediate the transport of specific cargoes. From (Clarke and Zhang, 2008b).

VIII.B2- The Ran-GTP dependent microtubule assembly pathway

During mitosis, cells take advantage of this complex transport mechanism in order to assemble bipolar spindles.

The role of Ran-GTP in microtubule assembly was first studied in *Xenopus* egg extracts. Using this system, several groups showed that a Ran-GTP gradient triggered around the chromosomes by its exchange factor RCC1 was essential for spindle formation, centrosomal microtubule stabilization and the assembly of chromosomal microtubules (Carazo-Salas et al., 1999; Kalab et al., 1999; Ohba et al., 1999; Wilde and Zheng, 1999; Zhang et al., 1999). Some years later, the Ran-GTP gradient was visualized (Kalab et al., 2002) and modelled in order to determine its properties in microtubule nucleation and

stabilization around chromosomes (Caudron et al., 2005). The existence of a Ran-GTP gradient essential for spindle assembly was shown as well in somatic cells (Gruss et al., 2002; Guarguaglini et al., 2000; Kaláb et al., 2006; Khodjakov et al., 2000b; Nachury et al., 2001). Many proteins identified as downstream effectors of this Ran-GTP gradient were identified and classified as spindle assembly factors (SAFs) due to their role in microtubule assembly. The first characterized SAF was TPX2 (Gruss et al., 2001). Although TPX2 was initially found to be involved in the targeting of the kinesin XKLP2 (*Xenopus* Kinesin like protein 2) to the spindle poles, the mechanism behind this targeting is still not known (reviewed in (Vanneste et al., 2011)). However, TPX2 has been extensively studied over the last decade and many of its important functions for spindle assembly have been characterized. First, TPX2 has been shown to be essential for chromatin-dependent microtubule nucleation because it promotes two necessary events: the activation of AurA and NEDD1 phosphorylation and a scaffolding activity needed for the recruitment of the MT nucleation complex (Scrofani et al., 2015). The mechanism of action of TPX2 during Ran-GTP dependent chromosomal microtubule nucleation involves the release of TPX2 from its inhibitory binding to importins around the chromosomes (Meunier and Vernos, 2012) (Figure 16). Once released, TPX2 interacts with RHAMM (hyaluronan-mediated motility receptor/HMMR), NEDD1 and γ-TuRC to promote MT nucleation around the chromosomes (Scrofani et al., 2015).

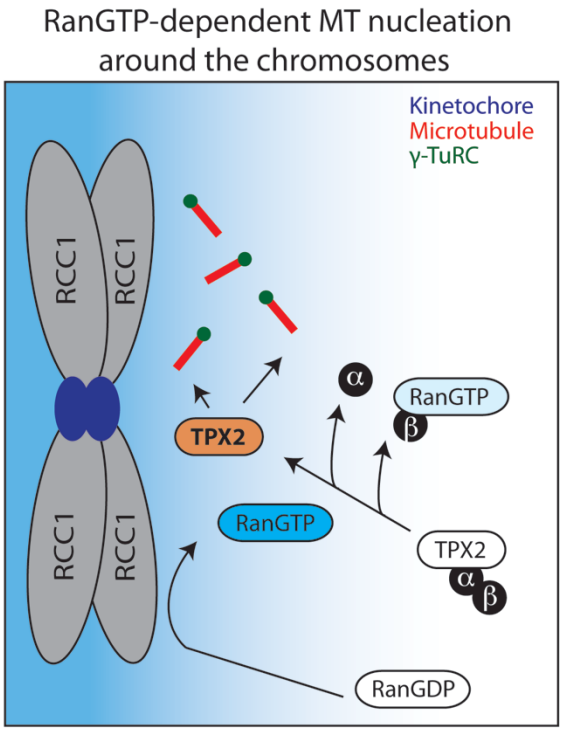

Figure 16: Model of a Ran-GTP dependent microtubule assembly pathway.

RCC1, bound to chromosomes, induces a local high concentration of Ran-GTP around chromatin. The Ran-GTP gradient (blue) promotes the local dissociation of spindle assembly factors, such as TPX2, from their inhibitory binding to importins (black). This promotes the local nucleation of acentrosomal MTs around chromosomes, in a process that is dependent on TPX2 and γ-TuRC. From (Meunier and Vernos, 2016).

Second, TPX2 (activated by AurA) was also shown to be important for centrosome maturation and microtubule assembly (Eckerdt et al., 2009; Sardon et al., 2008). Third, a role of TPX2 in regulating the localization and activity of the Kinesin-5 motor Eg5 was also described (Gable et al., 2012; Ma et al., 2011).

Apart from TPX2, many other SAFs have been characterized. Some of them have functions in microtubule dynamics (i.e MCRS1), in microtubule organization (i.e kinesin-14) or microtubule focusing (i.e NuMA). In the next table I summarize some of the SAFs identified to date (Table I).

Table I: RanGTP regulated factors in mitosis.
*Only amphibians have Lamin B3. Adapted from (Cavazza and Vernos, 2016).

Table I	Protein name	Mitotic function	Mitotic localization
Chromatin remodeling	CHD4	Stabilizes MTs	MTs and DNA
	ISWI1	Stabilizes MTs, mostly in anaphase	Centrosomes, Spindle poles and DNA
	MCRS1	Protects MT-end, favors Chromatin MT assembly and K-fiber formation	Spindle poles, K-fibers-ends
Kinesins	Kif14-NabKin	+end directed motor, important for chromosome congression and cytokinesis	MTs
	Kid (Kif22)	+end directed chromokinesin, important for for chromosome arm congression	MTs and Chromatin
	HSET/XCTK2/KIFC1	-end directed kinesin, important for pole focusing	MTs
	Kif2a	MT depolymerizing kinesin. Important for spindle length, pole coalescence, and chromosome congression	MTs
Nuclear Pore Complex	Mel28/ELYS	Ran Dependent MT nucleation, interacts with γ-Tubulin	Spindle poles, kinetochores
	Nup107-160 complex	Ran Dependent MT nucleation, interacts with γ-Tubulin, CPC localization	Spindle poles, kinetochores
	Nup98	Inhibits MCAK activity	Not described
	Rae1	Spindle organization; counteracts NuMA function	Spindle poles
	Laminin B3*	Spindle organization, supposedly through the spindle matrix	MTs
Others	TPX2	MT nucleation, MT bundling, AurA activation	MTs
	NuMA	Spindle pole formation and Spindle positioning	MTs
	NuSAP	Important for MT stabilization and crosslinking, favors MT assembly in proximity of chromatin	MTs and chromatin
	HURP	Stabilizes and bundles MTs, specially K-fibers	K-fibers
	TACC3	MT elongation and K-fiber formation	Spindle poles and MTs
	CDK11	Centrosome maturation and MT stability	Spindle poles/centrosomes
	APC	Bundles MTs	MTs and kinetochores
	Anillin	Cytokinesis, membranes elongation in anaphase	Cell cortex

VIII.C- Augmin-dependent microtubule amplification pathway

Recently, an additional mechanism for acentrosomal MT assembly in mitosis was identified. This pathway depends on the octameric Augmin complex (termed HAUS in mammalian systems) (Table II).

Associated Human Gene Name	*Drosophila* Augmin Gene name	Human Augmin Gene Name
CCDC5		HAUS1
CEP27		HAUS2
C4ORF15	Dgt3	HAUS3
C14ORF94		HAUS4
KIAA0841	Dgt5	HAUS5
FAM29A	Dgt6	HAUS6
UCHL5IP		HAUS7
HICE1		HAUS8

Table II: Proposed nomenclature for HAUS and associated subunits.
HAUS for homologues to Augmin subunits 1 to 8. Current genes names and homologues detected in *Drosophila* Augmin are indicated. Adapted from (Lawo et al., 2009).

Augmin was first identified in a RNAi genome wide screen for mitotic assembly factors performed in *Drosophila melanogaster* (Goshima et al., 2007). The 8-subunit complex can be reconstituted *in vitro* (Hsia et al., 2014; Lawo et al., 2009; Uehara et al., 2009) and it is conserved in animal and plant cells (Goshima et al., 2008; Kimmy Ho et al., 2011; Wainman et al., 2009). The subunit FAM29A (family with sequence similarity 29, member A/ HAUS6), binds to γ-TuRC while the subunit HICE1(Hec1-interacting and centrosome-associated 1/HAUS8) directly binds to the lattice of a pre-existing MT (Tsai et al., 2011; Zhu et al., 2008). The nucleation of a new microtubule on the lattice of a pre-existing one generates a "branching" effect where the newly formed microtubules are either disposed parallel to the extant ones or in a low angle with respect of the "mother"

microtubule (≈20º to 40º according to different studies) (Chan et al., 2009; Kamasaki et al., 2013; Murata et al., 2005; Nakamura et al., 2010; Petry et al., 2013). The branched microtubules are transported with their minus ends leading along pre-existing microtubules towards the spindle poles (Lecland and Lüders, 2014). As the Augmin complex can presumably associate to any microtubule, it is plausible to think that this pathway could be active throughout the cell cycle. In mitosis it acts on both centrosomal and acentrosomal microtubules (Hayward et al., 2014; Lawo et al., 2009) (Figure 17) while in interphase it generates microtubules in the cortical microtubule array (Liu et al., 2014; Murata et al., 2005; Nakaoka et al., 2015; Sánchez-Huertas and Lüders, 2015). The Augmin-dependent branching effect contributes to the generation of a robust mitotic spindle by exponentially amplifying the number of microtubules in mitosis (Hayward et al., 2014; Petry et al., 2011; Uehara et al., 2009). Recently, Augmin has been shown to be crucial for microtubule organization in post-mitotic neurons, controlling axonal microtubule polarity (Sánchez-Huertas et al., 2016).

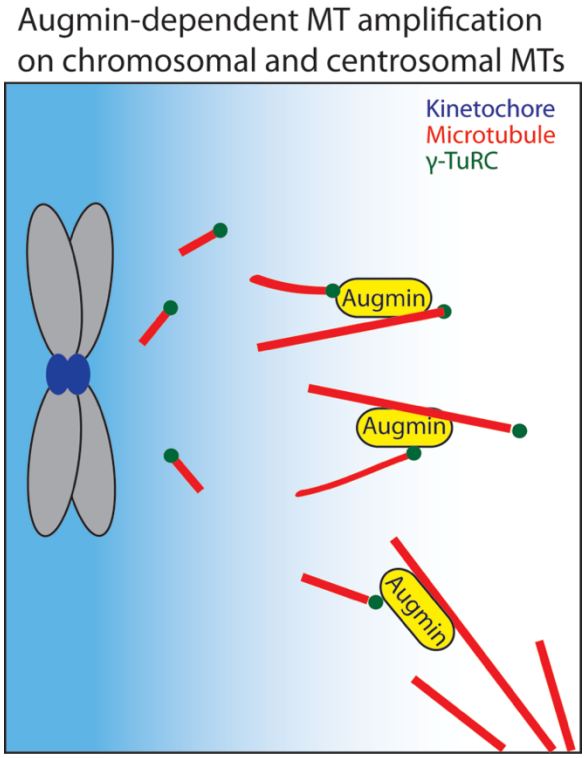

Figure 17: Model of an Augmin-dependent microtubule assembly pathway.
The augmin complex is recruited to MTs nucleated through the Ran-GTP pathway and to centrosomal MTs. Augmin promotes MT branching and amplification by a mechanism that may be potentiated by the Ran-GTP pathway. Adapted from (Meunier and Vernos, 2016).

The function of the Augmin pathway in mitotic cells has been explored in different systems (mammalian cells, *Drosophila* cells and *Xenopus* egg extracts) by several groups over the last decade. Augmin depletion in cells results in various mitotic defects as a reduction in the number of central spindle microtubules and in sister kinetochore tension, impairing metaphase progression (Goshima et al., 2008; Uehara et al., 2009). Augmin silencing also resulted in a phenotype of multipolar spindles probably caused by centrosome fragmentation (Lawo et al., 2009; Uehara et al., 2009).

Augmin depletion in *Xenopus* egg extracts resulted in a very similar phenotype to that of Augmin depleted cells, with a reduced rate of microtubule formation in a majority of multipolar spindles (Petry et al., 2011), although this phenotype was more severe in the absence of centrosomes. In addition, the coimmuprecipitation of Augmin with TPX2 (the main Ran-GTP effector) indicated a link between both Ran-GTP dependent and Augmin dependent microtubule assembly pathways. In fact, Augmin depletion significantly reduced the assembly of microtubules generated by the Ran-GTP pathway whereas addition of Ran-GTP increased the efficiency of the Augmin pathway in *Xenopus* egg extracts (Petry et al., 2011, 2013). This observation indicated that the Ran-GTP pathway is necessary for the activity of Augmin. However, spindles do assemble in absence of centrosomal and Augmin activity, indicating that the Ran-GTP pathway does not require the Augmin pathway, even if the Ran-GTP dependent microtubules are amplified by Augmin.

IX- NEDD1, γ-TuRC and regulation of microtubule nucleation in mitosis

During mitosis, there is a spatial and temporal regulation of microtubule nucleation: before NEBD, microtubules are nucleated at the two centrosomes. Then, after NEBD, nucleation occurs in the vicinity of the chromatin through the Ran-GTP pathway and microtubules are also nucleated on the lattice of pre-existing microtubules through the Augmin mediated amplification pathway.

A common element shared by the three pathways is the γ-TuRC and its adaptor protein NEDD1, essential for MT nucleation. As explained in section II, NEDD1 targets the γ-

TuRC to the different sites of microtubule nucleation in the cell, specifically regulating microtubule assembly by the different pathways. When the cell enters mitosis, NEDD1 becomes hyper phosphorylated. To date at least 42 NEDD1 residues have been described to be phosphorylated in mitosis by different kinases (Gomez-Ferreria et al., 2012a).

NEDD1-dependent targeting of the γ-TuRC is regulated by three NEDD1 specific phosphorylations that control the activity of each microtubule nucleation pathway in mitosis: the centrosomal, the chromosomal and the augmin pathways.

The phosphorylation of NEDD1 by the kinase Nek9 at S377 (downstream of Plk1) promotes the recruitment of NEDD1 and thus the γ-TuRC to the centrosomes in G2/prophase (Sdelci et al., 2012). Phosphorylation at S405 by the kinase AurA promotes microtubule nucleation around the chromatin in a Ran-GTP dependent manner (Pinyol et al., 2013). Phosphorylation of NEDD1 at the S411 by the kinase Cdk1 is required for the interaction of the γ-TuRC with the Augmin complex, mediating the microtubule amplification pathway (Johmura et al., 2011; Lüders et al., 2006; Uehara et al., 2009) (Figure 18).

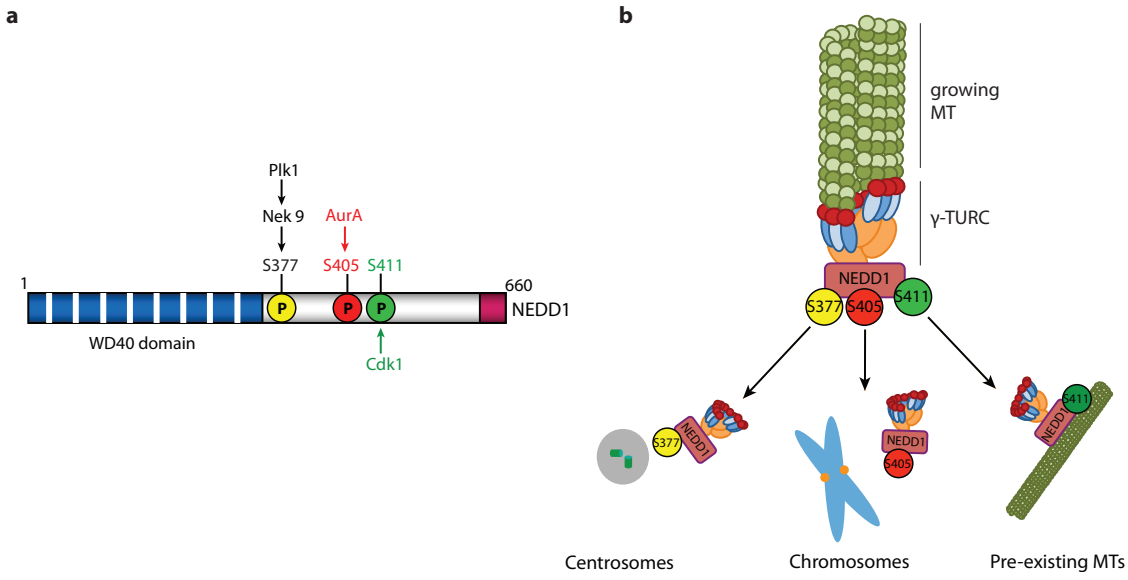

Figure 18: NEDD1-γ-TuRC targeting to specific microtubule nucleation sites.

a)NEDD1 structure showing the specific residues and kinases responsible for NEDD1-γ-TuRC targeting to the differerent microtubule nucleation sites. **b)** Schematic drawing of NEDD1-γ-TuRC targeting to centrosomes, chromosomes or pre-existing MTs depending on NEDD1 specific phosphorylation.

The consequences of interfering with each of the three different microtubule nucleation pathways by perturbing NEDD1 phosphorylation at each individual site have been explored in mitotic cells. First, expression of a phosphorylation-null mutant in which the S377 was substituted by an alanine: The S377A mutant, impaired NEDD1 and γ-tubulin recruitment to the mitotic centrosomes. Cell expressing this mutant showed an increase in the mitotic index as a result of a cell arrest in a prometaphase-like state, thereby interfering with spindle formation and mitotic progression (Sdelci et al., 2012). Expression of a S405A mutant allowed the formation of bipolar spindles with scattered or misaligned chromosomes and K-fibers that were less stable under depolymerization conditions (Pinyol et al., 2013). Finally, expression of a S411A mutant resulted in several defective spindle morphologies together with a high reduction of microtubule density in the central region of the spindle and an increase of the mitotic index (Johmura et al., 2011; Lüders et al., 2006).

Altogether, these data indicate an important role for each specific phosphorylation in regulating NEDD1 targeting and, thereby, microtubule nucleation at the three sites. However, the specific contribution of each of the pathways to the assembly of the mitotic spindle and how the three pathways are integrated to build a functional spindle is still unknown. During this thesis I aimed at investigating this question.

OBJECTIVES

The main objective of this thesis was to understand the respective contribution of each microtubule nucleation pathway in mitosis and how these pathways are integrated to support the formation of a functional bipolar spindle.

Specifically, the objectives were:

I. To set up a method to manipulate at will the three microtubule nucleation pathways during mitosis through the expression of specific phosphorylation variants of NEDD1, individually or in combination.

II. To obtain a full functional characterization of the consequences on spindle assembly of interfering with the microtubule nucleation pathways individually or in combination.

III. To define the temporal and spatial regulation of the NEDD1 phosphorylation events responsible for each of the three microtubule nucleation pathways.

RESULTS

The goal of my PhD project was to understand the specific contribution of the centrosomal, chromosomal and microtubule-based nucleation pathways in the assembly of the mitotic spindle. I focused on NEDD1 since its phosphorylation at S377, S405 and S411 has been shown to specifically regulate microtubule nucleation through each of the pathways individually.

As a first goal, we wanted to detect when and where the phosphorylation at each individual site occurs during mitosis. With this aim we attempted at generating phosphorylation specific antibodies for each of the three residues S377, S405 and S411 to follow the different phosphorylated NEDD1 residues in the cell. We injected synthetic peptides (15 amino acids maximum) with an attached phosphate group to S377, S405 and S411 into rabbits. Affinity purified antibodies were first tested by immunofluorescence. They generated a signal at the centrosomes but when we tested them by western blot none of them recognized specifically phosphorylated NEDD1. Therefore, we could not use them for studying the time and location of the different phosphorylated forms of NEDD1 (results not shown).

In parallel, we decided to establish a system that would allow me to manipulate the three microtubule nucleation pathways at will. The strategy that we followed was to generate siRNA resistant inducible Hela-FRT/TR cell lines expressing different variants of NEDD1 mutated at these specific residues.

I- Establishing an inducible system in tissue culture cells

The first goal of this project was to define the experimental conditions to fully rescue the NEDD1 silencing phenotype by expressing exogenous Flag-hNEDD1 WT in the siRNA resistant inducible cell line.

I followed an experimental approach that included different times of induction of the exogenous Flag-hNEDD1 WT at 0,1 µg/ml of tetracycline after silencing endogenous NEDD1 during 48h (Figure 19A, left).

At the 48h time point, I took samples to perform western blot analysis and immunofluorescence. I quantified the percentage of mitotic structures in fixed cells under both conditions (Figure 19A, right). The proportion of monopolar spindles is a good read

out of NEDD1 silencing efficiency. In control cells it was less than 5% whereas in NEDD1 silenced cells it was around 43%. In addition, NEDD1 silenced cells showed a low proportion of prometaphases (≈22%) and metaphases (≈23%). The remaining 12% of mitotic structures were multipolar, aberrant and tilted spindles. Expression of Flag-hNEDD1 WT protein in the silenced cells during 36h did decrease the number of monopolar structures to 17%, together with an increase in the number of prometaphases (≈37%) and metaphases (≈38%), suggesting a partial rescue. However, the proportion of monopolar structures was still higher than in control cells. Expression of Flag-hNEDD1 WT during 24h was less efficient than the previous condition. We concluded that the tested conditions were not good enough to analyze the phenotypes of NEDD1 mutants, and it was important to spend some time in finding good rescue conditions that would reduce the proportion of monopolar structures to that of control cells (less than 5%).

We focused on three main aspects to improve the rescue of NEDD1 silencing phenotype: first, the kinetics of expression of exogenous Flag-hNEDD1 WT (time of induction and tetracycline concentration). Second, the optimization of NEDD1 silencing (time post siRNA transfection) and third, the potential effects of overexpressing Flag-hNEDD1 WT.

The first test was to investigate whether it would be better to control the expression of the exogenous protein with a pulse of tetracycline induction to avoid the accumulation of the exogenous Flag-hNEDD1 WT. To test this, I performed a pulse of tetracycline induction (14h and 24h) at a concentration of 0,1µg/ml, followed by a wash to try to adjust the total levels of NEDD1 (endogenous versus exogenous) and rescue spindle assembly (Figure 19B, schemes on the left). The quantifications of the mitotic structures for the 14 and 24h pulse (Figure 19B, right) indicated that the 24h tetracycline pulse was the best condition but the rescue was still not good enough.

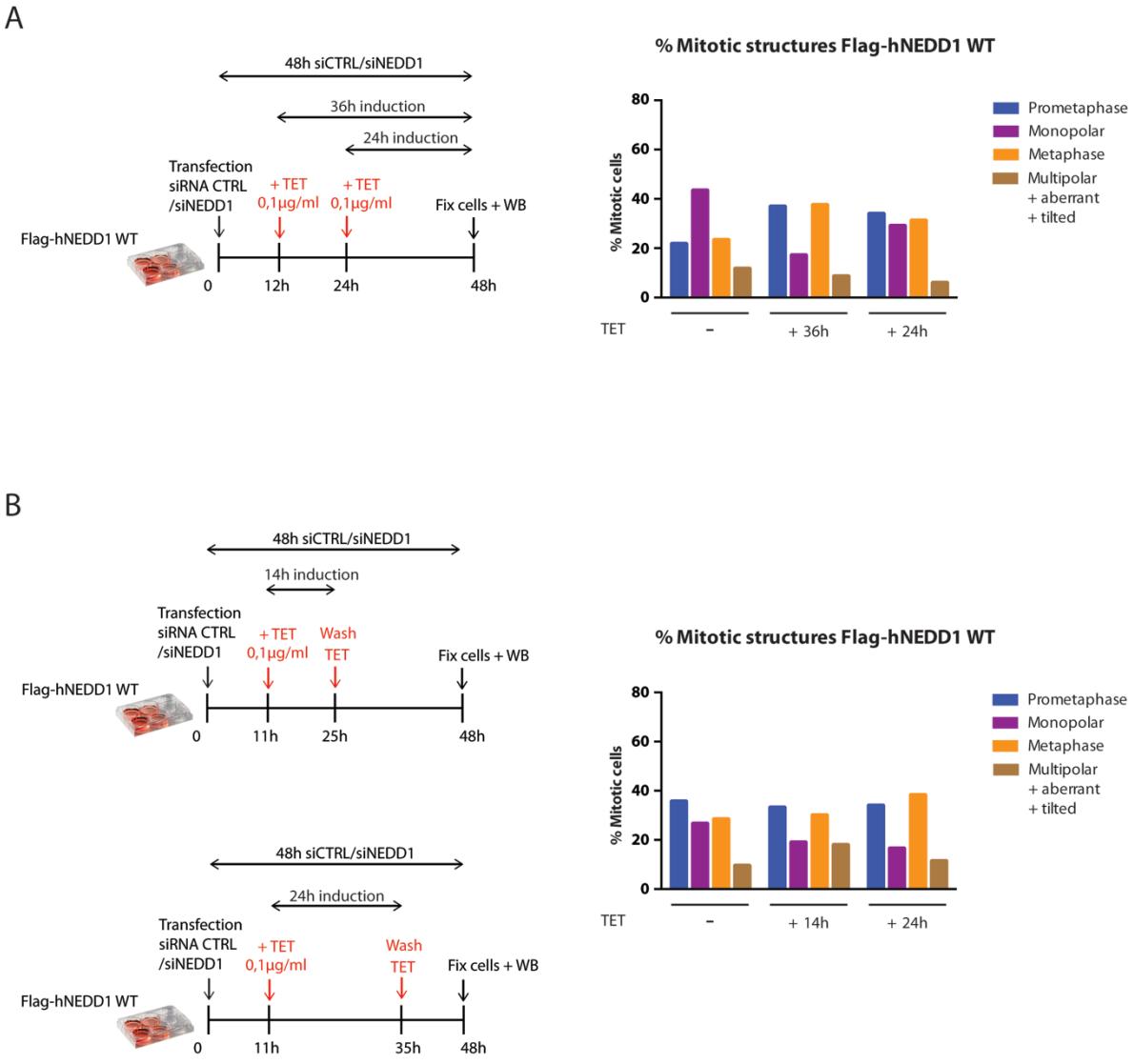

Figure 19: Rescue of NEDD1 silencing by inducible expression of Flag-hNEDD1-WT; testing different conditions of tetracycline induction.

Experimental protocol and quantification of the distribution of mitotic structures in NEDD1 silenced cells (for 48h) upon different tetracycline induction conditions (at 0,1 µg/ml).

A) Induction for 24h and 36h. **B)** Pulse of induction for 14h.

Next, we tested whether leaving more time after the tetracycline pulse would improve the rescue. I performed another experiment fixing the cells after different silencing times, keeping the 24h tetracycline pulse at 0,1 μg/ml (Figure 20A, left). The quantification shows that the longer the incubation time was, the lower the efficiency of rescue (Figure 20A, right). We reasoned that this could be due to the reduction of the exogenous protein levels over time (Figure 20B, left). Indeed, 37h after tetracycline wash out the cells had approximately 75% less Flag-hNEDD1 WT than after 13h (Figure 20B, right).

These results indicated that both overexpressing the exogenous protein (36h) and reducing the induction time with a tetracycline pulse (14 and 24h) at 0,1μg/ml were not good strategies to promote a full rescue. Therefore, we decided to characterize the kinetics of the endogenous protein depletion and exogenous protein expression by obtaining curves of these two parameters overtime.

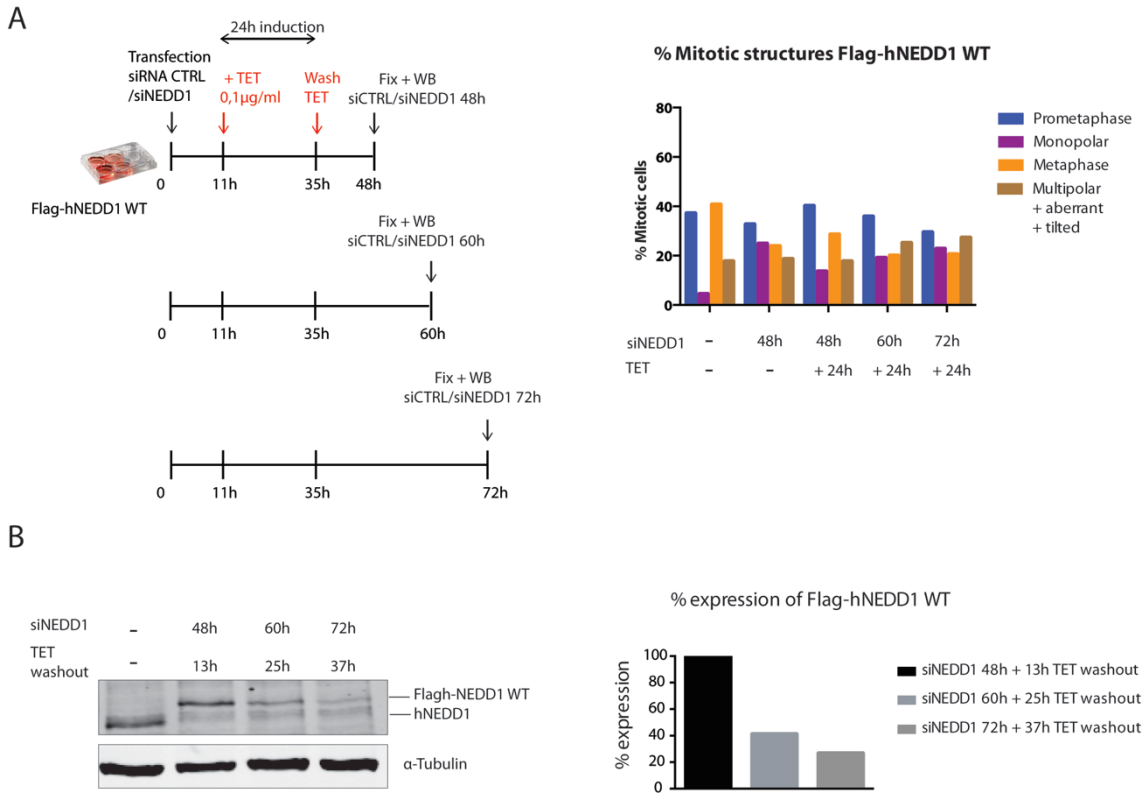

Figure 20: Rescue of NEDD1 silencing by inducible expression of Flag-hNEDD1-WT; testing different times of siRNA incubation with a 24h tetracycline pulse.

A) On the left, schematic representation of the experimental protocol followed. On the right the corresponding quantification of the mitotic phenotypes. **B)** On the left, western blot showing levels of endogenous and exogenous NEDD1 over different times of siRNA incubation and tetracycline washout. On the right, percentage of expression of exogenous NEDD1 after different times of tetracycline washout.

Ideally, as the endogenous protein decreases, the exogenous protein should increase to replace the function of the endogenous by keeping a constant level of active NEDD1, starting with 100% of endogenous NEDD1 and finishing with a majority of exogenous Flag-hNEDD1 WT. A schematic representation of this ideal silencing (black line) and expression curve (red line) is shown in Figure 21A. To establish how to obtain such an ideal situation, I first performed a tetracycline induction experiment, collecting samples after different times of induction and also at different concentrations of tetracycline (Figure 21B).

Figure 21C shows the expression levels of Flag-hNEDD1 WT after different times of induction and at different concentrations of tetracycline. For all the conditions tested, there was a peak of expression after 48h of induction that did not significantly change at

longer times. I then checked the levels of the endogenous protein with the anti NEDD1 antibody. The induction condition resulting in expression levels similar to the endogenous NEDD1 levels was 24h at 0,01 µg/ml of tetracycline. The rest of the time points at 0,01 µg/ml showed an overexpression of the exogenous Flag-hNEDD1 WT protein and this was also the case for the tetracycline induction at 0,05 µg/ml and 0,1 µg/ml (blot not shown).

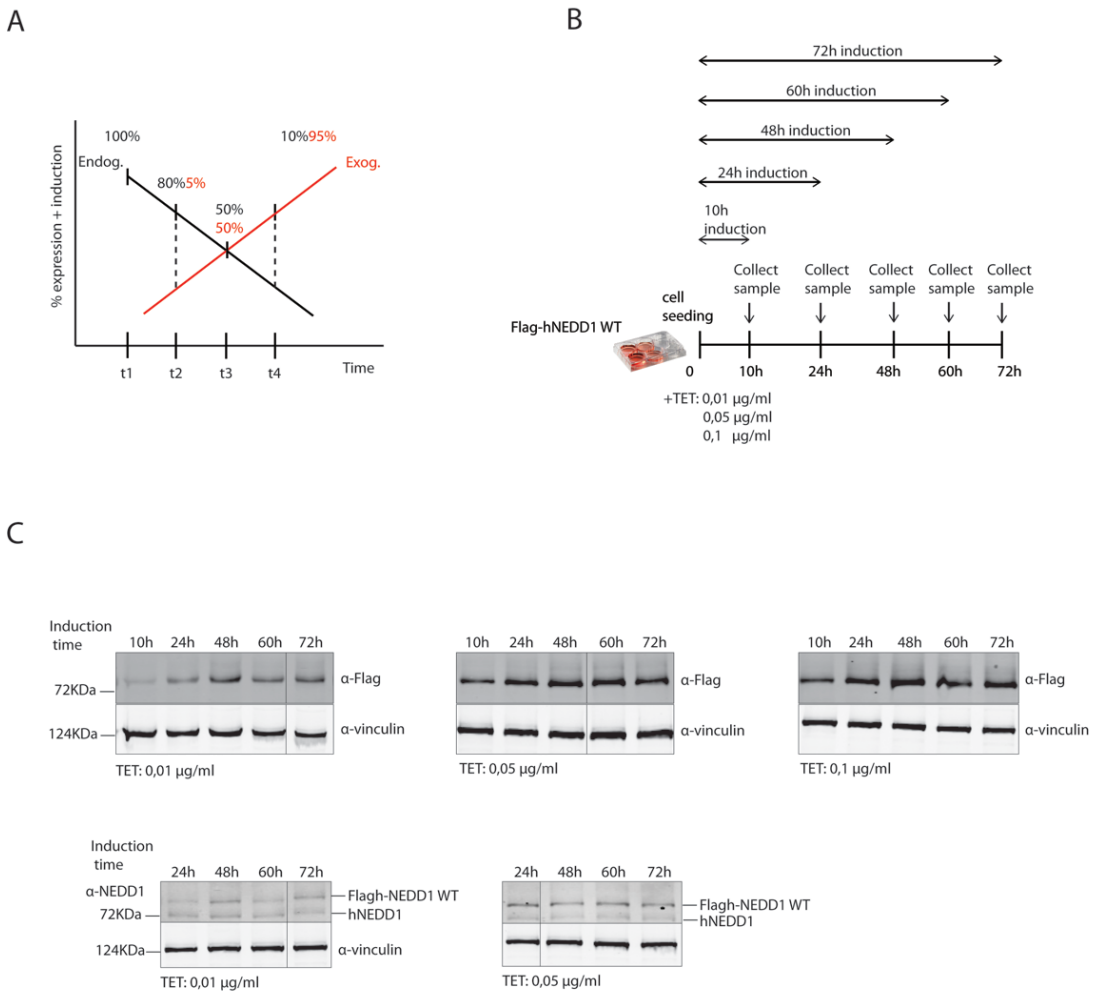

Figure 21: Kinetics of exogenous protein expression.

A) Schematic representation of the optimal balance of silencing and expression curves overtime in a putative rescue experiment. **B)** Schematic representation of the experimental protocol followed to obtain the kinetics of Flag-hNEDD1 WT expression. **C)** Western blots showing the levels of Flag-hNEDD1 WT expression upon different times and concentrations of tetracycline indicated in B).

We then aimed at optimizing NEDD1 silencing by checking the levels of the protein at different times after siRNA transfection. In parallel, I used the conditions previously selected (0,01 μg/ml) to check if I could rescue the NEDD1 silencing phenotype (Figure 22A). Figure 22B shows the efficiency of the silencing overtime together with the expression of the exogenous protein at different times. The silencing efficiency increased over time with minor changes after 54h while the expression of the exogenous protein reached a peak between 30-48h that was later maintained and slightly reduced over time, as expected. Then, I performed a quantification of the different mitotic structures in fixed cells to check the progression through mitosis (Figure 22C). I first looked at control cells expressing exogenous NEDD1 to determine if increasing the levels of NEDD1 had any effect on spindle assembly. Indeed, it has been previously described that overexpression of NEDD1 is detrimental for the cell (Haren et al., 2006; Kumar et al., 1994). Overexpression of Flag-hNEDD1 WT protein in control cells during 48 hours showed a small increase in the percentage of monopolar structures, a decrease in the number of metaphases, and also an increase in aberrant structures but the effect was mild. The highest expression levels (60 hours of tetracycline induction) resulted in a stronger detrimental effect with a decrease in the number of metaphases (≈15%) and an increase of around 13% in the proportion of aberrant structures compared with control cells. Overexpression of Flag-hNEDD1 WT in NEDD1 silenced cells did not rescue the high proportion of monopolar structures at any of the induction times tested (48 and 60h). From this experiment I concluded that the expression of exogenous Flag-hNEDD1 WT overtime at 0,01 μg/ml while silencing endogenous NEDD1 was not good enough to fully rescue the silencing phenotype.

A

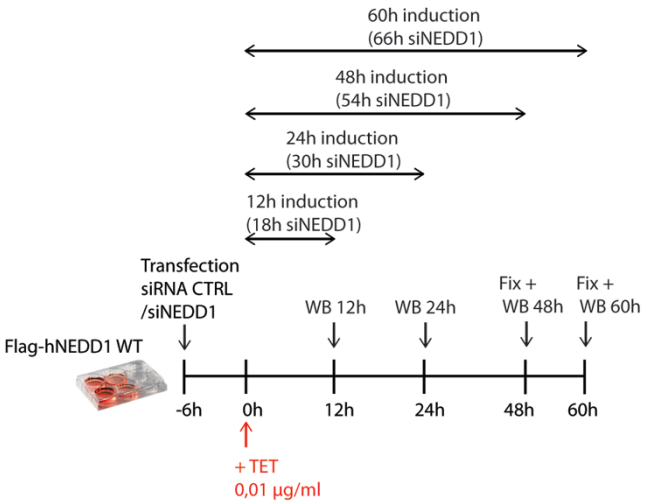
60h induction
(66h siNEDD1)
48h induction
(54h siNEDD1)
24h induction
(30h siNEDD1)
12h induction
(18h siNEDD1)
Transfection
siRNA CTRL
/siNEDD1
WB 12h
WB 24h
Fix +
WB 48h
Fix +
WB 60h
Flag-hNEDD1 WT
-6h
0h
12h
24h
48h
60h
+ TET
0,01 µg/ml

B

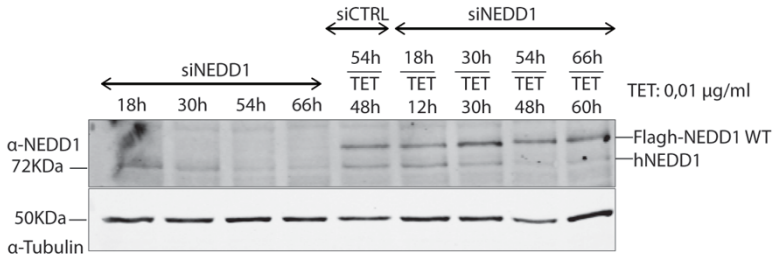
siCTRL
siNEDD1
siNEDD1
18h
30h
54h
66h
54h TET 48h
18h TET 12h
30h TET 30h
54h TET 48h
66h TET 60h
TET: 0,01 µg/ml
α-NEDD1
72KDa
Flagh-NEDD1 WT
hNEDD1
50KDa
α-Tubulin

C

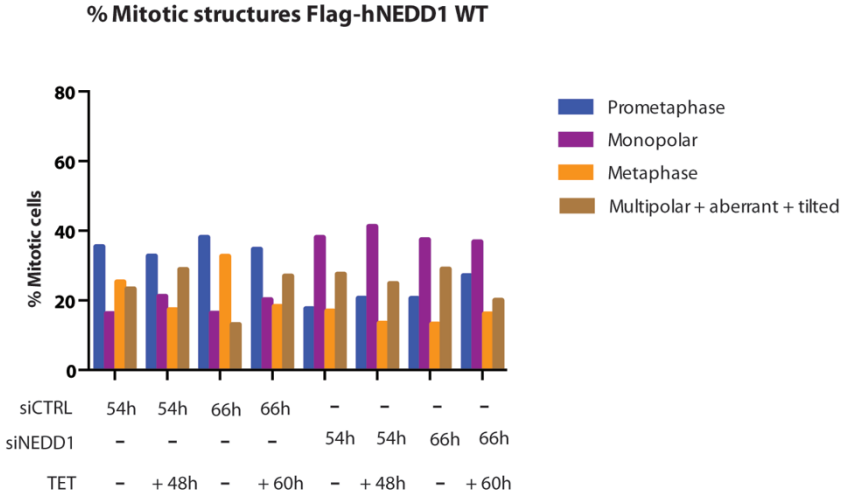
% Mitotic structures Flag-hNEDD1 WT
% Mitotic cells
80
60
40
20
0
Prometaphase
Monopolar
Metaphase
Multipolar + aberrant + tilted
siCTRL 54h 54h 66h 66h – – – –
siNEDD1 – – – – 54h 54h 66h 66h
TET – + 48h – + 60h – + 48h – + 60h

Figure 22: Kinetics of endogenous protein depletion at different times of tetracycline induction.
A) Schematic representation of the experimental protocol followed to obtain the kinetics of NEDD1 depletion after tetracycline induction. **B)** Western blot showing the levels of NEDD1 depletion over time in absence of tetracycline or after different times of tetracycline induction. **C)** Quantification of the mitotic phenotypes corresponding to the different conditions indicated in A).

Since the overexpression of exogenous protein at the chosen concentration did not seem to be deleterious for the cell, we tested whether increasing the levels of the exogenous protein could work in our rescue assays. The scheme from Figure 23A shows the protocol applied. Western blot analysis showed that the best silencing condition is after 55h of siRNA transfection with little variations when there was also induction of the exogenous protein (Figure 23B). I quantified the intensities of the bands corresponding to this blot and the graph shows that, indeed, the best level of NEDD1 silencing occurred after 55h post-transfection with siRNA, with around 80% of the endogenous protein being silenced (Figure 23C, top plot). I also calculated the ratio between endogenous and exogenous protein (Figure 23C, bottom plot) and, as expected, only the concentration of 0,01 µg/ml had a similar expression level to endogenous NEDD1. The other two conditions tested were 6-7 fold overexpressed.

The quantification of the mitotic structures (Figures 23D and 23E) also showed that silencing of NEDD1 during 55h had more detrimental consequences for the cell than 48h of silencing, with less prometaphases and metaphases and an increased proportion of aberrant structures. Unfortunately, none of the tested conditions was able to fully rescue the NEDD1 silencing phenotype still.

A

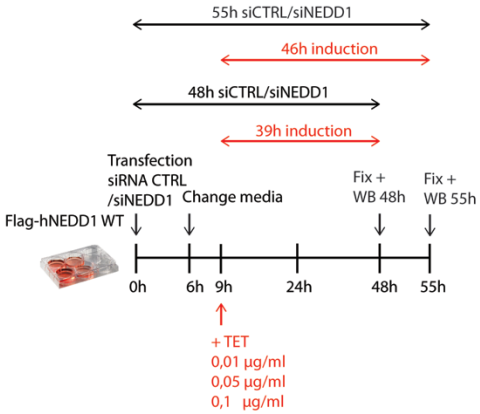
55h siCTRL/siNEDD1
46h induction
48h siCTRL/siNEDD1
39h induction
Transfection
siRNA CTRL
/siNEDD1
Change media
Fix +
WB 48h
Fix +
WB 55h
Flag-hNEDD1 WT
0h
6h
9h
24h
48h
55h
+ TET
0,01 µg/ml
0,05 µg/ml
0,1 µg/ml

B

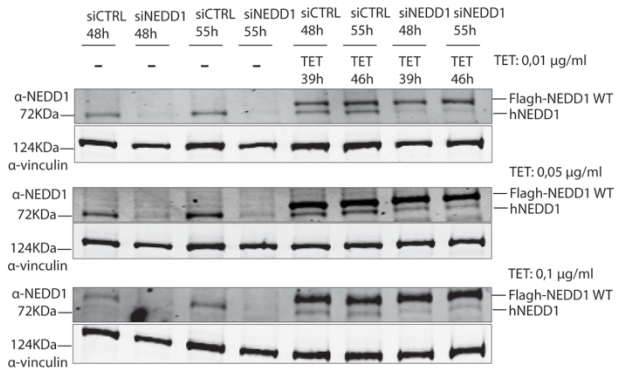
siCTRL 48h
siNEDD1 48h
siCTRL 55h
siNEDD1 55h
siCTRL 48h
siCTRL 55h
siNEDD1 48h
siNEDD1 55h
TET 39h
TET 46h
TET 39h
TET 46h
TET: 0,01 µg/ml
α-NEDD1 72KDa
Flagh-NEDD1 WT
hNEDD1
124KDa α-vinculin
TET: 0,05 µg/ml
TET: 0,1 µg/ml

C

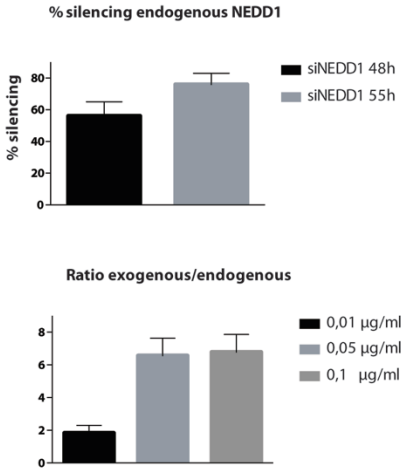
% silencing endogenous NEDD1
% silencing
siNEDD1 48h
siNEDD1 55h
Ratio exogenous/endogenous
0,01 µg/ml
0,05 µg/ml
0,1 µg/ml

D

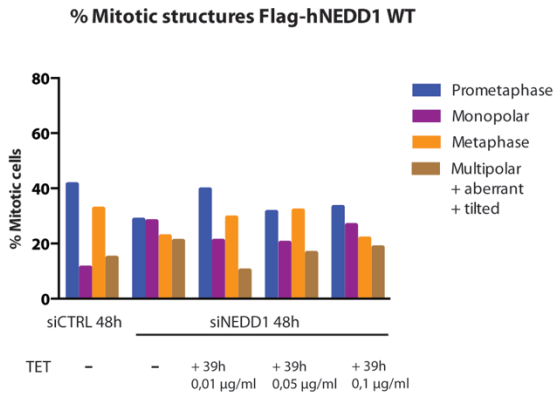
% Mitotic structures Flag-hNEDD1 WT
% Mitotic cells
Prometaphase
Monopolar
Metaphase
Multipolar
+ aberrant
+ tilted
siCTRL 48h
siNEDD1 48h
TET
+ 39h
0,01 µg/ml
+ 39h
0,05 µg/ml
+ 39h
0,1 µg/ml

E

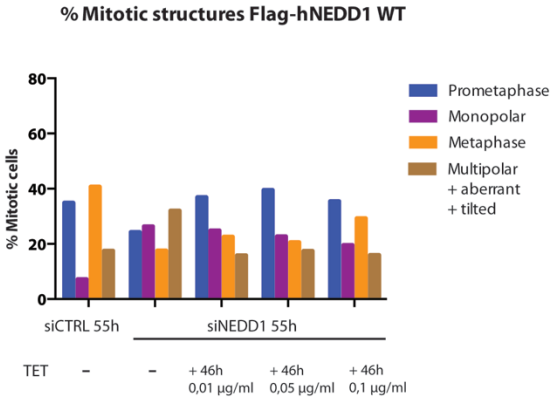
% Mitotic structures Flag-hNEDD1 WT
% Mitotic cells
Prometaphase
Monopolar
Metaphase
Multipolar
+ aberrant
+ tilted
siCTRL 55h
siNEDD1 55h
TET
+ 46h
0,01 µg/ml
+ 46h
0,05 µg/ml
+ 46h
0,1 µg/ml

Figure 23: Rescue of NEDD1 silencing by inducible expression of Flag-hNEDD1-WT; increasing the levels of exogenous Flag-hNEDD1 WT expression.

A) Schematic representation of the experimental protocol followed to determine the best condition for the rescue of NEDD1 silencing phenotype. **B)** Western blot showing endogenous and exogenous protein levels upon different times of silencing and tetracycline induction at several concentrations. **C)** Graphs showing the percentage of silencing of endogenous NEDD1 after different times of incubation with siRNA (top) and the ratio of exogenous/endogenous NEDD1 in the different concentrations of tetracycline used (bottom). **D)** and **E)** Quantification of the mitotic phenotypes corresponding to the different conditions indicated in A).

After trying many different conditions, we were disappointed because although we had optimized NEDD1 silencing in our cell line and we had perfectly established how to induce expression of exogenous Flag-hNEDD1 WT to keep appropriate endogenous levels, this was not enough to fully rescue the mitotic defects in NEDD1 silenced cells. However, we observed that overexpression of exogenous Flag-hNEDD1 WT was not deleterious.

Since the overexpression of exogenous protein by transient transfection (which drives very high levels of expression) had been shown to fully rescue NEDD1 silencing phenotypes (Pinyol et al., 2013), we then reasoned that reaching high levels of expression in our system could be the right approach to rescue spindle assembly in NEDD1 silenced cells. We therefore decided to change the strategy and induce expression of exogenous Flag-hNEDD1 WT before silencing the endogenous protein.

II- Inducible expression of Flag-hNEDD1 WT fully rescues mitotic progression in NEDD1 silenced cells

Based on our last hypothesis, I performed another trial inducing the expression of Flag-hNEDD1 WT protein the day before siRNA transfection and changing the media every 24h to keep the tetracycline concentration constant as shown in the scheme (Figure 24A).

Figure 24B shows the efficiency of NEDD1 silencing after 55h of transfection with siRNA, which was higher than 80% (quantification not shown). Upon induction with tetracycline an upper band corresponding to the exogenous Flag-hNEDD1 WT appeared. This band showed a slight overexpression of Flag-hNEDD1 WT compared with endogenous levels.

Next, I performed immunofluorescence in fixed cells to look at the localization of both endogenous NEDD1 and exogenous Flag-hNEDD1 WT (Figure 24C). In control cells NEDD1 signal strongly decorated the spindle poles and also the spindle microtubules. After silencing, NEDD1 signal was highly reduced and almost undetectable. In addition, tubulin intensity was reduced as expected since microtubule nucleation is impaired in the absence of NEDD1. Upon expression of Flag-hNEDD1 WT, the localization of NEDD1 to the poles and to the spindle microtubules was rescued. Staining with α-Flag antibodies confirmed the localization of the exogenous protein to the centrosomes and spindle microtubules, similarly to endogenous NEDD1.

Then, I quantified the mitotic structures as I previously did for the other conditions (Figure 24D). NEDD1 silenced cells presented the expected increase in the number of monopolar (≈20%) and aberrant structures (≈59%) while there was a reduction in the number of prometaphases (≈15%) and metaphases (≈6%) compared with control cells (≈46% and ≈32% respectively). Silenced cells expressing exogenous Flag-hNEDD1 WT had a highly reduced percentage of monopolar (≈8%) and aberrant structures (≈26%) and a percentage of prometaphases (≈41%) and metaphases (≈25%) that was comparable to control levels, suggesting almost a full rescue. It is important to mention that in control and silenced cells expressing Flag-hNEDD1 WT the multipolar structures are the majority of the figures found between the three categories classified as a single group (multipolar + aberrant + tilted) whereas in NEDD1 silenced cells the aberrant structures are the most representative figures within the group.

In parallel, I quantified the mitotic index in the three conditions tested: control cells transfected with scrambled siRNA (siCTRL), NEDD1 silenced cells and NEDD1 silenced cells expressing the exogenous Flag-hNEDD1 WT (Figure 24E). Control cells exhibited a mitotic index of less than 5%. After silencing of NEDD1, this mitotic index increased to levels around 15%, a percentage that was fully rescued with the expression of exogenous Flag-hNEDD1 WT.

In addition, I monitored Flag-hNEDD1 WT migration pattern in SDS-PAGE (Figure 24F). NEDD1 has been described to be hyper phosphorylated in mitosis at least on 42 residues (Gomez-Ferreria et al., 2012a). The objective of the experiment was to observe a migration shift between asynchronous and mitotic samples as it has been previously

shown (Haren et al., 2006, 2009; Lüders et al., 2006). To do this I prepared samples from asynchronous cultures and cultures that were synchronized in mitosis with nocodazole and later collected by mitotic shake-off. The blot shows a big shift between asynchronous and mitotic samples, where the upper band corresponds to the phosphorylated fraction of the protein. Phosphorylation (not ubiquitination, sumoylation or other modifications) was causing the migration shift because after treating the samples with lambda phosphatase, the upper band disappeared. Both endogenous and exogenous Flag-hNEDD1 WT showed the same migration pattern in mitosis. From this experiment I concluded that exogenously expressed Flag-hNEDD1 WT was phosphorylated as the endogenous NEDD1. Altogether, these results suggested that exogenous Flag-hNEDD1 WT protein was fully functional. We therefore used these optimized rescue conditions to explore the consequences of interfering with the phosphorylation state of NEDD1 by expressing the different NEDD1 phosphorylation variants.

Figure 24: Rescue of NEDD1 silencing by inducible expression of Flag-hNEDD1-WT; optimized protocol.

A) Schematic representation of the experimental approach followed to fully rescue NEDD1 silencing phenotype by expression of Flag-hNEDD1 WT. **B)** Western blot showing the silencing levels of endogenous NEDD1 and the expression levels of exogenous Flag-hNEDD1 WT in a typical rescue experiment. **C)** Representative immunofluorescence images showing the localization of endogenous and exogenous NEDD1 in mitotic cells. The first row of the panel shows the localization of NEDD1 in control cells. The second row of the panel shows the localization of NEDD1 in silenced cells. The third row of the panel shows the localization of NEDD1 in silenced cells expressing Flag-hNEDD1 WT and the last row of the panel shows the localization of exogenous Flag-hNEDD1 WT in silenced cells. Tubulin is shown in red, NEDD1 in green and DNA in blue. Scale bar 5μm. **D)** Quantification of the mitotic structures. Three replicas with ≈200 cells quantified per condition and experiment were performed. Columns represent the average percentage of cells in each category. Standard deviation between replicas is represented with a line on top of each column. **E)** Quantification of the mitotic index. >1000 cells per condition were counted. The plot shows the average of three independent experiments. Standard deviation between replicas is represented with a line on top of each column. Two-way ANOVA test: ns, non-significant differences. **** indicates p-value <0,0001. **F)** Western blot showing NEDD1 in asynchronous and mitotic cells collected by shake-off after an overnight nocodazole block at 0,33μM. Flag-hNEDD1 WT induced cells were incubated with tetracycline at 1μg/ml during 24h and λ-Phosphatase was added for 30 minutes when indicated.

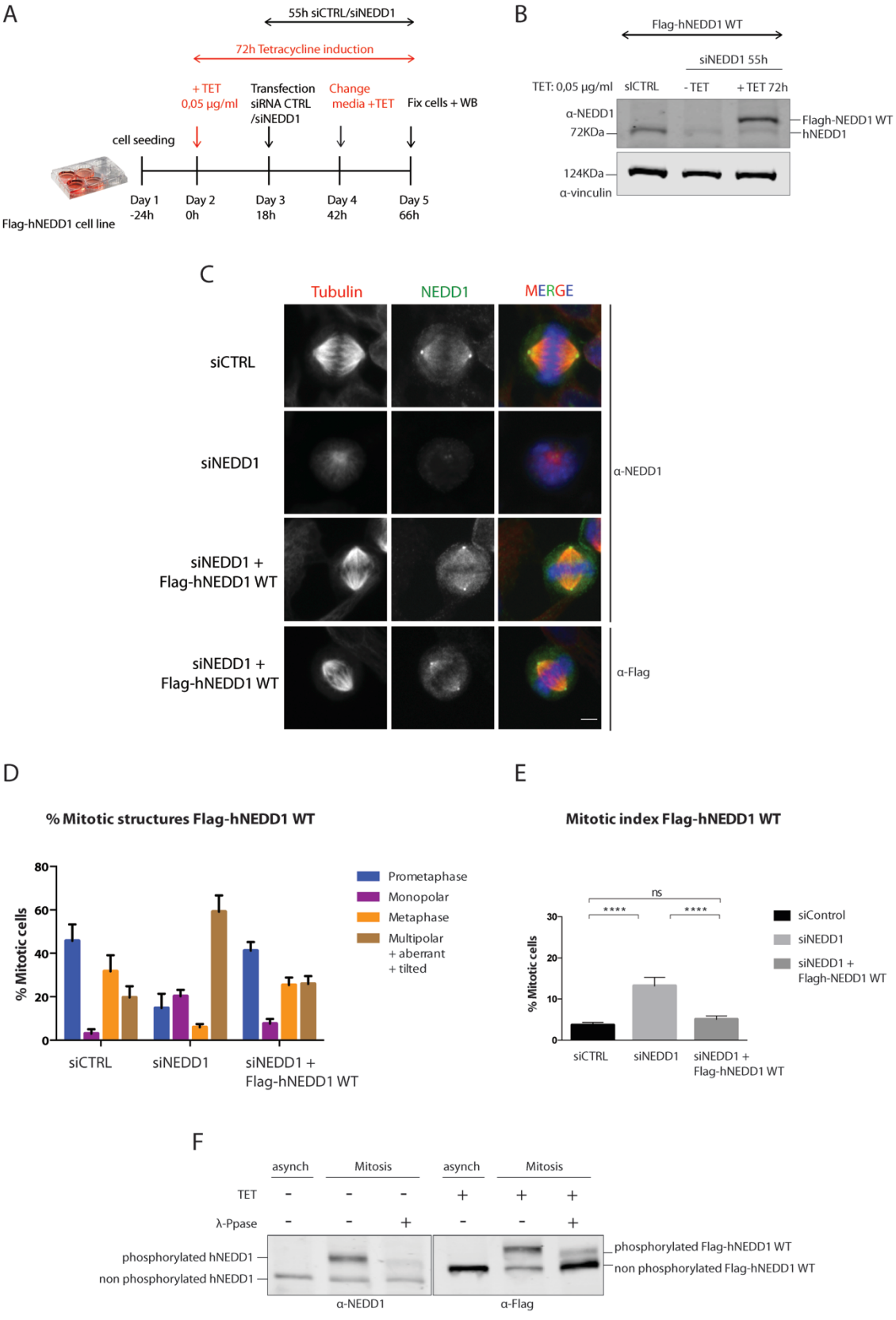
A
55h siCTRL/siNEDD1
72h Tetracycline induction
+ TET 0,05 µg/ml
Transfection siRNA CTRL /siNEDD1
Change media +TET
Fix cells + WB
cell seeding
Flag-hNEDD1 cell line
Day 1 -24h
Day 2 0h
Day 3 18h
Day 4 42h
Day 5 66h
B
Flag-hNEDD1 WT
siNEDD1 55h
TET: 0,05 µg/ml
siCTRL
- TET
+ TET 72h
α-NEDD1 72KDa
Flagh-NEDD1 WT
hNEDD1
124KDa
α-vinculin
C
Tubulin
NEDD1
MERGE
siCTRL
siNEDD1
siNEDD1 + Flag-hNEDD1 WT
siNEDD1 + Flag-hNEDD1 WT
α-NEDD1
α-Flag
D
% Mitotic structures Flag-hNEDD1 WT
% Mitotic cells
Prometaphase
Monopolar
Metaphase
Multipolar + aberrant + tilted
siCTRL
siNEDD1
siNEDD1 + Flag-hNEDD1 WT
E
Mitotic index Flag-hNEDD1 WT
ns
****
****
% Mitotic cells
siControl
siNEDD1
siNEDD1 + Flagh-NEDD1 WT
siCTRL
siNEDD1
siNEDD1 + Flag-hNEDD1 WT
F
asynch
Mitosis
asynch
Mitosis
TET
λ-Ppase
phosphorylated hNEDD1
non phosphorylated hNEDD1
phosphorylated Flag-hNEDD1 WT
non phosphorylated Flag-hNEDD1 WT
α-NEDD1
α-Flag

III- Characterization of the three single phosphorylation-null NEDD1 variants

Different laboratories previously expressed several NEDD1 phosphorylation mutants in a variety of systems, obtaining interesting results about the role of specific NEDD1 residues in spindle assembly. However, one advantage of our experimental approach is that we could compare side by side the phenotypes of the different mutants in the same cell line. In addition, some of the studies did not include several aspects of the phenotypic characterization and I aimed at completing this description.

I prepared three stable cell lines for the inducible expression of Flag-hNEDD1 phospho-null variants in which each of the three residues responsible for microtubule nucleation through the different pathways (S377, S405 and S411) were individually mutated to an alanine. By expressing the single phosphorylation-null mutants S377A, S405A or S411A, we should have switched off one specific microtubule nucleation pathway without in principle affecting the others.

III.A- Functional characterization of NEDD1-S377A expressing cells

Phosphorylation of NEDD1 at the S377 was shown to be necessary for γ-Tubulin recruitment to the centrosome in prophase and mitotic progression (Sdelci et al., 2012). However, these studies did not report the consequences for bipolar spindle formation. To address this question, I characterized the mitotic phenotypes of mitotic cells expressing the single phosphorylation-null mutant S377A.

Western blot analysis confirmed that endogenous NEDD1 in the parental cell line expressing Flag-hNEDD1 S377A could be efficiently silenced and that exogenous Flag-hNEDD1 S377A was correctly expressed (Figure 25A).

Then, I performed immunofluorescence in fixed cells to study the localization of NEDD1 in cells expressing Flag-hNEDD1 S377A as well as to count the number of mitotic cells in the three conditions: control, NEDD1 silenced cells and NEDD1 silenced cells expressing the mutant. Figure 25B shows the localization of NEDD1. In control cells NEDD1 localized to the spindle poles and spindle microtubules as expected. In NEDD1 silenced cells the signal for NEDD1 was very reduced as well as the tubulin signal. In

silenced cells expressing the mutant S377A, NEDD1 localized to the centrosomes, although this localization seemed to be reduced in comparison with control cells. Staining with α-flag antibodies confirmed the specific localization of Flag-hNEDD1 S377A to the centrosomes but not on the microtubules.

I then analyzed the distribution of the mitotic phases. As shown in Figure 25C, silenced cells expressing the mutant Flag-hNEDD1 S377A presented a reduced number of monopolar (≈20%) and aberrant structures (≈26%) in comparison with NEDD1 silenced cells (≈33% and ≈41% respectively). This reduction in the number of abnormal structures was accompanied by an increase in the number of normal prometaphase (≈26%) and metaphase structures (≈28%) compared with silenced cells (≈12% and ≈14% respectively).

On the other hand, silenced cells expressing Flag-hNEDD1 S377A showed a mitotic index of ≈13% instead of 21% for silenced cells (Figure 25D). Although the rescue by expression of Flag-hNEDD1 S377A was not comparable to WT levels, cells expressing this mutant presented a small degree of improvement in comparison with NEDD1 silenced cells. To establish if a mutant is able to rescue the NEDD1 silencing phenotype, we will use a combination of the distribution of the mitotic structures and mitotic index levels. The mitotic index and the phenotype of cells expressing Flag-hNEDD1 S377A seemed to be intermediate between control and silenced cells, therefore suggesting that this phospho-null mutant was able to partially rescue spindle assembly and cell division.

I also performed a band shift assay to look at the phosphorylation state of Flag-hNEDD1 S377A. As previously described, endogenous NEDD1 had a slow migrating form specifically in mitotic cells. Interestingly, Flag-hNEDD1 S377A was also phosphorylated in mitosis (Figure 25E).

Altogether, the data suggested that expression of Flag-hNEDD1 S377A mutant partially rescued the NEDD1 silencing phenotype. Since S377 phosphorylation was shown to be necessary for the recruitment of γ-tubulin to the centrosomes in prophase, these results suggest that although the centrosomal microtubule nucleation pathway is important for bipolar spindle assembly and mitotic progression, the other pathways may be sufficient.

A

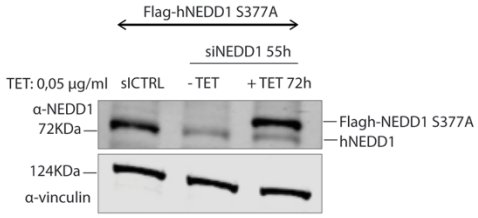
Flag-hNEDD1 S377A
siNEDD1 55h
TET: 0,05 µg/ml
siCTRL
- TET
+ TET 72h
α-NEDD1
72KDa
Flagh-NEDD1 S377A
hNEDD1
124KDa
α-vinculin

B

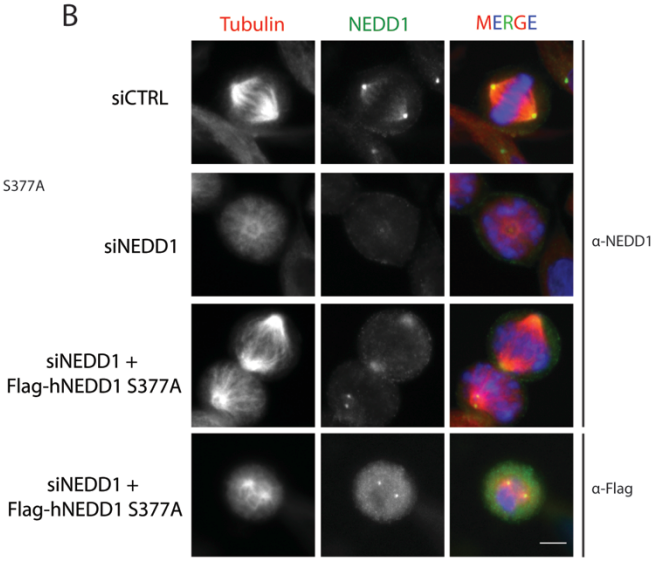
Tubulin
NEDD1
MERGE
siCTRL
siNEDD1
siNEDD1 +
Flag-hNEDD1 S377A
siNEDD1 +
Flag-hNEDD1 S377A
α-NEDD1
α-Flag

C

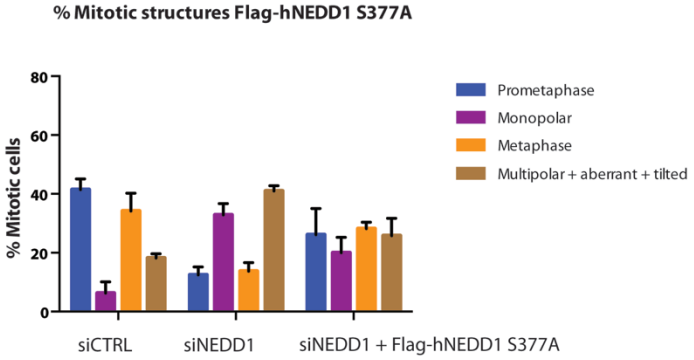
% Mitotic structures Flag-hNEDD1 S377A
% Mitotic cells
80
60
40
20
0
Prometaphase
Monopolar
Metaphase
Multipolar + aberrant + tilted
siCTRL
siNEDD1
siNEDD1 + Flag-hNEDD1 S377A

D

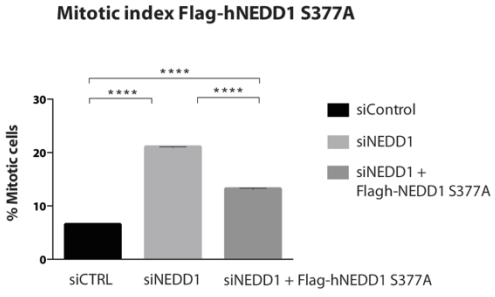
Mitotic index Flag-hNEDD1 S377A
****
****
****
% Mitotic cells
30
20
10
0
siControl
siNEDD1
siNEDD1 +
Flagh-NEDD1 S377A
siCTRL
siNEDD1
siNEDD1 + Flag-hNEDD1 S377A

E

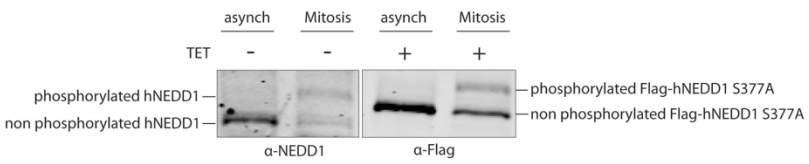
asynch
Mitosis
asynch
Mitosis
TET
-
-
+
+
phosphorylated hNEDD1
non phosphorylated hNEDD1
phosphorylated Flag-hNEDD1 S377A
non phosphorylated Flag-hNEDD1 S377A
α-NEDD1
α-Flag

Figure 25: NEDD1 phosphorylation at S377 is important for spindle assembly.

A) Western blot showing the silencing levels of endogenous NEDD1 and the expression levels of exogenous Flag-hNEDD1 S377A in a typical rescue experiment. **B)** Representative immunofluorescence images showing the localization of endogenous and exogenous NEDD1 in mitotic cells. The first row of the panel shows the localization of NEDD1 in control cells. The second row of the panel shows the localization of NEDD1 in silenced cells. The third row of the panel shows the localization of NEDD1 in silenced cells expressing Flag-hNEDD1 S377A and the last row of the panel shows the localization of exogenous Flag-hNEDD1 S377A in silenced cells. Tubulin is shown in red, NEDD1 in green and DNA in blue. Scale bar 5µm. **C)** Quantification of the mitotic structures. Three replicas with ≈200 cells quantified per condition and experiment were performed. Columns represent the average percentage of cells in each category. Standard deviation between replicas is represented with a line on top of each column. **D)** Quantification of the mitotic index. >1000 cells per condition were counted. The plot shows the average of three independent experiments. Standard deviation between replicas is represented with a line on top of each column. Two-way ANOVA test: **** indicates p-value <0,0001. **E)** Western blot showing NEDD1 in asynchronous and mitotic cells collected by shake-off after an overnight nocodazole block at 0,33µM. Flag-hNEDD1 S377A induced cells were incubated with tetracycline at 1µg/ml during 24h.

III.B- Functional characterization of NEDD1-S405A expressing cells

Although the consequences of expressing both S405A and S411A mutants have already been described, I also wanted to characterize the phenotypes in the same system. Therefore, I first described the phenotype of the single phosphorylation-null mutant S405A.

It has been previously shown that expression of a S405A mutant still allows the formation of bipolar spindles, although the phenotype is characterized by the presence of scattered or misaligned chromosomes (Pinyol et al., 2013). To test if the expression of the same mutant in a different experimental system leads to a similar phenotype, I used the inducible cell line following the optimized protocol.

First, I confirmed that the silencing of endogenous NEDD1 and expression of the exogenous protein Flag-hNEDD1 S405A worked efficiently (Figure 26A). Second, I looked at the localization of this mutant in fixed mitotic cells (Figure 26B). NEDD1 localized to the centrosomes in a dot-like manner in silenced cells expressing Flag-hNEDD1 S405A. This localization was not as strong as in control cells but it was stronger than in cells expressing the centrosomal mutant Flag-hNEDD1 377A. In contrast, I could not detect NEDD1 localization to the microtubules as previously described (Pinyol et al., 2013).

I then quantified the different structures found in mitotic cells (Figure 26C). NEDD1 silenced cells presented a high proportion of monopolar (≈18%) and aberrant/abnormal structures (≈64%) with different defects at the level of microtubule organization, together

with a reduced number of normal prometaphase (≈11%) and metaphase spindles (≈8%). Expression of Flag-hNEDD1 S405A in silenced cells resulted in a phenotype in between control and silenced cells, with a reduction of monopolar (≈11%) and aberrant structures (≈43%) and an increase in prometaphases (≈28%) and metaphases (≈18%).

Next, I quantified the mitotic index in silenced cells expressing Flag-hNEDD1 S405A (Figure 26D). While NEDD1 silenced cells exhibited a mitotic index of around 15%, silenced cells expressing Flag-hNEDD1 S405A showed similar levels (≈12%). Although the distribution of mitotic structures in silenced cells expressing Flag-hNEDD1 S405A was not as detrimental as in NEDD1 silenced cells, the high mitotic index levels of this mutant suggested that its expression did not rescue NEDD1 silencing phenotype.

I also examined whether Flag-hNEDD1 S405A was phosphorylated in mitosis. Figure 26E shows that mitotic Flag-hNEDD1 S405A ran as two different bands. The band running at a higher molecular weight was reduced upon treatment with lambda phosphatase, suggesting that the mutated protein was phosphorylated in mitosis.

Altogether, the data suggested that expression of Flag-hNEDD1 S405A was detrimental for the cell. It did not rescue the NEDD1 silencing phenotype nor the normal progression through mitosis. We could then conclude that the chromosomal microtubule nucleation pathway is essential for spindle assembly and mitosis, as previously described in other systems.

Figure 26: NEDD1 phosphorylation at S405 is essential for spindle assembly and mitosis.

A) Western blot showing the silencing levels of endogenous NEDD1 and the expression levels of exogenous Flag-hNEDD1 S405A in a typical rescue experiment. **B)** Representative immunofluorescence images showing the localization of endogenous and exogenous NEDD1 in mitotic cells. The first row of the panel shows the localization of NEDD1 in control cells. The second row of the panel shows the localization of NEDD1 in silenced cells. The third row of the panel shows the localization of NEDD1 in silenced cells expressing Flag-hNEDD1 S405A and the last row of the panel shows the localization of exogenous Flag-hNEDD1 S405A in silenced cells. Tubulin is shown in red, NEDD1 in green and DNA in blue. Scale bar 5µm. **C)** Quantification of the mitotic structures. Three replicas with ≈200 cells quantified per condition and experiment were performed. Columns represent the average percentage of cells in each category. Standard deviation between replicas is represented with a line on top of each column. **D)** Quantification of the mitotic index. >1000 cells per condition were counted. The plot shows the average of three independent experiments. Standard deviation between replicas is represented with a line on top of each column. Two-way ANOVA test: * indicates p-value = 0,0214, **** indicates p-value <0,0001. **E)** Western blot showing NEDD1 in asynchronous and mitotic cells collected by shake-off after an overnight nocodazole block at 0,33µM. Flag-hNEDD1 S405A induced cells were incubated with tetracycline at 1µg/ml during 24h and λ-Phosphatase was added for 30 minutes when indicated.

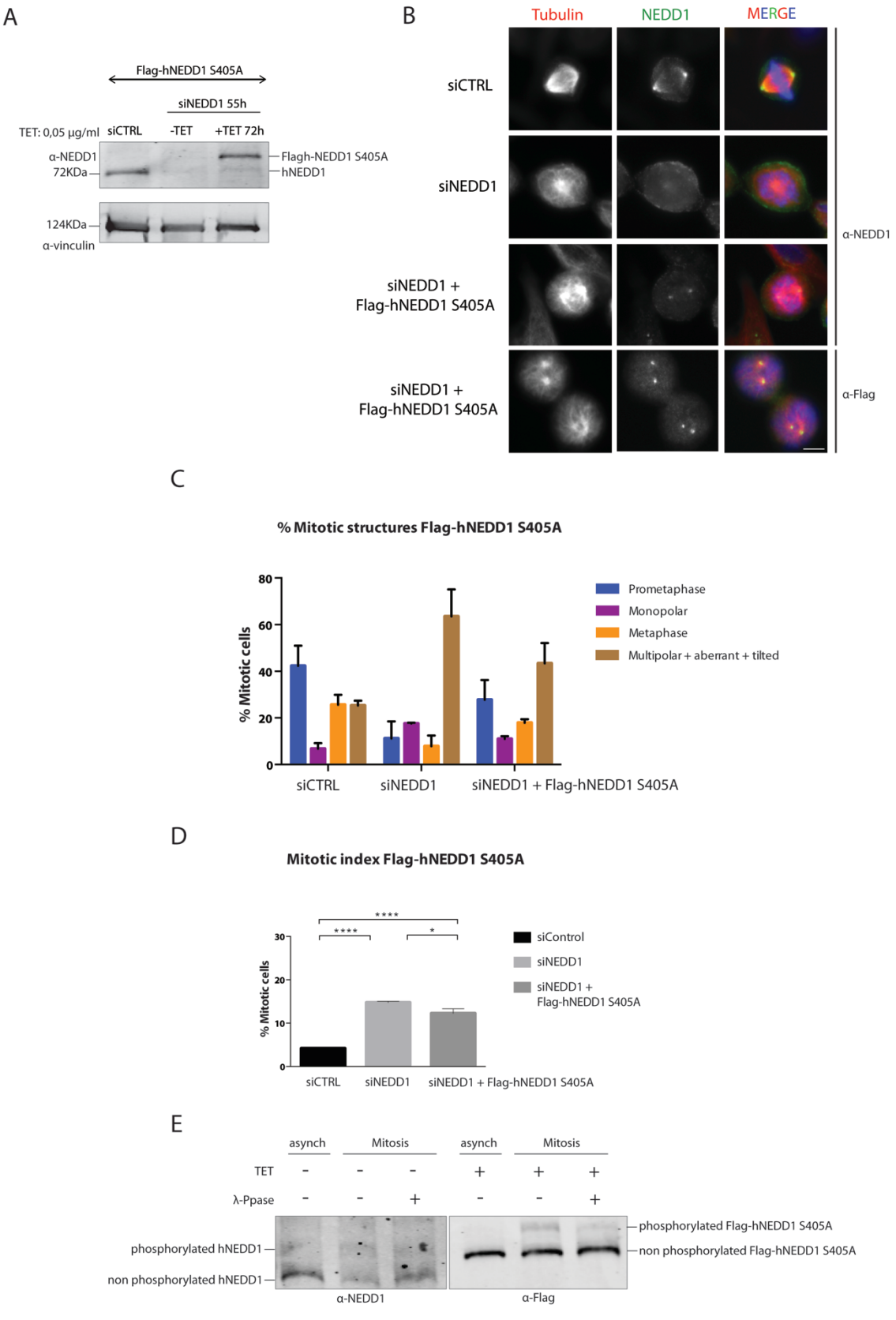
A
Flag-hNEDD1 S405A
siNEDD1 55h
TET: 0,05 µg/ml
siCTRL
-TET
+TET 72h
α-NEDD1
72KDa
Flagh-NEDD1 S405A
hNEDD1
124KDa
α-vinculin
B
Tubulin
NEDD1
MERGE
siCTRL
siNEDD1
siNEDD1 +
Flag-hNEDD1 S405A
siNEDD1 +
Flag-hNEDD1 S405A
α-NEDD1
α-Flag
C
% Mitotic structures Flag-hNEDD1 S405A
% Mitotic cells
80
60
40
20
0
siCTRL
siNEDD1
siNEDD1 + Flag-hNEDD1 S405A
Prometaphase
Monopolar
Metaphase
Multipolar + aberrant + tilted
D
Mitotic index Flag-hNEDD1 S405A
****
****
*
% Mitotic cells
30
20
10
0
siCTRL
siNEDD1
siNEDD1 + Flag-hNEDD1 S405A
siControl
siNEDD1
siNEDD1 +
Flag-hNEDD1 S405A
E
asynch
Mitosis
asynch
Mitosis
TET
λ-Ppase
phosphorylated hNEDD1
non phosphorylated hNEDD1
α-NEDD1
α-Flag
phosphorylated Flag-hNEDD1 S405A
non phosphorylated Flag-hNEDD1 S405A

III.C- Functional characterization of NEDD1-S411A expressing cells

To complete the study of all the phosphorylation-null mutants I explored the phenotype of the S411A mutant. According to published data, the lack of NEDD1 phosphorylation at the S411 by the kinase Cdk1, prevents the nucleation from pre-existing microtubules (Johmura et al., 2011). Indeed, it has been shown that expression of a S411A mutant leads to several defective spindle morphologies together with a high reduction of microtubule density in the central region of the spindle and an increase of the mitotic index (Johmura et al., 2011; Lüders et al., 2006). Moreover, NEDD1-S411A cannot co-immunoprecipitate Augmin, in contrast to the endogenous protein (Johmura et al., 2011; Uehara et al., 2009).

I first checked the silencing and expression levels of Flag-hNEDD1 S411A induced cells. Figure 27A shows the high efficiency of NEDD1 silencing and the proper expression of the exogenous protein. Then, I looked at the localization of NEDD1 in cells expressing Flag-hNEDD1 S411A (Figure 27B). Flag-hNEDD1 S411A strongly localized only to the centrosomes as previously described (Lüders et al., 2006; Pinyol et al., 2013); the distribution of NEDD1 staining followed a dot-like pattern at the poles in mitotic cells.

I quantified the percentage of mitotic structures in fixed cells (Figure 27C). Expression of Flag-hNEDD1 S411A in silenced cells led to a phenotype very similar to that of NEDD1 silencing, showing a very high number of aberrant structures (≈44%) and almost no rescue in the number of normal prometaphase and metaphase structures (≈ 22% and ≈20% versus ≈21% and ≈12% of silenced cells).

I then counted the number of mitosis in silenced cells expressing Flag-hNEDD1 S411A (Figure 27D). As expected, the mutant S411A did not rescue the mitotic index levels, showing a 23% of mitotic cells versus the 22% of silenced cells.

These data indicated that expression of Flag-hNEDD1 S411A was as detrimental for the cell as the lack of endogenous NEDD1.

To complete the characterization of the Flag-hNEDD1 S411A phenotype, I performed a band shift assay (Figure 27E). Mitotic samples showed a very small phosphorylation shift of this phospho-null variant that became highly reduced upon treatment with lambda phosphatase, indicating that the exogenous Flag-hNEDD1 S411A was phosphorylated in mitosis but to lower levels than the endogenous protein. Since mitotic Flag-hNEDD1

S411A had a smaller phosphorylation shift than mitotic Flag-hNEDD1 S377A/S405A, this indicates that S411 is in large part responsible for the shift of migration of NEDD1 in mitotic cell lysates. This also suggests that Flag-hNEDD1 S377A and S405A are probably phosphorylated on S411, since they both shifted in mitosis.

All this set of data suggested that expression of Flag-hNEDD1 S411A was as detrimental for the cell as silencing NEDD1. Cells expressing this mutant were blocked in mitosis, accumulating different kind of aberrant structures with disorganized microtubules.

If we compare the phenotypes resulting from the expression of the three individual phosphorylation-null mutants in silenced cells, the S411A mutant was the most detrimental in terms of mitosis progression and accumulation of aberrant structures. This result suggested a key major role for S411 phosphorylation in mitosis. One possibility was that S411A could not be phosphorylated on S377 and S405 and thereby all the nucleation pathways were inactive (as in silenced cells).

We concluded that although each individual microtubule nucleation pathway has an important role in mitosis progression, preventing S411 phosphorylation that has been associated to the Augmin pathway has the worst consequences for the spindle assembly and cell division.

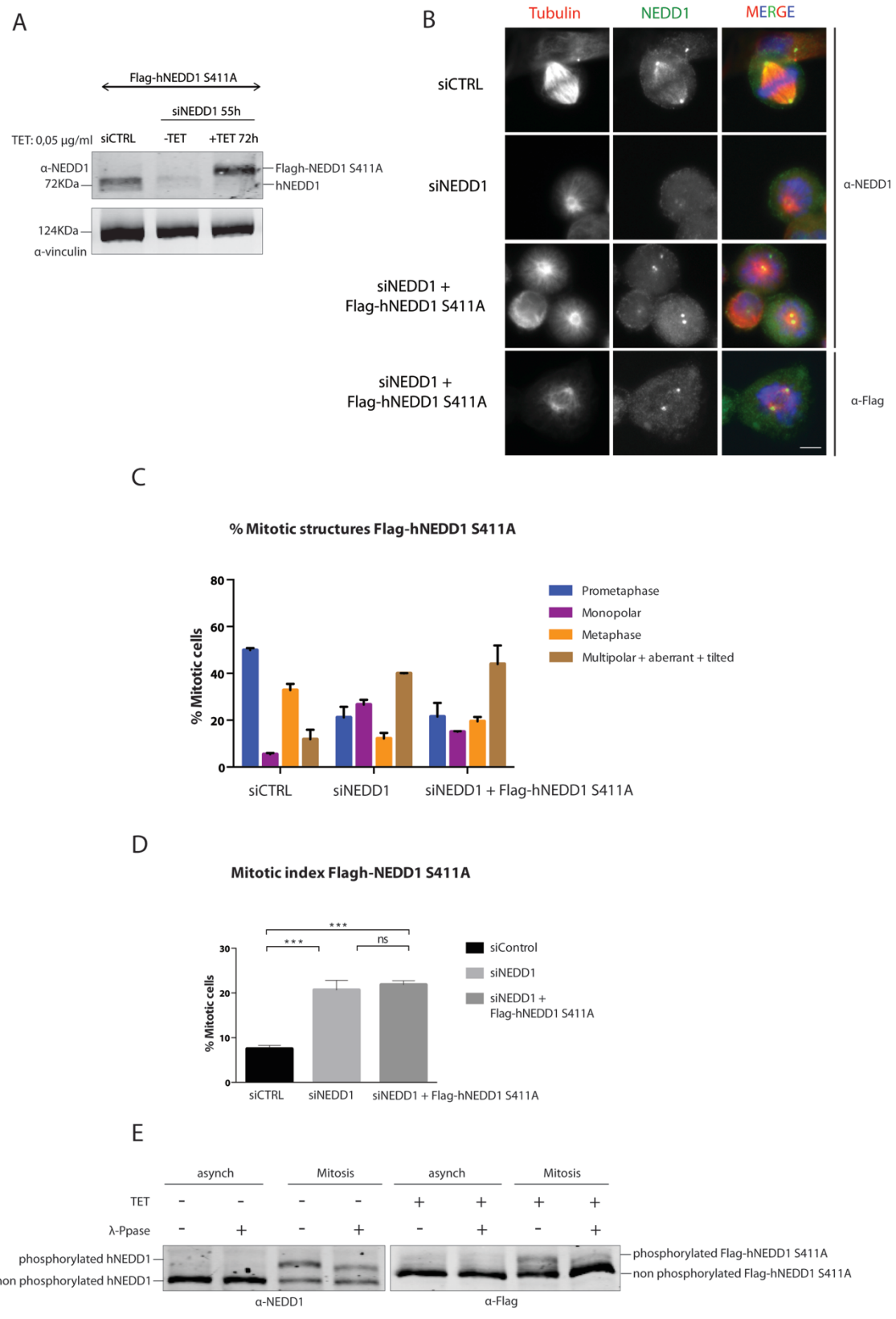
A
Flag-hNEDD1 S411A
siNEDD1 55h
TET: 0,05 µg/ml
siCTRL
-TET
+TET 72h
α-NEDD1
72KDa
Flagh-NEDD1 S411A
hNEDD1
124KDa
α-vinculin
B
Tubulin
NEDD1
MERGE
siCTRL
siNEDD1
siNEDD1 +
Flag-hNEDD1 S411A
siNEDD1 +
Flag-hNEDD1 S411A
α-NEDD1
α-Flag
C
% Mitotic structures Flag-hNEDD1 S411A
% Mitotic cells
80
60
40
20
0
Prometaphase
Monopolar
Metaphase
Multipolar + aberrant + tilted
siCTRL
siNEDD1
siNEDD1 + Flag-hNEDD1 S411A
D
Mitotic index Flagh-NEDD1 S411A
***
***
ns
% Mitotic cells
30
20
10
0
siControl
siNEDD1
siNEDD1 +
Flag-hNEDD1 S411A
siCTRL
siNEDD1
siNEDD1 + Flag-hNEDD1 S411A
E
asynch
Mitosis
asynch
Mitosis
TET
λ-Ppase
phosphorylated hNEDD1
non phosphorylated hNEDD1
α-NEDD1
α-Flag
phosphorylated Flag-hNEDD1 S411A
non phosphorylated Flag-hNEDD1 S411A

Figure 27: NEDD1 phosphorylation at S411 has a major role in the formation of bipolar spindles.

A) Western blot showing the silencing levels of endogenous NEDD1 and the expression levels of exogenous Flag-hNEDD1 S411A in a typical rescue experiment. **B)** Representative immunofluorescence images showing the localization of endogenous and exogenous NEDD1 in mitotic cells. The first row of the panel shows the localization of NEDD1 in control cells. The second row of the panel shows the localization of NEDD1 in silenced cells. The third row of the panel shows the localization of NEDD1 in silenced cells expressing Flag-hNEDD1 S411A and the last row of the panel shows the localization of exogenous Flag-hNEDD1 S411A in silenced cells. Tubulin is shown in red, NEDD1 in green and DNA in blue. Scale bar 5µm. **C)** Quantification of the mitotic structures. Three replicas with ≈200 cells quantified per condition and experiment were performed. Columns represent the average percentage of cells in each category. Standard deviation between replicas is represented with a line on top of each column. **D)** Quantification of the mitotic index. >1000 cells per condition were counted. The plot shows the average of three independent experiments. Standard deviation between replicas is represented with a line on top of each column. Two-way ANOVA test: ns, non-significant differences. *** indicates p-value = 0,0002. **E)** Western blot showing NEDD1 in asynchronous and mitotic cells collected by shake-off after an overnight nocodazole block at 0,33µM. Flag-hNEDD1 S411A induced cells were incubated with tetracycline at 1µg/ml during 24h and λ-Phosphatase was added for 30 minutes when indicated.

IV- Functional characterization of a triple phosphorylation-null NEDD1 variant (NEDD1- AAA)

The correct balance between the mitotic microtubule assembly pathways has been proposed to be crucial for bipolar spindle assembly. Preventing chromosome-dependent MT nucleation promotes an increase of centrosomal MT nucleation suggesting a competition for a limiting component. Therefore switching off one microtubule nucleation pathway creates an unbalance that compromises correct bipolar spindle formation (Cavazza et al., 2016).

We then reasoned that the detrimental effects of expressing a single phosphorylation-null mutant could result from an unbalance among the three pathways rather than being specific to one pathway. Therefore, removing the three regulatory phosphorylations at the same time could potentially eliminate the unbalance by having the same background levels of nucleation through all the pathways. To test this possibility, we used a triple phosphorylation null version of NEDD1 on S377, S405 and S411: the AAA mutant. In this mutant the three sites responsible for microtubule nucleation were substituted by alanines, impairing NEDD1 phosphorylation on any of the three sites and presumably downregulating microtubule nucleation through the three pathways.

I first checked the silencing efficiency and the expression levels of Flag-hNEDD1 AAA in induced cells. Figure 28A shows a good silencing efficiency of endogenous NEDD1 and high expression of the exogenous mutated protein. Then I performed

immunofluorescence in fixed cells to look at NEDD1 localization in cells expressing Flag-hNEDD1 AAA (Figure 28B). Flag-hNEDD1 AAA localized only to the spindle poles in a dot-like manner. This centrosome-specific localization was confirmed with an α-flag staining; Flag-hNEDD1 AAA localized to the poles of aberrant spindles.

I looked in more detail at the mitotic figures found in silenced cells expressing Flag-hNEDD1 AAA (Figure 28C). The quantification of the mitotic structures indicated that silenced cells expressing the triple phosphorylation-null mutant presented a higher number of aberrant structures (≈64%) than NEDD1 silenced cells (≈50%). Usually in NEDD1 silenced cells the proportion of monopolar and aberrant structures may vary but the percentage of both structures altogether is always similar. This was also the case in silenced cells expressing Flag-hNEDD1 AAA: the number of monopolar structures (≈17%) was lower than in NEDD1 silenced cells (≈25%) but the number of aberrant figures increased instead. In agreement with this result, the number of prometaphases (≈13%) and metaphases (≈6%) was also lower than in NEDD1 silenced cells (≈ 16% and ≈9% respectively).

I then quantified the mitotic index in control, NEDD1 silenced cells and NEDD1 silenced cells expressing the triple phosphorylation-null mutant (Figure 28D). I found that silenced cells expressing Flag-hNEDD1 AAA exhibited a high mitotic index of ≈25%, like NEDD1 silenced cells.

According with these results, the phenotypical differences between NEDD1 silenced cells and silenced cells expressing Flag-hNEDD1 AAA were not significant suggesting that the function of NEDD1 is fully dependent on its phosphorylation on these three residues.

To look at the phosphorylation state of the mutant Flag-hNEDD1 AAA, I performed a band shift assay treating mitotic samples from cells expressing WT and Flag-hNEDD1 AAA in parallel (Figure 28E). Endogenous NEDD1 was phosphorylated to normal levels in the parental Hela/FTR/TR cell line for both WT and Flag-hNEDD1 AAA. Exogenous mitotic Flag-hNEDD1 WT presented a big migration shift that disappeared upon treatment with lambda phosphatase. In contrast, exogenous mitotic Flag-hNEDD1 AAA did not show this migration shift before treatment with lambda phosphatase. The blot shows a small smear instead of an upper band corresponding to the phosphorylated version of the protein, indicating that the triple phospho-null mutant was not

phosphorylated efficiently in mitosis. Upon treatment with phosphatase the smear disappeared and the fraction of the protein corresponding to the non-phosphorylated Flag-hNEDD1 AAA became enriched. This result is interesting. It is in agreement with our previous hypothesis that S411 phosphorylation is responsible for the shift.

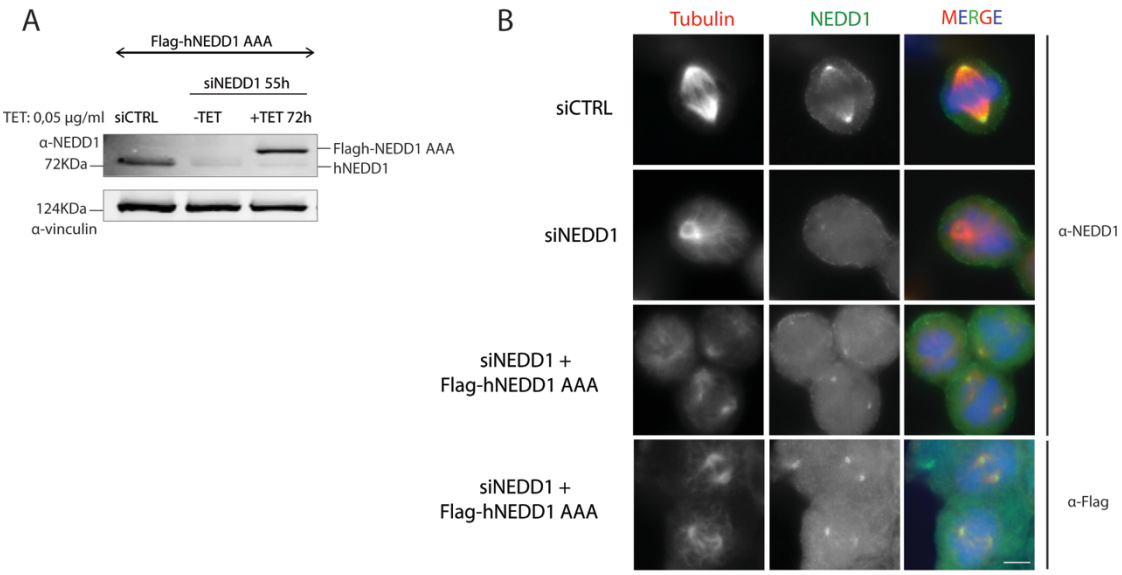
A
Flag-hNEDD1 AAA
siNEDD1 55h
TET: 0,05 µg/ml
siCTRL
-TET
+TET 72h
α-NEDD1
72KDa
Flagh-NEDD1 AAA
hNEDD1
124KDa
α-vinculin
B
Tubulin
NEDD1
MERGE
siCTRL
siNEDD1
siNEDD1 +
Flag-hNEDD1 AAA
siNEDD1 +
Flag-hNEDD1 AAA
α-NEDD1
α-Flag

C

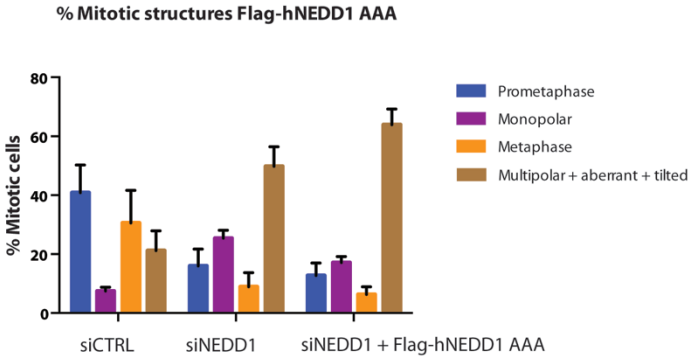
% Mitotic structures Flag-hNEDD1 AAA
% Mitotic cells
80
60
40
20
0
Prometaphase
Monopolar
Metaphase
Multipolar + aberrant + tilted
siCTRL
siNEDD1
siNEDD1 + Flag-hNEDD1 AAA

D

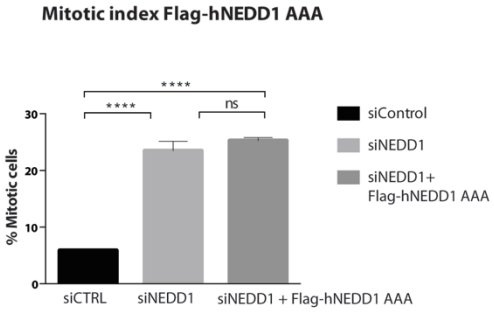
Mitotic index Flag-hNEDD1 AAA
****
****
ns
% Mitotic cells
30
20
10
0
siControl
siNEDD1
siNEDD1+
Flag-hNEDD1 AAA
siCTRL
siNEDD1
siNEDD1 + Flag-hNEDD1 AAA

E

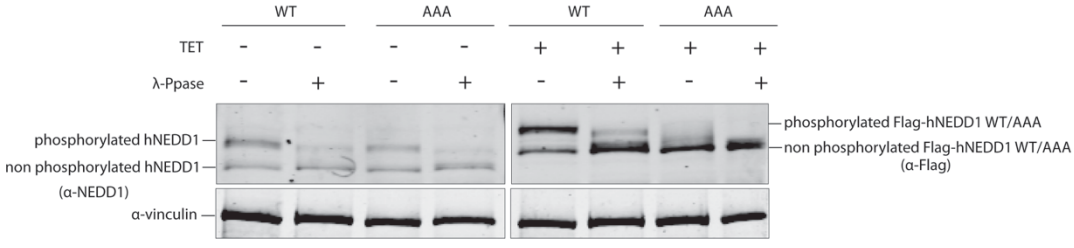
WT
AAA
WT
AAA
TET
λ-Ppase
phosphorylated hNEDD1
non phosphorylated hNEDD1
(α-NEDD1)
α-vinculin
phosphorylated Flag-hNEDD1 WT/AAA
non phosphorylated Flag-hNEDD1 WT/AAA
(α-Flag)

Figure 28: Characterization of a triple phosphorylation-null NEDD1 variant (NEDD1-AAA).

A) Western blot showing the silencing levels of endogenous NEDD1 and the expression levels of exogenous Flag-hNEDD1 AAA in a typical rescue experiment. **B)** Representative immunofluorescence images showing the localization of endogenous and exogenous NEDD1 in mitotic cells. The first row of the panel shows the localization of NEDD1 in control cells. The second row of the panel shows the localization of NEDD1 in silenced cells. The third row of the panel shows the localization of NEDD1 in silenced cells expressing Flag-hNEDD1 AAA (from the three cells shown in the picture only the cell in the bottom is well focused at the centrosomes). The last row of the panel shows the localization of exogenous Flag-hNEDD1 AAA in silenced cells. Tubulin is shown in red, NEDD1 in green and DNA in blue. Scale bar 5µm. **C)** Quantification of the mitotic structures. Three replicas with ≈200 cells quantified per condition and experiment were performed. Columns represent the average percentage of cells in each category. Standard deviation between replicas is represented with a line on top of each column. **D)** Quantification of the mitotic index. >1000 cells per condition were counted. The plot shows the average of three independent experiments. Standard deviation between replicas is represented with a line on top of each column. Two-way ANOVA test: ns, non-significant differences. **** indicates p-value<0,0001. **E)** Western blot showing NEDD1 in asynchronous and mitotic cells collected by shake-off after an overnight nocodazole block at 0,33µM. Flag-hNEDD1 AAA induced cells were incubated with tetracycline at 1µg/ml during 24h and λ-Phosphatase was added for 30 minutes when indicated.

V- Investigating NEDD1 interactions and their putative regulation by phosphorylation

As an initial approach, I performed Flag-hNEDD1 pulldowns and posterior western blot analysis in order to detect Flag-hNEDD1 interactors. The goal was to first confirm known interactors of NEDD1 and then check if these interactions were dependent on phosphorylation at 377, 405 and/or 411. I performed a pulldown from Flag-hNEDD1 WT induced cells synchronized in mitosis. Figure 29 shows efficient pulldown of exogenous Flag-hNEDD1 WT with α-flag magnetic coated beads. I then blotted against a known NEDD1 interactor, Plk1. The blot shows that exogenous Flag-hNEDD1 WT immunoprecipitated Plk1, but a faint band also appeared in the control sample (non-induced sample). Since the control sample was less concentrated this prevented us from concluding that Flag-hNEDD1 WT did co-immunoprecipitate Plk1 with our experimental conditions. I tried to optimize the Flag-hNEDD1 pulldown, testing many different conditions of beads incubation time and beads washing but, unfortunately, I was not able to completely eliminate Plk1 signal in control samples, precluding any further analysis with the NEDD1 phosphorylation mutants.

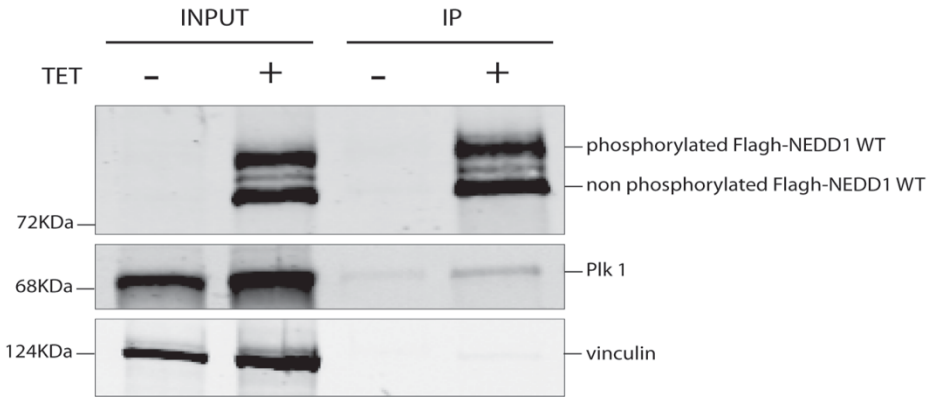

Figure 29: Flag-hNEDD1 WT pulldown and Plk1 interaction.

Hela Flag-hNEDD1 WT cells were grown in the absence or presence of tetracycline (24h incubation at 1 µg/ml) to induce the stable expression of the exogenous Flag-hNEDD1 WT protein. Both induced and non-induced cell populations were synchronized in mitosis by an overnight nocodazole block. Mitotic cell lysates were collected by mitotic shake-off and then immunoprecipitated (IP) with α-flag magnetic coated beads. Mitotic cell lysates and the α-flag and α-Plk1 immunoprecipitates (IP) were analyzed by western blotting to detect NEDD1 (upper row), Plk1 (middle row) and α-vinculin (lower row) as loading control.

As an alternative approach, we then tried to identify NEDD1 interactors regulated by phosphorylation by combining a SILAC based method and mass spectrometry using the Flag-hNEDD1 WT cell line and the different phosphorylation mutants expressing cell lines. The aim was to identify putative phosphorylation dependent specific interactors of NEDD1 that could be playing a different role in each of the three microtubule assembly pathways. The SILAC method uses in vivo metabolic incorporation of "heavy" 13C- or 15N-labeled amino acids into proteins followed by mass spectrometry (MS) analysis for identification, characterization and quantitation of proteins. We performed a first pilot experiment using Flag-hNEDD1 WT (cells grown in light medium) versus Flag-hNEDD1 AAA (cells grown in heavy medium) as we expected to see bigger differences between them at the level of interaction (Figure 30). Such a result would indicate the existence of putative specific complexes acting under the regulation of these particular phosphorylations. In this experiment, I recovered more than 800 proteins, including some of the components that are part of the γ-TuRC and also some proteins that are specific for the chromosomal pathway as TPX2 and RHAMM. In addition, the results from this experiment suggested that there were differences in NEDD1 interactions in both populations of cells: Flag-hNEDD1 AAA induced cells presented more protein interactions than cells expressing Flag-hNEDD1 WT. I performed a second replica of this SILAC experiment but, unexpectedly, the results were very different from the first pilot experiment (Figure 30).

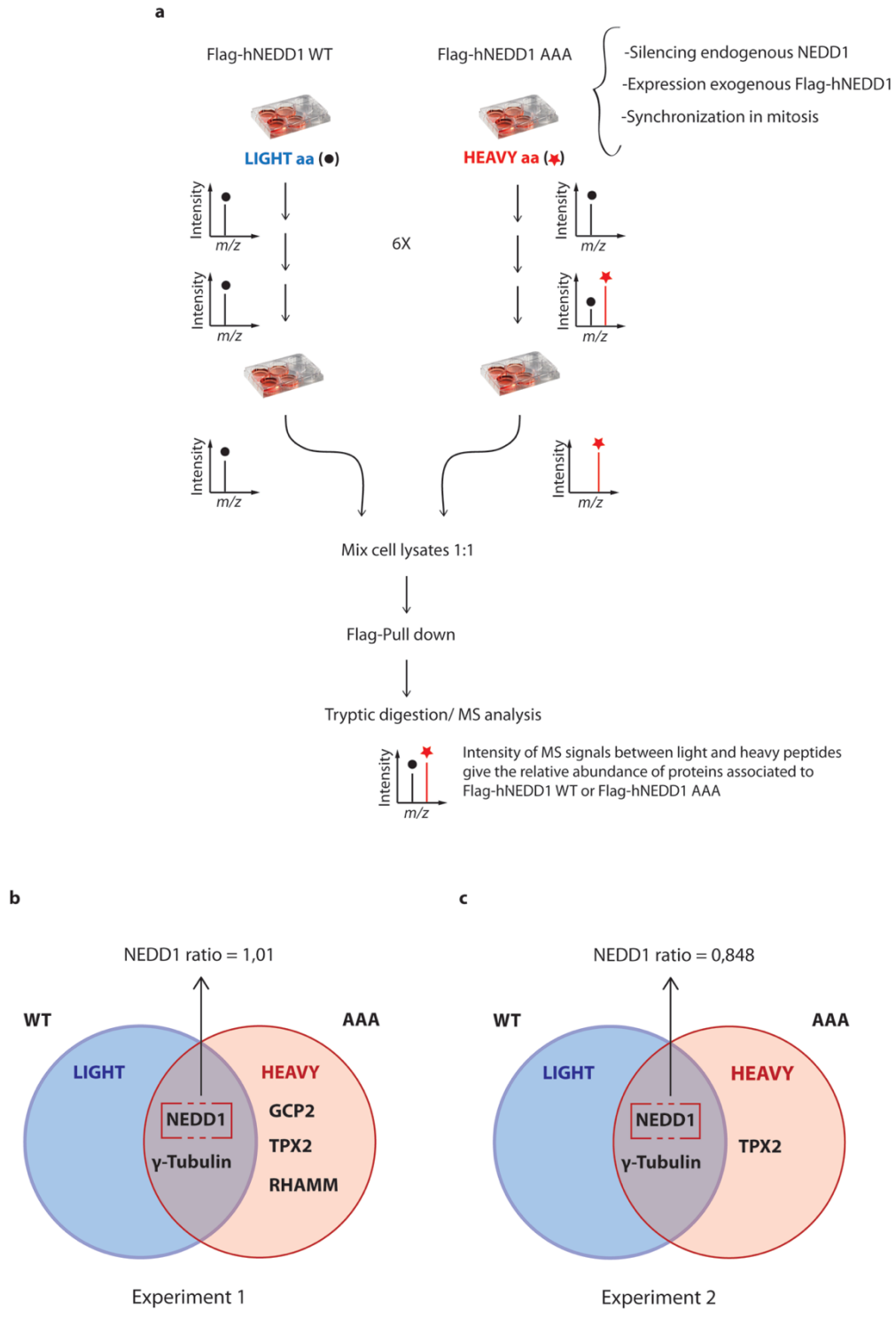

Figure 30: NEDD1 interactors identified by Mass Spectrometry using a SILAC based approach.
a) Schematic representation of the SILAC experimental workflow. **b)** Venn diagram showing the NEDD1 ratio and selected proteins identified in the first experiment. **c)** Venn diagram showing the NEDD1 ratio and some of the proteins identified in the second replica.

In the second experiment, less peptides were identified. As a result, some proteins that were identified in the first experiment could not be identified the second time. In addition, there were some contradictory results as for example the heavy/light ratio for TACC3 (see table below). We classified the identified proteins according to the heavy/light ratios. Proteins having a ratio below 0,5 were considered as enriched in the light sample (Flag-hNEDD1 WT) and those having a ratio above 1,5 were considered enriched in the heavy sample (Flag-hNEDD1 AAA). Those with a ratio between 0,5-1,5 were considered to be equally abundant. In the two replicas we found more interactors in the triple alanine mutant AAA than in the WT.

The next table shows the comparison between heavy/light ratios for some of the identified proteins. In the first experiment the ratio for NEDD1 was 1,01, indicating that the light and heavy samples were mixed in the right proportion 1:1 and that NEDD1 pulldown was properly performed. In the second experiment, as previously explained, the ratios in general were much lower and the interactors specific to each sample category (with the same filter applied) were as well very different from the first experiment.

Ratio Heavy/Light	**Experiment 1**	**Experiment 2**
NEDD1	1,01	0,848
γ-Tubulin	1,54	0,557
TACC3	6,31	0,972
Ran-GTP	2,46	0,972
TPX2	4,16	1,609

Table III: Heavy/Light ratio of selected proteins identified by Mass Spectrometry in the two replicas.

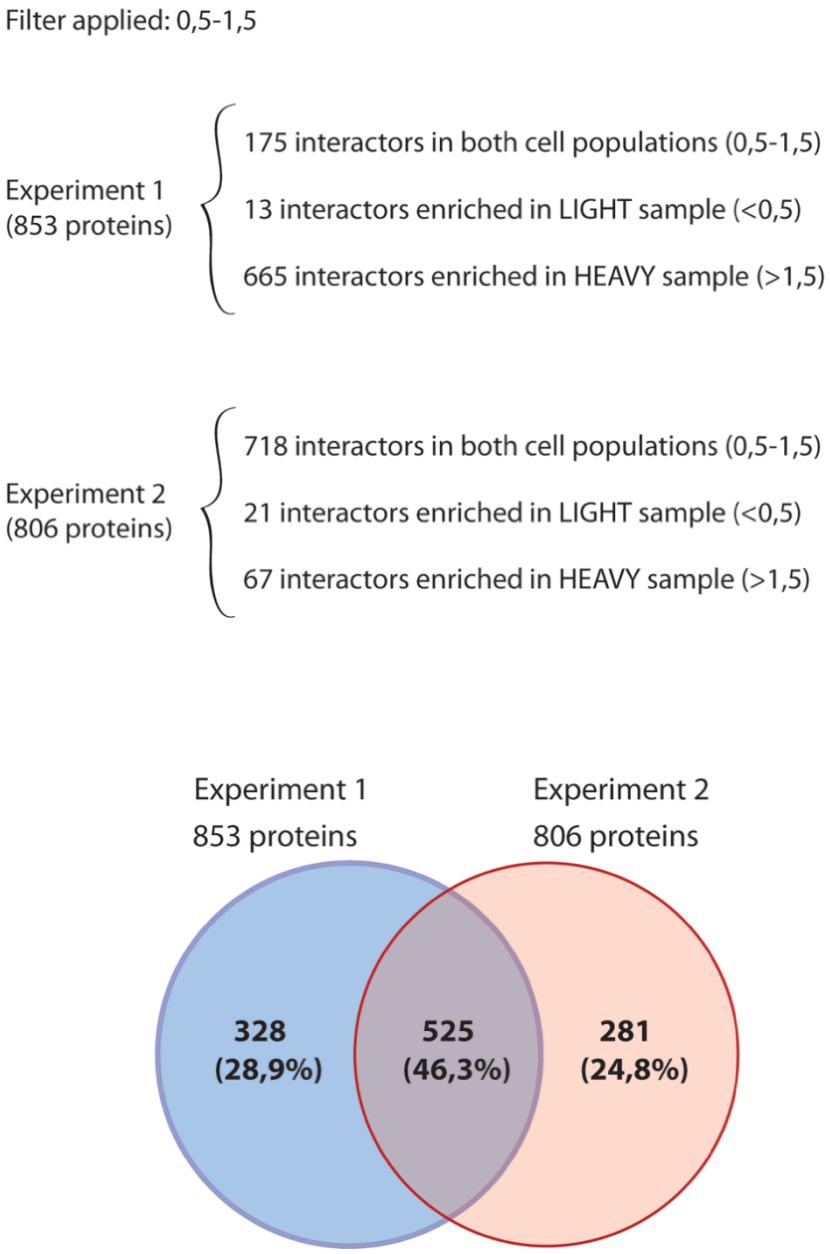

Figure 31:Number of proteins identified in the two SILAC experiments and Venn diagram showing the percentage of overlap.

As the results from both experiments were quite unrelated, we could not make any conclusion about the differences in interactors between Flag-hNEDD1 WT and Flag-hNEDD1 AAA expressing cells. We tried to improve the experimental conditions of this SILAC experiment to obtain NEDD1 as one of the top identified proteins, which was not the case for any of the two experiments. As we were doing the pulldown of NEDD1, we should have got NEDD1 as the first protein identified and then, the potential interactors

would also have appeared in a bigger ratio. We think that many of the proteins that appeared in the highest ratios were contaminants. In order to solve this problem, we performed different conditions of beads washing to try to eliminate all the protein contaminants. After testing many experimental conditions, we were still having technical difficulties that made impossible to get consistent results. Therefore, we decided not to continue performing SILAC on these two particular cell lines.

VI- Functional characterization of a triple phosphorylation-mimicking NEDD1 variant (NEDD1-DDD)

We wanted to use our system to test whether the timing of activation of the three pathways is important for spindle assembly as previously suggested (Cavazza et al., 2016). Microtubule nucleation at the centrosomes starts before nuclear envelope breakdown (NEBD) in G2, then nucleation around the chromosomes is promoted by a Ran-GTP gradient after NEBD. Nucleation from pre-existing microtubules also takes place, most probably after NEBD too.

To abolish the temporal regulation still ensuring that the three pathways are active we used a triple phospho-mimicking variant: Flag-hNEDD1 DDD. In this mutant, the three sites responsible for microtubule nucleation were substituted to an aspartic acid that mimics the phosphorylation state at the three sites, presumably upregulating microtubule nucleation simultaneously through the three pathways.

To start characterizing the phenotype of this mutant, I performed western blot to check whether endogenous protein was properly silenced and exogenous Flag-hNEDD1 DDD was well expressed (Figure 32A). The blot shows good levels of both silencing efficiency and expression of exogenous protein. Then, I looked at the localization of Flag-hNEDD1 DDD in mitotic cells (Figure 32B). Silenced cells expressing Flag-hNEDD1 DDD presented a high number of structures with incomplete pole separation and aberrant figures. In these figures NEDD1 localized to the poles and not to the microtubules.

The distribution of the mitotic structures (Figure 32C) showed that the phenotype of cells expressing Flag-hNEDD1 DDD was very detrimental, with a percentage of aberrant structures higher than 70% and a very low number of prometaphases (≈12%) and metaphases (≈4%). The phenotype of the DDD mutant was even more dramatic than the

absence of endogenous NEDD1, meaning that expression of Flag-hNEDD1 DDD did not support spindle assembly and it was really harmful for the cell.

The quantification of the mitotic index in silenced cells expressing the DDD mutant was in agreement with the previous result. Both silenced and silenced cells expressing the triple phospho-mimicking mutant exhibited a mitotic index of ≈13%, indicating that expression of Flag-hNEDD1 DDD did not rescue the mitotic arrest resulting from NEDD1 silencing (Figure 32D). These results indicated that the phosphorylation at S377, S405 and S411 from early mitotic phases is deleterious suggesting that spindle assembly requires a very tight spatial and temporal regulation of microtubule nucleation

In addition, I performed a band shift assay from cells expressing Flag-hNEDD1 DDD (Figure 32E). Exogenous Flag-hNEDD1 DDD showed an abnormal migration pattern with two bands in asynchronous and mitotic cells although cells were correctly synchronized as checked with the α-TPX2 antibody. Possibly introducing an aspartic acid in the 411 site (as we hypothesized in the 411A experiment) is sufficient to produce the band shift which is not sensitive to phosphatase.

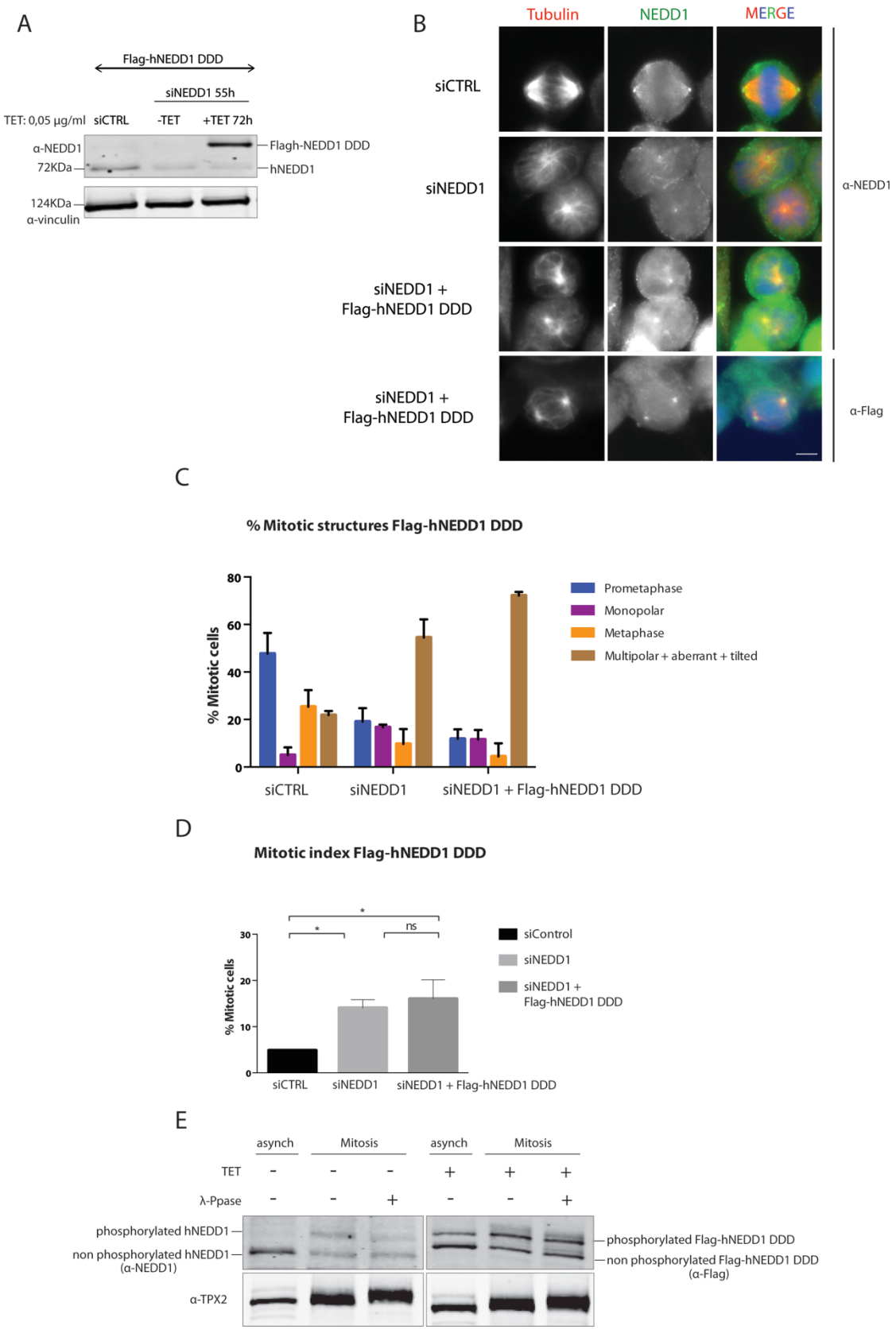
A
Flag-hNEDD1 DDD
siNEDD1 55h
TET: 0,05 µg/ml siCTRL -TET +TET 72h
α-NEDD1
72KDa
Flagh-NEDD1 DDD
hNEDD1
124KDa
α-vinculin
B
Tubulin
NEDD1
MERGE
siCTRL
siNEDD1
siNEDD1 + Flag-hNEDD1 DDD
siNEDD1 + Flag-hNEDD1 DDD
α-NEDD1
α-Flag
C
% Mitotic structures Flag-hNEDD1 DDD
% Mitotic cells
80
60
40
20
0
siCTRL
siNEDD1
siNEDD1 + Flag-hNEDD1 DDD
Prometaphase
Monopolar
Metaphase
Multipolar + aberrant + tilted
D
Mitotic index Flag-hNEDD1 DDD
% Mitotic cells
30
20
10
0
*
*
ns
siCTRL
siNEDD1
siNEDD1 + Flag-hNEDD1 DDD
siControl
siNEDD1
siNEDD1 + Flag-hNEDD1 DDD
E
asynch
Mitosis
asynch
Mitosis
TET - - - + + +
λ-Ppase - - + - - +
phosphorylated hNEDD1
non phosphorylated hNEDD1 (α-NEDD1)
α-TPX2
phosphorylated Flag-hNEDD1 DDD
non phosphorylated Flag-hNEDD1 DDD (α-Flag)

Figure 32: Characterization of a triple phosphorylation-mimicking NEDD1 variant (NEDD1-DDD). **A)** Western blot showing the silencing levels of endogenous NEDD1 and the expression levels of exogenous Flag-hNEDD1 DDD in a typical rescue experiment. **B)** Representative immunofluorescence images showing the localization of endogenous and exogenous NEDD1 in mitotic cells. The first row of the panel shows the localization of NEDD1 in control cells. The second row of the panel shows the localization of NEDD1 in silenced cells. The third row of the panel shows the localization of NEDD1 in silenced cells expressing Flag-hNEDD1 DDD and the last row of the panel shows the localization of exogenous Flag-hNEDD1 DDD in silenced cells. Tubulin is shown in red, NEDD1 in green and DNA in blue. Scale bar 5µm. **C)** Quantification of the mitotic structures. Three replicas with ≈200 cells quantified per condition and experiment were performed. Columns represent the average percentage of cells in each category. Standard deviation between replicas is represented with a line on top of each column. **D)** Quantification of the mitotic index. >1000 cells per condition were counted. The plot shows the average of three independent experiments. Standard deviation between replicas is represented with a line on top of each column. Two-way ANOVA test: ns, non-significant differences. * indicates p-value=0,0283 between control and NEDD1 silenced samples and p-value = 0,0120 between control and NEDD1 silenced cells expressing Flag-hNEDD1 DDD. **E)** Western blot showing NEDD1 in asynchronous and mitotic cells collected by shake-off after an overnight nocodazole block at 0,33µM. Flag-hNEDD1 DDD induced cells were incubated with tetracycline at 1µg/ml during 24h and λ-Phosphatase was added for 30 minutes when indicated.

VII- Characterization of the single phosphorylation-mimicking NEDD1 variants

Altogether the data show that neither the triple phosphorylation-null mutant S377A+S405A+S411A (AAA) nor the triple phosphorylation-mimicking mutant S377D+S405D+S411D (DDD) support spindle assembly, suggesting that spindle assembly requires a tight control of all the spatial and temporal events occurring during microtubule nucleation.

Although the rescue of the mitotic defects in NEDD1 silenced cells by expression of a phospho-mimicking version was previously shown with a S405D mutant (Pinyol et al., 2013); there was no information about the phospho-mimicking versions of the other two sites: S377D and S411D. To obtain confirmation of our hypothesis, we decided to characterize the mitotic phenotypes of cells expressing any of the three single phospho-mimicking NEDD1 variants: S377D, S405D and S411D.

VII.A- Functional characterization of the single phosphorylation-mimicking mutant S405D

It has been previously shown that a phospho-mimicking mutant S405D was able to rescue different mitotic defects when expressed in NEDD1 silenced cells as for example: chromosome misalignment phenotypes, K-fiber instability under cold conditions and microtubule regrowth after nocodazole release from both centrosomes and chromosomes

(Pinyol et al., 2013). Therefore, I checked if we could reproduce similar results in our experimental system. I first performed western blot to check the silencing and expression levels of the mutated protein (Figure 33A). Endogenous NEDD1 was well silenced and exogenous Flag-hNEDD1 S405D was also properly expressed. I then looked at the localization of NEDD1 in mitotic cells expressing this mutant (Figure 33B). Bipolar spindles presented the chromosomes perfectly aligned in the metaphase plate and NEDD1 localized strongly to the centrosomes but also to the spindle microtubules, like the endogenous protein. I quantified the distribution of the different mitotic structures (Figure 33C). NEDD1 silenced cells exhibited a high percentage of monopolar (≈28%) and aberrant figures (≈%38) and a low number of prometaphase and metaphase structures (≈19% and ≈14% respectively). Expression of Flag-hNEDD1 S405D resulted in a decrease in the number of monopolar (≈19%) and aberrant structures (26%) together with an increase in the percentage of normal prometaphase (≈39%) and metaphase figures (≈16%) compared with silenced cells. This result suggested a partial rescue of the NEDD1 silencing phenotype upon expression of Flag-hNEDD1 S405D mutant. However, the rescue was not as efficient as the rescue with Flag-hNEDD1 WT, therefore we looked at the mitotic index levels to confirm it. I counted the number of mitotic cells in the three conditions: control, NEDD1 silenced cells and NEDD1 silenced cells expressing Flag-hNEDD1 S405D (Figure 33D). Expression of the phospho-mimicking mutant S405D rescued the increase in the mitotic index (≈12%) caused by NEDD1 silencing. The rescue was really efficient as the differences in the mitotic index between control (≈4%) and silenced cells expressing Flag-hNEDD1 S405D (≈5%) were not significant. Altogether, the data are in agreement with previous observations indicating a rescue of the NEDD1 silencing phenotype by expression of a S405D mutant.

Figure 33: Functional characterization of the single phosphorylation-mimicking mutant S405D.
A) WB showing the silencing levels of endogenous NEDD1 and the expression levels of exogenous Flag-hNEDD1 S405D in a typical rescue experiment. **B)** Representative IF images showing the localization of endogenous and exogenous NEDD1 in mitotic cells. 1st row of the panel shows the localization of NEDD1 in control cells. 2nd row of the panel shows the localization of NEDD1 in silenced cells. The 3rd row of the panel shows the localization of NEDD1 in silenced cells expressing Flag-hNEDD1 S405D and the last row of the panel shows the localization of exogenous Flag-hNEDD1 S405D in silenced cells. Tubulin is shown in red, NEDD1 in green and DNA in blue. Scale bar 5µm. **C)** Quantification of the mitotic structures. Three replicas with ≈200 cells quantified per condition and experiment were performed. Columns represent the average percentage of cells in each category. SD between replicas is represented with a line on top of each column. **D)** Quantification of the mitotic index. >1000 cells per condition were counted. The plot shows the average of three independent experiments. Standard deviation between replicas is represented with a line on top of each column. Two-way ANOVA test: ns, non-significant differences. **** indicates p-value<0,0001.

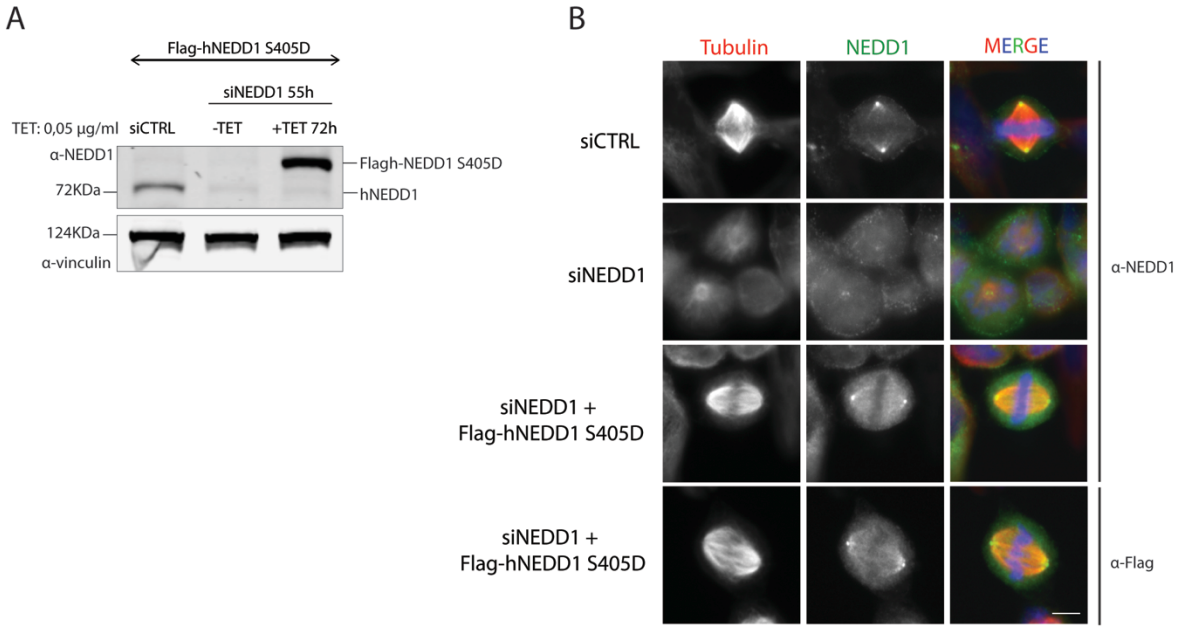
A
Flag-hNEDD1 S405D
siNEDD1 55h
TET: 0,05 µg/ml
siCTRL
-TET
+TET 72h
α-NEDD1
72KDa
Flagh-NEDD1 S405D
hNEDD1
124KDa
α-vinculin
B
Tubulin
NEDD1
MERGE
siCTRL
siNEDD1
siNEDD1 +
Flag-hNEDD1 S405D
siNEDD1 +
Flag-hNEDD1 S405D
α-NEDD1
α-Flag

C

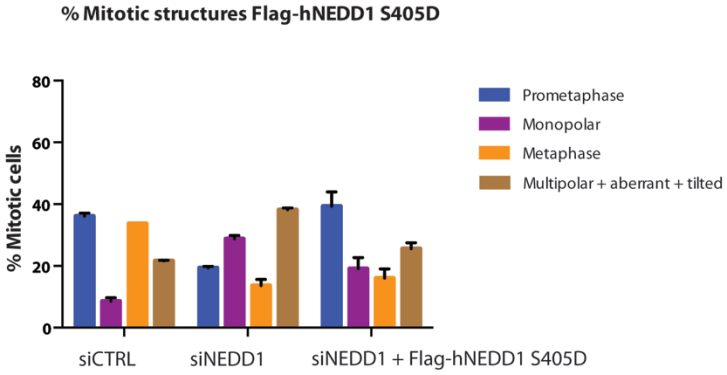
% Mitotic structures Flag-hNEDD1 S405D
% Mitotic cells
80
60
40
20
0
Prometaphase
Monopolar
Metaphase
Multipolar + aberrant + tilted
siCTRL
siNEDD1
siNEDD1 + Flag-hNEDD1 S405D

D

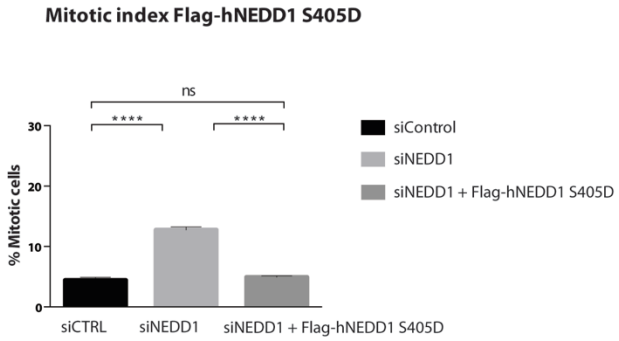
Mitotic index Flag-hNEDD1 S405D
ns
****
****
% Mitotic cells
30
20
10
0
siControl
siNEDD1
siNEDD1 + Flag-hNEDD1 S405D
siCTRL
siNEDD1
siNEDD1 + Flag-hNEDD1 S405D

VII.B- Functional characterization of the single phosphorylation-mimicking mutant S377D

It has been previously described that a phospho-mimicking S377D mutant was able to rescue the mitotic recruitment of γ-tubulin to the centrosomes in Nek9 silenced cells (Sdelci et al., 2012), although the phenotype of mitotic cells expressing this mutant and its ability to rescue the NEDD1 silencing phenotype was not reported. Therefore, I expressed a Flag-hNEDD1 S377D mutant in our inducible system to explore its mitotic phenotypes.

Western blot analysis confirmed that endogenous NEDD1 was efficiently silenced and exogenous Flag-hNEDD1 S377D was properly expressed (Figure 34A). I then performed immunofluorescence in fixed cells to look at the localization of the exogenous protein in mitotic cells (Figure 34B). The monopolar and aberrant structures observed in NEDD1 silenced cells were substituted by a high number of prometaphase (≈39%) and metaphase spindles (≈20%) where NEDD1 clearly localized to the spindle poles.

I quantified the mitotic structures in Flag-hNEDD1 S377D induced cells (Figure 34C). Silenced cells expressing this mutant showed a big reduction in the number of aberrant structures (≈29%), together with an increase in the percentage of prometaphases and metaphases (≈39% and ≈20% respectively) compared with NEDD1 silenced cells that exhibited ≈58% of aberrant structures and around 11% of both prometaphases and metaphases. This phenotype could be considered as a partial rescue of the NEDD1 silencing phenotype, as it could overcome a big percentage of the mitotic defects but it was still not good enough to reach control levels.

This result was confirmed by the quantification of the mitotic index. I counted the number of mitosis in control, NEDD1 silenced cells and silenced cells expressing Flag-hNEDD1 S377D (Figure 34D). Interestingly, I found that cells expressing the mutant partially rescued the mitotic arrest due to NEDD1 silencing, going from a 17% of mitotic cells in NEDD1 silenced cells to an 8% in silenced cells expressing the mutant S377D.

The partial rescue at the level of mitotic structures suggested that expression of Flag-hNEDD1 S377D was sufficient to, at least in part, overcome the NEDD1 silencing phenotype and the mitotic index quantification confirmed this rescue.

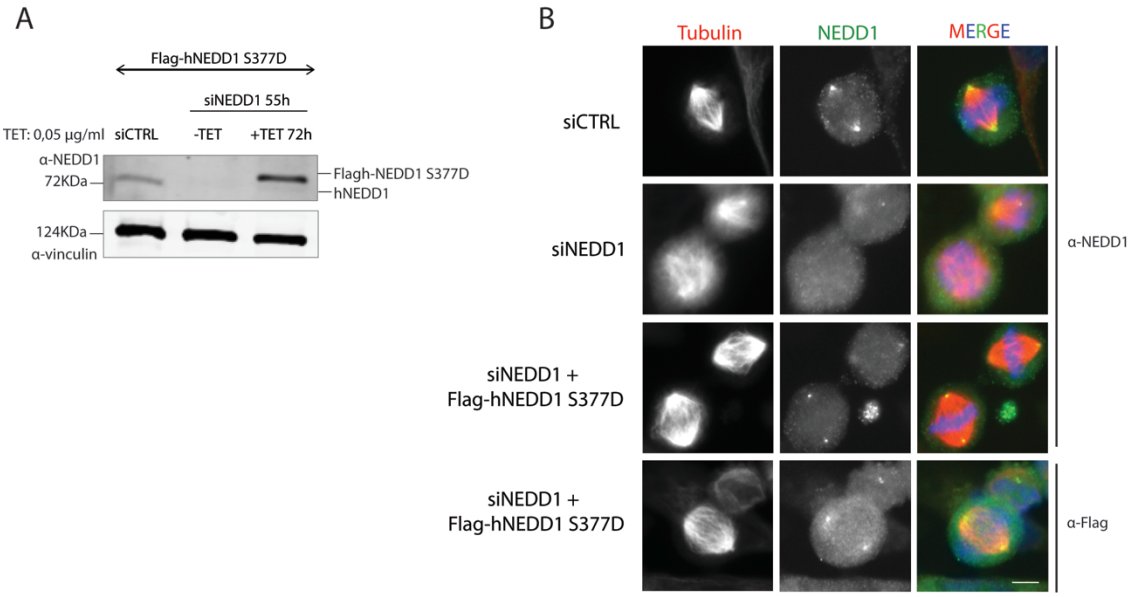
A
Flag-hNEDD1 S377D
siNEDD1 55h
TET: 0,05 µg/ml siCTRL -TET +TET 72h
α-NEDD1
72KDa
Flagh-NEDD1 S377D
hNEDD1
124KDa
α-vinculin
B
Tubulin
NEDD1
MERGE
siCTRL
siNEDD1
siNEDD1 +
Flag-hNEDD1 S377D
siNEDD1 +
Flag-hNEDD1 S377D
α-NEDD1
α-Flag

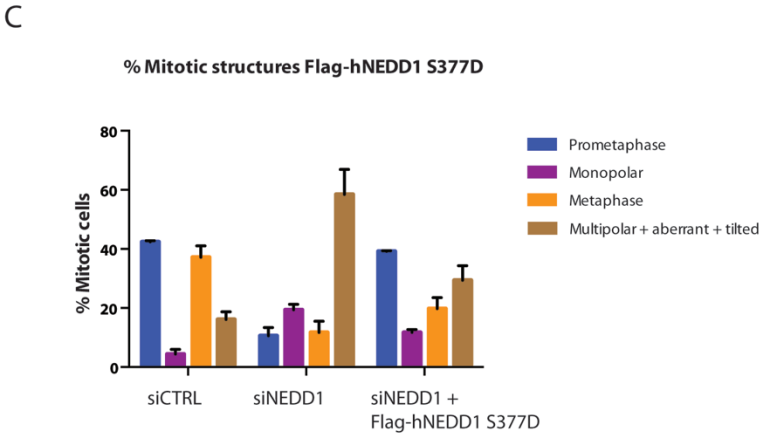
C
% Mitotic structures Flag-hNEDD1 S377D
% Mitotic cells
80
60
40
20
0
siCTRL
siNEDD1
siNEDD1 +
Flag-hNEDD1 S377D
Prometaphase
Monopolar
Metaphase
Multipolar + aberrant + tilted

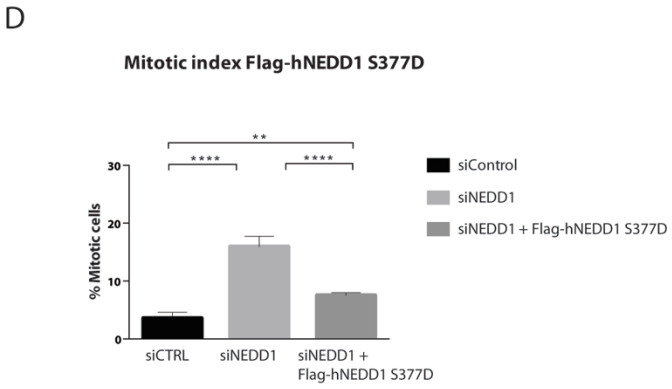
D
Mitotic index Flag-hNEDD1 S377D
% Mitotic cells
30
20
10
0
**
****
****
siCTRL
siNEDD1
siNEDD1 +
Flag-hNEDD1 S377D
siControl
siNEDD1
siNEDD1 + Flag-hNEDD1 S377D

Figure 34: Functional characterization of the single phosphorylation-mimicking mutant S377D.

A) Western blot showing the silencing levels of endogenous NEDD1 and the expression levels of exogenous Flag-hNEDD1 S377D in a typical rescue experiment. **B)** Representative immunofluorescence images showing the localization of endogenous and exogenous NEDD1 in mitotic cells. The first row of the panel shows the localization of NEDD1 in control cells. The second row of the panel shows the localization of NEDD1 in silenced cells. The third row of the panel shows the localization of NEDD1 in silenced cells expressing Flag-hNEDD1 S377D and the last row of the panel shows the localization of exogenous Flag-hNEDD1 S377D in silenced cells. Tubulin is shown in red, NEDD1 in green and DNA in blue. Scale bar 5μm. **C)** Quantification of the mitotic structures. Three replicas with ≈200 cells quantified per condition and experiment were performed. Columns represent the average percentage of cells in each category. Standard deviation between replicas is represented with a line on top of each column. **D)** Quantification of the mitotic index. >1000 cells per condition were counted. The plot shows the average of three independent experiments. Standard deviation between replicas is represented with a line on top of each column. Two-way ANOVA test: ns, non-significant differences. ** indicates p-value = 0,0054; **** indicates p-value<0,0001.

VII.C- Functional characterization of the single phosphorylation-mimicking mutant S411D

Some of the consequences of expressing a single phosphorylation null mutant S411A were already described (Johmura et al., 2011; Lüders et al., 2006) but the effects of expressing a phosphorylation mimicking mutant on that particular residue in NEDD1 silenced cells were not reported. Therefore, I followed the same experimental approach to explore the phenotype of the last single phospho-mimicking mutant: The S411D mutant.

I performed western blot to analyze the silencing and expression levels of the protein. Figure 35A shows a good silencing efficiency of endogenous NEDD1 and high expression levels of exogenous Flag-hNEDD1 S411D. I then looked at NEDD1 localization in mitotic cells expressing this phospho-mimicking mutant (Figure 35B). Interestingly, NEDD1 localized only to the centrosomes and not to the spindle microtubules in both monopolar and bipolar spindles from cells expressing Flag-hNEDD1 S411D. This specific centrosomal localization was confirmed by staining with α-Flag antibodies.

From this initial observation I could already notice that silenced cells expressing Flag-hNEDD1 S411D cells were arrested in a prometaphase-like state. I quantified the distribution of the mitotic structures in silenced cells expressing Flag-hNEDD1 S411D (Figure 35C). The graph shows that the majority of silenced cells expressing the S411D mutant arrested in mitosis forming monopolar (≈23%) and aberrant structures (≈41%). In agreement with this distribution, Flag-hNEDD1 S411D induced cells showed a reduced number of metaphases and prometaphases (≈18%) compared with control cells (≈34% and ≈47% respectively). This result suggested that, in contrast to the other two single phospho-mimicking mutants S377D and S405D, expression of Flag-hNEDD1 S411D highly interfered with normal mitotic progression and did not rescue the NEDD1 silencing detrimental phenotype.

This hypothesis was further confirmed with the quantification of the mitotic index (Figure 35D). Silenced cells expressing the 411D mutant presented an accumulation of mitosis, reaching a mitotic index of approximately 17%, similarly to NEDD1 silenced cells. This lack of rescue in the NEDD1 silencing phenotype was evident from the non-significant

differences between NEDD1 silenced cells and silenced cells expressing Flag-hNEDD1 S411D.

Collectively, the data indicated that the overexpression of Flag-hNEDD1 S411D was not sufficient to recover the mitotic defects due to the lack of endogenous NEDD1, precluding the formation of functional bipolar spindles.

I examined Flag-hNEDD1 S411D migration pattern in SDS-PAGE (Figure 35E). Endogenous NEDD1 was phosphorylated in mitosis, exhibiting an upper band corresponding to the phosphorylated fraction of NEDD1 that was reduced upon treatment with lambda phosphatase. Exogenous Flag-hNEDD1 S411D migrated both in asynchronous and mitotic conditions as a band that was higher than phosphorylated endogenous mitotic NEDD1. This migration is similar to the phosphorylated Flag-hNEDD1 WT. As previously suggested, the data indicated that the introduction of an aspartic acid in the site 411 is responsible for the shift, meaning that either phosphorylation or changing the amino acid in the residue 411 produces the mobility shift. However, in the mitotic lysates there was a small smear that disappeared upon treatment with phosphatase indicating that the protein is phosphorylated.

Altogether, the data supported the hypothesis of S411 as a critical residue for NEDD1 function.

Figure 35: Functional characterization of the single phosphorylation-mimicking mutant S411D.
A) Western blot showing the silencing levels of endogenous NEDD1 and the expression levels of exogenous Flag-hNEDD1 411D in a typical rescue experiment. **B)** Representative immunofluorescence images showing the localization of endogenous and exogenous NEDD1 in mitotic cells. The first row of the panel shows the localization of NEDD1 in control cells. The second row of the panel shows the localization of NEDD1 in silenced cells. The third row of the panel shows the localization of NEDD1 in silenced cells expressing Flag-hNEDD1 411D and the last row of the panel shows the localization of exogenous Flag-hNEDD1 411D in silenced cells. Tubulin is shown in red, NEDD1 in green and DNA in blue. Scale bar 5µm. **C)** Quantification of the mitotic structures. Three replicas with ≈200 cells quantified per condition and experiment were performed. Columns represent the average percentage of cells in each category. Standard deviation between replicas is represented with a line on top of each column. **D)** Quantification of the mitotic index. >1000 cells per condition were counted. The plot shows the average of three independent experiments. Standard deviation between replicas is represented with a line on top of each column. Two-way ANOVA test: ns, non-significant differences. ** indicates p-value = 0,0011, *** indicates p-value=0,0005. **E)** Western blot showing NEDD1 in asynchronous and mitotic cells collected by shake-off after an overnight nocodazole block at 0,33µM. Flag-hNEDD1 411D induced cells were incubated with tetracycline at 1µg/ml during 24h and λ-Phosphatase was added for 30 minutes when indicated.

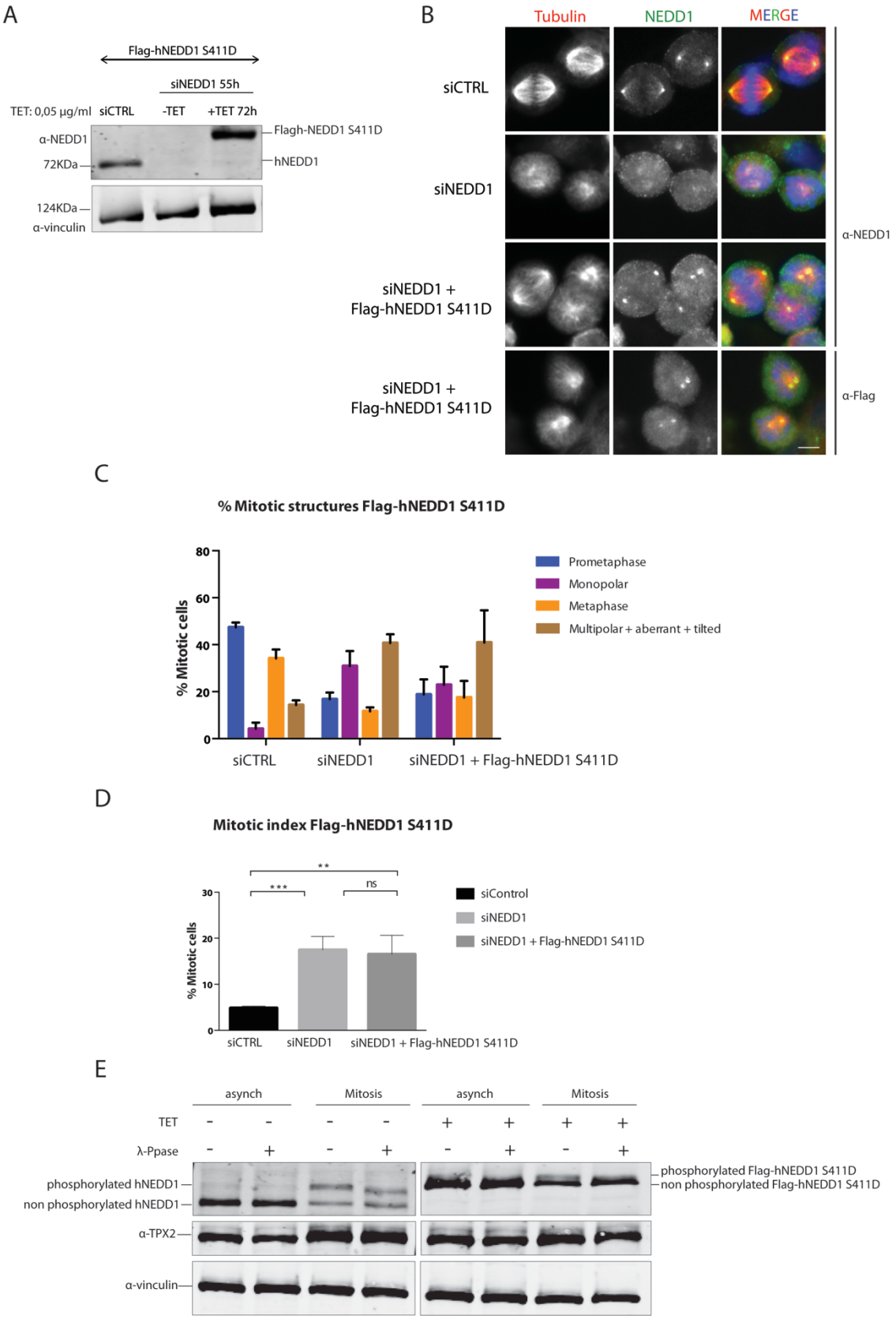
A
Flag-hNEDD1 S411D
siNEDD1 55h
TET: 0,05 µg/ml siCTRL -TET +TET 72h
α-NEDD1
72KDa
Flagh-NEDD1 S411D
hNEDD1
124KDa
α-vinculin
B
Tubulin
NEDD1
MERGE
siCTRL
siNEDD1
siNEDD1 + Flag-hNEDD1 S411D
siNEDD1 + Flag-hNEDD1 S411D
α-NEDD1
α-Flag
C
% Mitotic structures Flag-hNEDD1 S411D
% Mitotic cells
Prometaphase
Monopolar
Metaphase
Multipolar + aberrant + tilted
siCTRL
siNEDD1
siNEDD1 + Flag-hNEDD1 S411D
D
Mitotic index Flag-hNEDD1 S411D
% Mitotic cells
siControl
siNEDD1
siNEDD1 + Flag-hNEDD1 S411D
E
asynch
Mitosis
asynch
Mitosis
TET
λ-Ppase
phosphorylated hNEDD1
non phosphorylated hNEDD1
α-TPX2
α-vinculin
phosphorylated Flag-hNEDD1 S411D
non phosphorylated Flag-hNEDD1 S411D

VII.D- Functional characterization of the single phosphorylation-mimicking mutant S411E

The aspartic acid has been frequently used to mimic phosphorylation in proteins but in some cases it does not work. As an alternative, I mutagenized the S411 to a glutamic acid that has been used to simulate phosphorylation. I generated a new stable inducible cell line expressing the S411E mutant and I characterized its mitotic phenotypes.

Figure 36A shows good silencing levels of endogenous protein and high expression levels of exogenous Flag-hNEDD1 S411E protein.

Then, I performed immunofluorescence to examine the localization of NEDD1 in fixed cells expressing this second phospho-mimicking version S411E (Figure 36B). Interestingly, exogenous Flag-hNEDD1 S411E localized in a dot-like manner only to the centrosomes and not to the spindle microtubules. This result is in agreement with the observed NEDD1 localization in cells expressing the aspartic mutant S411D.

I then looked at the distribution of the mitotic phases (Figure 36C). Silenced cells expressing Flag-hNEDD1 S411E arrested in mitosis very similarly distributed to NEDD1 silenced cells. The graph shows comparable percentages of monopolar structures between these two categories, 32% in NEDD1 silenced cells versus 26% in silenced cells expressing Flag-hNEDD1 S411E. The number of aberrant structures was higher in silenced cells expressing the mutant (close to 50%) than in NEDD1 silenced cells (≈40%) and the number of prometaphase and metaphases (around 13%) was also not rescued with expression of S411E mutant. The data indicated that expression of a glutamic phospho-mimicking mutant was not sufficient to rescue NEDD1 silencing mitotic defects.

I confirmed this result by quantifying the number of mitotic cells (Figure 36D). I found that the mitotic index of silenced cells expressing the glutamic mutant was very similar to that of NEDD1 silenced cells, around a 20%, indicating that expression of Flag-hNEDD1 S411E did not rescue the NEDD1 silencing phenotype. In fact, statistical analysis showed non-significant differences between NEDD1 silenced and silenced cells expressing Flag-hNEDD1 S411E.

Altogether, the results confirmed that both aspartic and glutamic phospho-mimicking mutants did not support bipolar spindle assembly; cells expressing any of these mutants arrested in mitosis exhibiting a very similar phenotype with an accumulation of

monopolar and aberrant mitotic structures. I could conclude that the detrimental phenotypes observed in mitotic Flag-hNEDD1 S411D/E induced cells may not be caused by the change to a specific amino acid. However, it is difficult to define whether it is really due to a phospho-mimicking effect or to the introduction of a different amino acid at this specific position in the protein.

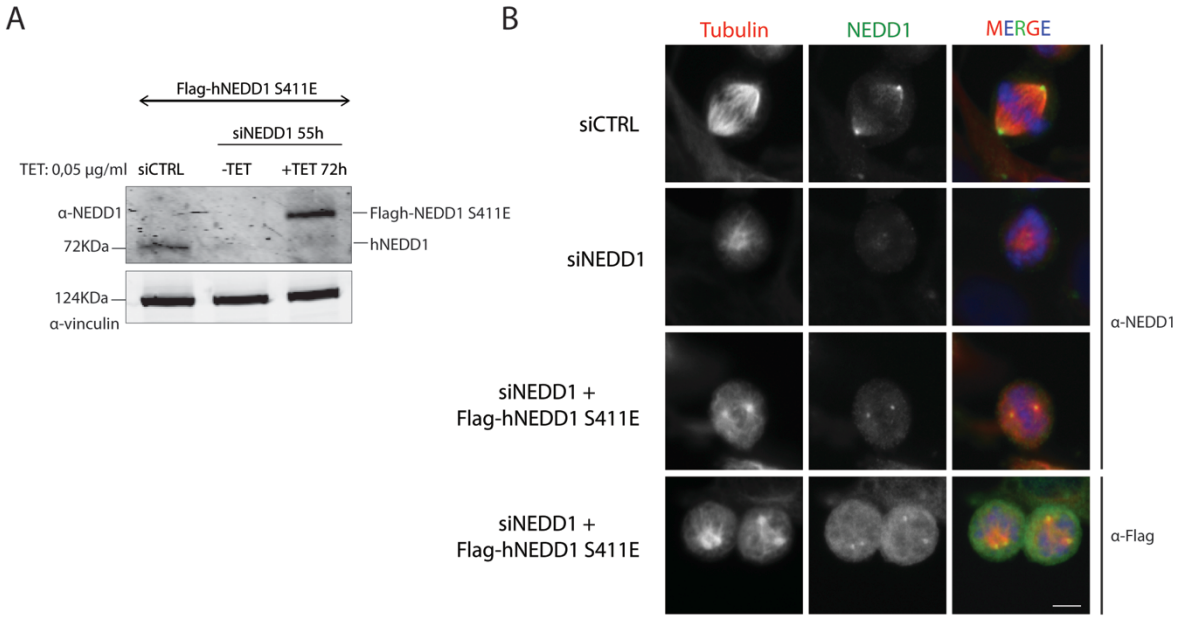
A
Flag-hNEDD1 S411E
siNEDD1 55h
TET: 0,05 µg/ml siCTRL -TET +TET 72h
α-NEDD1
72KDa
Flagh-NEDD1 S411E
hNEDD1
124KDa
α-vinculin
B
Tubulin
NEDD1
MERGE
siCTRL
siNEDD1
siNEDD1 +
Flag-hNEDD1 S411E
siNEDD1 +
Flag-hNEDD1 S411E
α-NEDD1
α-Flag

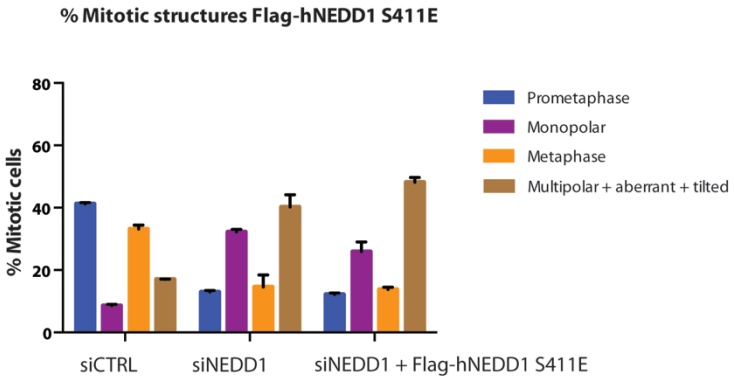
C
% Mitotic structures Flag-hNEDD1 S411E
% Mitotic cells
80
60
40
20
0
Prometaphase
Monopolar
Metaphase
Multipolar + aberrant + tilted
siCTRL
siNEDD1
siNEDD1 + Flag-hNEDD1 S411E

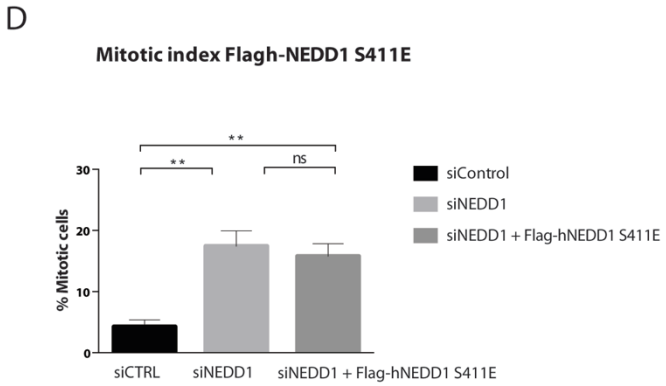
D
Mitotic index Flagh-NEDD1 S411E
% Mitotic cells
30
20
10
0
**
**
ns
siControl
siNEDD1
siNEDD1 + Flag-hNEDD1 S411E
siCTRL
siNEDD1
siNEDD1 + Flag-hNEDD1 S411E

Figure 36: Functional characterization of the single phosphorylation-mimicking mutant S411E.
A) Western blot showing the silencing levels of endogenous NEDD1 and the expression levels of exogenous Flag-hNEDD1 S411E in a typical rescue experiment. **B)** Representative immunofluorescence images showing the localization of endogenous and exogenous NEDD1 in mitotic cells. The first row of the panel shows the localization of NEDD1 in control cells. The second row of the panel shows the localization of NEDD1 in silenced cells. The third row of the panel shows the localization of NEDD1 in silenced cells expressing Flag-hNEDD1 S411E and the last row of the panel shows the localization of exogenous Flag-hNEDD1 S411E in silenced cells. Tubulin is shown in red, NEDD1 in green and DNA in blue. Scale bar 5µm. **C)** Quantification of the mitotic structures. Three replicas with ≈200 cells quantified per condition and experiment were performed. Columns represent the average percentage of cells in each category. Standard deviation between replicas is represented with a line on top of each column. **D)** Quantification of the mitotic index. >1000 cells per condition were counted. The plot shows the average of three independent experiments. Standard deviation between replicas is represented with a line on top of each column. Two-way ANOVA test: ns, non-significant differences. ** indicates p-value = 0,0014 between control and NEDD1 silenced cells and p-value = 0,0028 between control and NEDD1 silenced cells expressing Flag-hNEDD1 S411E.

VII.E- Phospho-mutant localization and γ-tubulin recruitment to the centrosomes

The unexpected phenotype of Flag-hNEDD1 NEDD1 S411 phosphorylation mutants made us wonder about the functionality of the exogenous Flag-hNEDD1 protein when mutated at this specific S411 residue. To investigate if the Flag-hNEDD1 S411A/D protein was active in centrosomal nucleation or if it was an unfolded/inactive protein, I looked at the recruitment of these proteins to the centrosome and whether they could recruit γ-tubulin to the centrosomes.

We had previously observed that both S411A/D mutants localize to the centrosomes (Figures 27B and 35B). To further confirm these data quantitatively, I looked at their recruitment to the centrosomes in silenced cells during microtubule regrowth. Cells were fixed after five minutes of nocodazole release. I then performed immunofluorescence and quantified NEDD1 signal at centrosomal asters using Fiji. Figure 37A-D shows that NEDD1 signal is strongly reduced at the centrosomes after silencing endogenous NEDD1, as expected. Expression of Flag-hNEDD1 S411A rescued the recruitment of NEDD1 to the centrosomes, although to lower levels than control cells (Figures 37A and 37C). Expression of Flag-hNEDD1 S411D rescued NEDD1 fluorescence intensity to levels comparable to control cells (Figures 37B and 37D).

I then quantified the γ-tubulin fluorescence intensity at the centrosomes of fixed control, NEDD1 silenced cells and silenced cells expressing Flag-hNEDD1 S411A (Figure 37E). The graph shows a reduction in γ-tubulin intensity from control to NEDD1 silenced cells,

indicating the loss of γ-tubulin localization to the centrosomes upon NEDD1 silencing, as it was previously shown (Haren et al., 2006; Lüders et al., 2006). Interestingly, the loss of γ-tubulin recruitment was rescued upon expression of the S411A mutant, as the fluorescence intensity at the centrosomes of cells expressing this mutant was recovered to control levels. Indeed, statistical analysis confirmed that there were no significant differences in γ-tubulin fluorescence between control and silenced cells expressing Flag-hNEDD1 S411A.

I performed the same experimental approach to quantify γ-tubulin fluorescence intensity in mitotic cells expressing the phospho-mimicking mutant S411D (Figure 37F). The loss of γ-tubulin recruitment to the centrosomes upon NEDD1 silencing was only partially rescued by expression of the S411D mutant, although the mutant was efficiently recruited to the centrosomes. This suggested that it is not very active for recruiting γ-tubulin.

Altogether, the results (although preliminary) suggested that the S411A mutant is at least partially active, since it retains an essential NEDD1 activity. However, introducing an aspartic acid at position 411 may affect NEDD1 functionality.

Figure 37: NEDD1-S411A/D phosphorylation mutants localize to the centrosome and recruit γ-tubulin.
A) Quantification of NEDD1 fluorescence intensity in the asters of control, silenced and silenced cells expressing Flag-hNEDD1 S411A subjected to a microtubule regrowth experiment. At the end of a typical rescue experiment (55h of siRNA transfection and 72h of tetracycline induction) cells were subjected to microtubule regrowth and fixed for NEDD1 5 min after nocodazole washout. The fluorescence intensity of ≈ 50 centrosomal asters per condition was quantified. **B)** Quantification of NEDD1 fluorescence intensity in the asters of control, silenced and silenced cells expressing Flag-hNEDD1 S411D subjected to a microtubule regrowth experiment. At the end of a typical rescue experiment (55h of siRNA transfection and 72h of tetracycline induction) cells were subjected to microtubule regrowth and fixed for NEDD1 5 min after nocodazole washout. The fluorescence intensity of ≈45 centrosomal asters per condition was quantified. **C)** Representative immunofluorescence microscopy images of microtubule asters in cells corresponding to experiment A). Samples were stained for NEDD1, tubulin and DNA. **D)** Representative immunofluorescence microscopy images of microtubule asters in cells corresponding to experiment B). NEDD1 (green), tubulin (red) and DNA (blue). Scale bar 5µm. **E)** Quantification of γ-tubulin fluorescence intensity in control, silenced and silenced cells expressing Flag-hNEDD1 S411A. At the end of a typical rescue experiment (55h of siRNA transfection and 72h of tetracycline induction) cells were fixed and stained for γ-tubulin. γ-tubulin fluorescence intensity was determined by quantifying the fluorescence intensity of a determined area for each centrosome. ≈ 30 centrosomes were quantified per condition. **F)** Quantification of γ-tubulin fluorescence intensity in control, silenced and silenced cells expressing Flag-hNEDD1 S411D. At the end of a typical rescue experiment (55h of siRNA transfection and 72h of tetracycline induction) cells were fixed and stained for γ-tubulin. γ-tubulin fluorescence intensity was determined by quantifying the fluorescence intensity of a determined area for each centrosome. ≈ 35 centrosomes were quantified per condition. Box-and-whisker plot: boxes show values between the 25th and the 75th quartiles, with a line at the median and a cross (+) at the mean, whiskers extend from the 10th to the 90th percentiles and dots correspond to outliers. One-way ANOVA test: ns, non-significant differences. **** indicates p-value<0,0001.

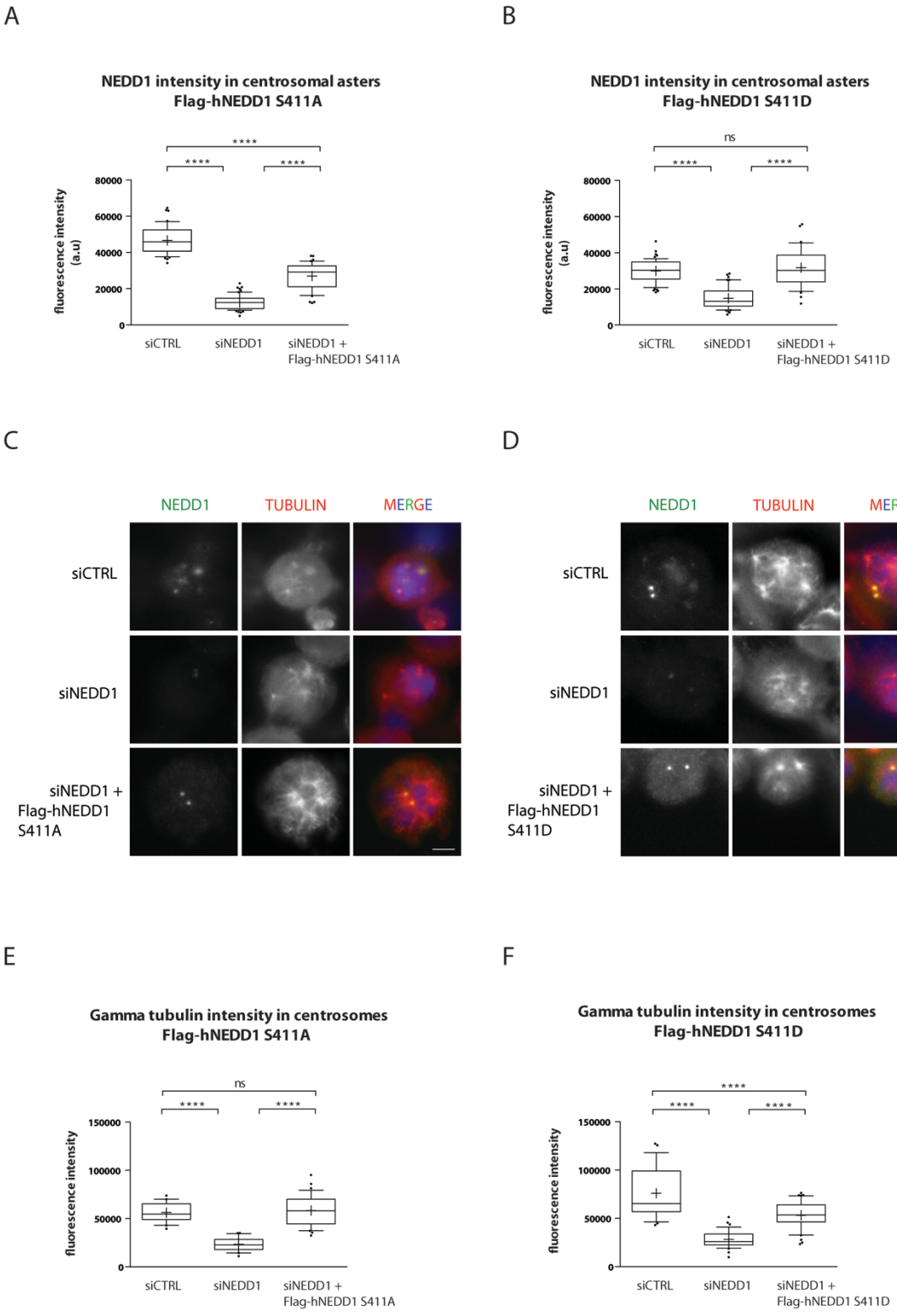
A
NEDD1 intensity in centrosomal asters
Flag-hNEDD1 S411A
fluorescence intensity (a.u)
80000
60000
40000
20000
0
****
****
****
siCTRL
siNEDD1
siNEDD1 + Flag-hNEDD1 S411A
B
NEDD1 intensity in centrosomal asters
Flag-hNEDD1 S411D
fluorescence intensity (a.u)
ns
****
****
siCTRL
siNEDD1
siNEDD1 + Flag-hNEDD1 S411D
C
NEDD1
TUBULIN
MERGE
siCTRL
siNEDD1
siNEDD1 + Flag-hNEDD1 S411A
D
NEDD1
TUBULIN
MERGE
siCTRL
siNEDD1
siNEDD1 + Flag-hNEDD1 S411D
E
Gamma tubulin intensity in centrosomes
Flag-hNEDD1 S411A
fluorescence intensity
150000
100000
50000
0
ns
****
****
siCTRL
siNEDD1
siNEDD1 + Flag-hNEDD1 S411A
F
Gamma tubulin intensity in centrosomes
Flag-hNEDD1 S411D
fluorescence intensity
150000
100000
50000
0
****
****
****
siCTRL
siNEDD1
siNEDD1 + Flag-hNEDD1 S411D

VII.F- Function of the chromosomal microtubule nucleation pathway in NEDD1-S411A/D phosphorylation mutants

Phosphorylation study of NEDD1 protein: Mass spectrometry analysis of Flag-hNEDD1 WT protein

As expression of the triple phosphorylation-null mutant AAA resulted in a very detrimental phenotype, we wondered if the phosphorylation on the 411 was absolutely necessary for the others to take place. Our preliminary data suggested that expressing either a phospho-null or a phospho-mimicking mutant S411A/D did not affect the centrosomal microtubule nucleation pathway but the nucleation around the chromatin upon expression of both mutants was not explored. The phosphorylation at the S405 is the one triggering the chromosomal pathway and we wanted to check if the expression of S411A/D mutants could affect this pathway by preventing NEDD1 phosphorylation at S405. In order to investigate this question, we decided to first examine the phosphorylation state of Flag-hNEDD1 by using mass spectrometry.

We first looked at the phosphorylation state of Flag-hNEDD1 pulled down from mitotic cell lysates expressing Flag-hNEDD1 WT, as we expected it to be phosphorylated at S377, S405 and S411. We performed a Flag-hNEDD1 WT pulldown from cells synchronized in mitosis, run the eluted protein in a SDS-8% acrylamide gel, cut the band corresponding to the phosphorylated version of Flag-hNEDD1 WT and sent it to the proteomics facility for mass spectrometry analysis. The results from this experiment were not ideal because, although the peptides containing the residues S377, S405 and S411 were detected, only the phosphorylation on the S411 was identified (Figure 38).

Our analysis corroborated some NEDD1 phosphorylation sites previously described as S282, S397, S411 and S516 (Gomez-Ferreria et al., 2012a), although these four identified residues are only a small part of all the NEDD1 phosphorylation residues reported to date. As this experimental approach was not useful for the detection of the phosphorylation at S377 and S405 in cells expressing Flag-hNEDD1 WT, we did not further explore the phosphorylation state of mitotic cells expressing S411A/D mutants.

Figure 38: NEDD1 protein coverage and PTMs identified by Mass Spectrometry.

NEDD1 sequence and position of phosphorylated residues and other PTMs identified. Although NEDD1 coverage was quite high (≈63%) and it included the peptides containing the residues S377, S405 and S411; only the phosphorylation at S411 was detected.

VIII- Haus-6 localization in Flag-hNEDD1 S411A/D phosphorylation mutants

As an additional way of investigating the role of S411 phosphorylation in regulating NEDD1 function, I looked at the localization of one component of the Augmin complex, the Haus-6 subunit, in cells expressing both Flag-hNEDD1 S411A/E mutants.

I performed the usual experimental approach for a rescue experiment, silencing endogenous NEDD1 during 55h and expressing Flag-hNEDD1 S411A/E during 72h. I then performed immunofluorescence against Haus-6 and tubulin to observe Haus-6 localization and microtubule organization in mitotic cells. Figure 39 shows representative pictures of the mitotic figures found in each condition. First, I confirmed Haus-6 localization to the centrosomes and spindle microtubules in control cells as previously published (Zhu et al., 2008). Control cells presented strong Haus-6 staining all along the spindle and also to centrosomes. In NEDD1 silenced cells Haus-6 also decorated the microtubules and the centrosomes, in agreement with previous observations (Zhu et al., 2008). Interestingly, Haus-6 strongly localized to the disorganized microtubules and to the poles of aberrant spindles found in silenced cells expressing Flag-hNEDD1 S411E phospho-mimicking mutant. Haus-6 also localized to the spindle microtubules and spindle poles in cells expressing Flag-hNEDD1 S411A phospho-null mutant.

These observations suggested that the Augmin complex binds to the microtubules independently of NEDD1 and recruits it on the lattice of pre-existing microtubules to drive amplification.

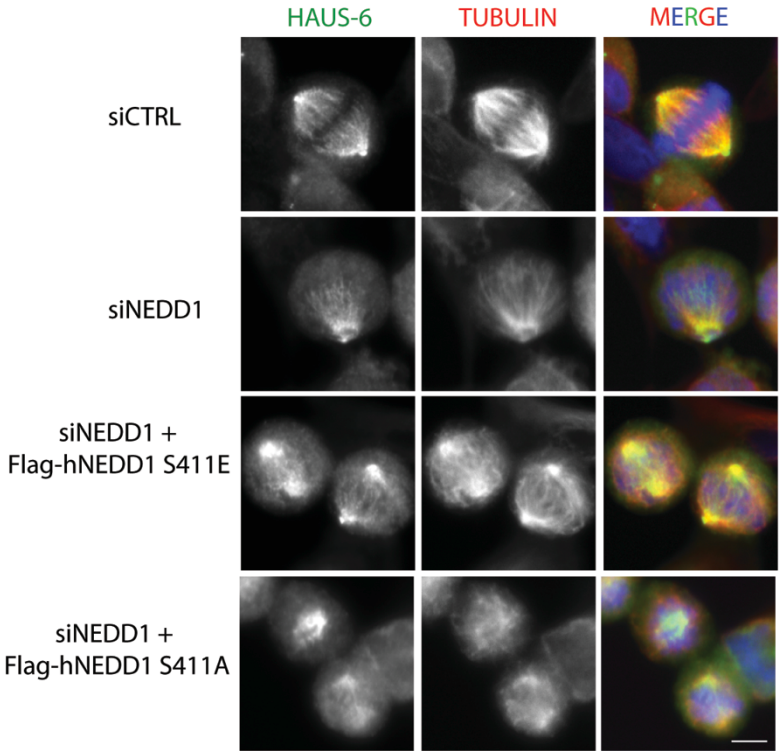

Figure 39: Haus-6 localizes to the centrosomes and spindle microtubules independently of NEDD1.

Cells were subjected to a typical rescue experiment (55h of siRNA transfection and 72h of tetracycline induction) and then were fixed and stained for Haus-6 (green), tubulin (red) and DNA (blue). The first row of the panel shows the localization of Haus-6 in control cells. The second row of the panel shows the localization of Haus-6 in NEDD1 silenced cells. The third row of the panel contains representative images of Haus-6 localization in cells expressing Flag-hNEDD1 S411E. The last row of the panel shows Haus-6 localization in cells expressing Flag-hNEDD1 S411A. Scale bar 5µm.

DISCUSSION

Several studies have addressed the role of centrosomes, chromosomes or microtubule amplification in spindle assembly. Most of them focused on one of the corresponding pathways and, therefore, a global understanding on the mechanism leading to their integration to assemble the bipolar spindle is still missing.

In summary, the main conclusions from these previous studies that are particularly relevant for this thesis are:

- Centrosomes: cells naturally build a bipolar spindle during meiosis without centrosomes. Eliminating the centrosome by laser ablation or through Plk4 activity interference does not impair spindle assembly, although it is less efficient (Khodjakov et al., 2000a; Lambrus et al., 2015; Wong et al., 2015).

- Microtubule amplification: silencing different subunits of the Augmin complex causes a reduction of microtubule density in the spindles and some organization defects depending on the system (Goshima et al., 2008; Lawo et al., 2009; Petry et al., 2011, 2013; Uehara et al., 2009).

- Chromosomes: interfering with microtubule nucleation through the chromosomal Ran-GTP dependent pathway (for example by silencing TPX2), impairs spindle assembly (Gruss et al., 2001, 2002; Tulu et al., 2006). However, this could also result from other functions of TPX2 in spindle assembly.

The data come from work performed by different groups, in distinct biological systems and with various experimental approaches. To gain a full understanding of how these pathways cooperate to support spindle assembly it is therefore important to obtain data in one system and with the same experimental approach. We decided to use NEDD1 phosphorylation as a way to alter specifically microtubule nucleation in a similar way for each of the pathways. In principle, it also offered the possibility to design specific combinations of activation/inactivation of microtubule nucleation.

I- Establishing an inducible system in tissue culture cells

To unravel the specific contribution of the different microtubule nucleation pathways activated in dividing cells (centrosomal, chromosomal and Augmin-mediated) to the assembly of the mitotic spindle we established a tetracycline inducible system. This system allowed the controlled expression of different phosphorylation variants of NEDD1 in NEDD1-silenced cells. The establishment of such a system was not trivial and required many optimization steps. However, the advantages of the system are many: first, it allows the manipulation of the pathways by "switching them-on and off" individually or in combination in the absence of the endogenous protein. Second, it allows to control the expression level of the exogenous protein simply by changing the concentration of tetracycline and the time of expression thus providing a better control than transient expression. Third, all cell lines are generated in the same parental cell line and therefore there should not be variations due to different experimental conditions.

In fact, as all the NEDD1 variants were generated in the same parental HeLa-FRT/TR cell line, we expected to obtain similar silencing efficiencies and exogenous protein expression levels in all cell lines. However, this was not always the case. Control cells for all cell lines did show only small variations in the distribution of the mitotic structures but their growth rates, cell morphologies and silencing efficiencies were not similar for all cell lines. Differences in the silencing efficiency for each particular cell line were reflected in distinct variations in the mitotic index and in the number of monopolar and aberrant mitotic structures. Moreover, we noticed that the expression of the different NEDD1 phospho-variants somehow affected endogenous NEDD1 levels, either by interfering with the silencing efficiency or by promoting endogenous NEDD1 stabilization.

Instead of trying to optimize conditions for each cell line we decided to perform all the experiments following the protocol we optimized for NEDD1 silencing and rescue by expression of NEDD1-WT protein. It is important to take into account that each NEDD1 variant has its own internal control, which is the non-silenced and non-induced stable cell line.

Optimizing the conditions for the rescue of the NEDD1 silencing phenotype with the controlled expression of the exogenous Flag-hNEDD1 WT was complicated and took

more time than initially expected. Indeed, we tried many different experimental conditions to obtain a satisfactory level of rescue (detailed in the results section).

Several factors could be behind the difficulties in optimizing the rescue. We initially aimed at getting levels of exogenous NEDD1 close to endogenous levels. We obtained curves for endogenous protein levels upon silencing and for exogenous protein expression levels after induction. We then selected the tetracycline concentration and induction time that resulted in levels of exogenous protein similar to the endogenous one. However, under these conditions the rescue was only partial; one possibility is that the exogenous NEDD1-WT was only partially active and therefore the cells needed a higher level of expression to rescue NEDD1 function. However, since raising exogenous NEDD1 levels required longer incubation times, this resulted in more detrimental defects due to the increased silencing time and it was complicated to find the right balance between silencing and overexpression levels. We therefore reasoned that expression of NEDD1-WT should be induced before the levels of endogenous NEDD1 were reduced by silencing. Such a condition would be more similar to rescue experiments performed by transient expression of exogenous protein in silenced cells.

Indeed, we finally found that inducing exogenous NEDD1 expression before silencing provided optimal conditions for rescuing NEDD1 silencing.

II- Control of microtubule nucleation through NEDD1 phosphorylation at S377, S405 and S411

Based on the literature, our initial hypothesis was that each of the three phosphorylation events at S377, S405 and S411 individually controls one specific microtubule assembly pathway. Thereby we could dissect the role of each pathway in spindle assembly by modifying these sites individually or in combination.

In general, our work on the NEDD1-S377A expressing cells is consistent with published data and its role in centrosomal microtubule nucleation. Similarly, we also obtained consistent results regarding the mutants S405A and S411A although I will review the phenotypes of these two mutants in more detail later in the discussion.

However, our results suggest that the 411 site may not be specifically associated with the activation of the Augmin pathway.

II.A- Phosphorylation at the S411 and the Augmin pathway

Previous results showed that expression of NEDD1-S411A led to aberrant spindle morphologies with a reduced microtubule density in the spindle and an increase of the mitotic index (Johmura et al., 2011; Lüders et al., 2006). In addition, NEDD1-S411A was shown to localize only to the centrosomes and not to the spindle microtubules (Lüders et al., 2006; Pinyol et al., 2013). On the other hand, NEDD1-S411A was shown to be unable to pull down proteins from the Augmin complex like endogenous NEDD1 (Johmura et al., 2011; Uehara et al., 2009), suggesting that phosphorylation at this specific residue was essential for this interaction and the Augmin-dependent microtubule amplification pathway.

In agreement with these data, we also found that NEDD1-S411A localized only to the centrosomes. However, the phenotypes of NEDD1-silenced cells expressing NEDD1-S411A were more deleterious in our system than previously described. In fact, the phenotype of these cells was as detrimental as the lack of endogenous NEDD1 with a block in mitosis progression and an accumulation of aberrant mitotic structures.

We expected that expression of a phospho-mimicking version S411D should rescue the mitotic defects associated with the silencing and expression of the S411A mutant, an experiment not reported previously. Unexpectedly, cells expressing the S411D mutant exhibited a very detrimental phenotype similar to that of NEDD1-silenced cells; expression of NEDD1-S411D highly interfered with normal mitotic progression and impaired functional bipolar spindle assembly.

To try to rule out that this was due specifically to the introduction of an aspartic acid amino acid, we expressed a different phosphorylation mimicking mutant: S411E. The phenotype of cells expressing this mutant was identical to that of NEDD1-silenced cells expressing NEDD1-S411D: the majority of cells were blocked in mitosis presenting an accumulation of monopolar and aberrant mitotic structures.

Altogether, the results confirmed that changing S411 to another amino acid interferes strongly with bipolar spindle assembly.

However, the reasons behind these detrimental phenotypes were not clear: is S411 a critical site that needs to be phosphorylated for NEDD1 to be functional in mitosis? Has the introduction of an aspartic (D) or a glutamic (E) acid an effect on the structural conformation of NEDD1? Maybe the presence of a D/E induces a conformational change in the protein that abrogates its function in mitosis. Regarding this last possibility, it would be useful to have the crystal structure of NEDD1 and analyze the position of the 411 amino acid in the core 3D structure. S411 is positioned after the WD40 N-terminal domain not very far away from the other two sites we have investigated S377 and S405. Yet the consequences of changing S411 to A or D/E were more detrimental than changing S377 or S405 to A, suggesting that more than its position in NEDD1 structure, S411 may be particularly important for NEDD1 function.

In fact, several data indicate that NEDD1 oligomerizes (Manning et al., 2010). Moreover, its C-terminal region that is required for interaction with γ-tubulin (Manning et al., 2010) has been shown to form a tetrameric helical coiled-coil structure. Phosphorylation at the 411 site may play a role in NEDD1 oligomerization, a question that remains unexplored. Disruption of 411 site could affect the folding of the protein or perturb its oligomerization that might be important for the recruitment of γ-tubulin.

To test whether the NEDD1-S411A/D could really fully interfere with NEDD1 activity as expected if the structure is fundamentally altered, we tested whether NEDD1-S411A and S411D retained some basic activities such as the recruitment of γ-tubulin to the centrosomes in mitosis. Indeed, both mutants localized to the centrosome and recruited γ-tubulin. However, preliminary data indicate that NEDD1-S411D was less efficient than NEDD1-S411A in such activity.

To further test proper centrosomal activity in cells expressing these mutants, we looked at NEDD1 recruitment to the centrosomes during microtubule regrowth conditions. Again, both NEDD1-S411A/D mutants localized to the centrosomes. However, preliminary data indicate that NEDD1-S411A recruited NEDD1 less efficiently than the S411D mutant.

Altogether, these data suggest that the substitution of S411 by an alanine (A) may not be fundamentally detrimental for NEDD1 organization. In fact, S411 is most probably

phosphorylated by Cdk1 and not phosphorylated in interphase when NEDD1 is also active.

On the other hand, the minimal capacity of NEDD1-S411D in recruiting γ-tubulin to the centrosome suggests that this protein is not fully functional beyond any specific phosphorylation effect. Actually, there are several examples in the literature showing that these substitutions are not always successful in mimicking phosphorylation.

Our data therefore indicate that S411 may have an important role in NEDD1 structure/function, not always related to its phosphorylation. Although NEDD1-S411A may provide the evidence for the essential role of S411 phosphorylation in NEDD1 function in mitosis, it is not clear that this function is to promote interaction with Augmin and thus the activation of microtubule amplification specifically. Indeed, the phenotype of NEDD1-S411A is as detrimental as NEDD1 silencing and much worse than Augmin silencing.

Altogether, S411 phosphorylation may not be specific for the Augmin-dependent microtubule amplification pathway. Therefore, the study of NEDD1 phosphorylation at S411 site is not a useful tool to investigate the specific contribution of Augmin to spindle assembly.

II.B- Phosphorylation at S377 and S405 are important for spindle assembly

The phenotypes of the different NEDD1 phospho-variants on S377 and S405 showed similarities with previously published observations but also some differences.

Previous data showed that expression of NEDD1-S377A in HeLa cells resulted in the loss of γ-tubulin recruitment to the centrosome in prophase as well as a mitotic arrest in prometaphase (Sdelci et al., 2012). I observed a similar phenotype upon expression of NEDD1-S377A in NEDD1-silenced cells. These cells had an elevated mitotic index and I found that there was an accumulation of monopolar and aberrant mitotic structures. However, expressing this mutant was not as detrimental for the cells as the lack of NEDD1, in contrast with published observations (Sdelci et al., 2012). Indeed, the mitotic index of NEDD1-S377A expressing cells was intermediate between that of control and

NEDD1-silenced cells (Figure 25D), whereas in the previous report it was even higher than for silenced cells (Sdelci et al., 2012).

On the other hand, our work provides for the first time data on the rescue of NEDD1 silencing by expressing a phospho-mimicking mutant S377D. I found that NEDD1-S377D improved substantially mitotic spindle assembly in NEDD1-silenced cells and lowered the mitotic index although not to control levels.

Unexpectedly, I could not detect NEDD1-S377A or NEDD1-S377D on the spindle microtubules. This had not been checked in previous reports and it suggests that the Augmin pathway may also be compromised when altering S377 phosphorylation.

Altogether, our data support that S377 phosphorylation is important for spindle assembly most probably by promoting microtubule nucleation at the centrosome but maybe also by altering microtubule-microtubule amplification through Augmin.

However, S377 phosphorylation may need to be regulated since NEDD1-S377A has apparently some function but NEDD1-S377D is not able to fully restore spindle assembly and mitotic progression.

Concerning S405 phosphorylation, it was previously shown that NEDD1-S405A did support bipolar spindle formation but chromosomes were scattered or misaligned and K-fibers were less stable (Pinyol et al., 2013). In contrast, our data indicate that expression of NEDD1-S405A interferes with mitotic progression promoting accumulation of aberrant mitotic structures and a high mitotic index. Previous studies reported that NEDD1-S405A localized to the centrosomes and to the spindle microtubules, a result that I was not able to reproduce as NEDD1-S405A localized only to the centrosomes in my experimental system.

These differences in NEDD1-S405A localization may be due to distinct levels of expression; transient transfection usually promotes high exogenous protein levels that may favor the localization at both centrosomes and microtubules. On the other hand, since in my experimental conditions most of the cells expressing NEDD1-S405A have aberrant mitotic structures with less microtubules, the detection of NEDD1-S405A on these remaining microtubules may be difficult.

Our results regarding NEDD1-S405D mutant are also in agreement with previous observations indicating a rescue of the mitotic defects upon NEDD1 silencing. The progression through mitosis was rescued with a mitotic index similar to control cells and cells expressing this mutant formed bipolar spindles. Moreover, NEDD1 localization to the spindle microtubules was also rescued, indicating proper targeting and function throughout the mitotic spindle of NEDD1-S405D.

The specific role for S405 phosphorylation in the chromosomal microtubule nucleation pathway has been dissected; NEDD1 phosphorylation on S405 by AurA (activated by TPX2) and the recruitment of a RHAMM-NEDD1-γ-TuRC complex onto a TPX2-dependent scaffold is essential for the activation of the Ran-GTP-dependent microtubule nucleation pathway. In fact, NEDD1-S405D was shown to be sufficient for microtubule nucleation in the absence of active AurA, indicating that NEDD1-S405 is the only AurA target essential for the Ran-GTP-dependent MT nucleation (Scrofani et al., 2015).

This information is in contrast with the phosphorylation at the S377, which has not been characterized in detail.

Altogether my data confirm that NEDD1-S405 phosphorylation is essential for spindle assembly. They indicate that it may not need to be regulated temporally since the constitutive phospho-mimicking mutant does fully rescue spindle assembly and mitotic progression. These data suggest a dominant role for the chromosomal pathway in ensuring the assembly of a functional spindle.

III- Temporal and spatial regulation of microtubule nucleation in mitosis

We reasoned that by abolishing or mimicking phosphorylation on the three sites by expressing NEDD1-AAA or NEDD1-DDD we could test the following two points:

- The role of the temporal regulation of the three pathways.
- The role of the spatial regulation of the three pathways.

Unfortunately, after discovering that the mutation at the S411 had a dominant negative effect, we could not make relevant conclusions from our studies using these triple

mutants. It could still be possible to study the contribution of centrosomal and chromosomal microtubule assembly pathways by generating NEDD1 phosphorylation mutants in which the 411 site is not affected.

However, the reasoning behind the use of these two mutants can be discussed. First, the effect of "switching-off/on" the three microtubule nucleation pathways at the same time had not been explored previously. Former reports indicated that "switching-off" a single pathway led to an unbalance effect that compromised correct bipolar spindle formation (Cavazza et al., 2016). Therefore, lowering the microtubule nucleation activity of the three pathways to the same levels might have re-balanced the system and we aimed at testing this hypothesis by expressing NEDD1-AAA. Second, even in the absence of NEDD1 there are still microtubules, although they are not able to organize a bipolar spindle thus leading to mitotic defects. Therefore, we reasoned that the presence of unregulated NEDD1 (by the expression of NEDD1-AAA) might partially rescue the NEDD1 silencing phenotype or at least improve the phenotype of silenced cells. This hypothesis was based on the results obtained for NEDD1-S377A and NEDD1-S405A; although they were not able to rescue the defects associated with NEDD1 silencing, cells had phenotypes not as detrimental as NEDD1-silenced cells. Therefore, with the expression of NEDD1-AAA we wanted to test whether a partial rescue of the NEDD1 silencing phenotype would occur. A partial rescue would have indicated additional functions for NEDD1 in spindle assembly.

Third, coinciding with the idea of a balance amongst the three pathways, another relevant point is the timing of activation of each pathway, which has been proposed to be important for spindle assembly (Cavazza et al., 2016). In fact, the cell naturally imposes a temporal regulation of microtubule nucleation through mitosis since centrosomes nucleate microtubules before nuclear envelope breakdown (NEBD) in G2; then, Ran-GTP dependent microtubule nucleation around the chromatin is only promoted after NEBD and microtubule-based nucleation occurs, probably after NEBD too. To date there are no studies addressing this issue directly. We aimed at doing this by having the three microtubule nucleation pathways constitutively active throughout cell division. In addition, since the phospho-mimicking NEDD1-S377D and S405D were able to rescue NEDD1 silencing defects, we expected a similar or even better rescue by expressing NEDD1-DDD. Such rescue would have indicated that the phosphorylation at the three

sites could occur simultaneously in the cell from the beginning of mitosis without having deleterious effects in spindle assembly. In fact, we observed phenotypes for both phospho-variants AAA/DDD at least as severe as the silencing ones.

These detrimental effects associated with the change of amino acid at the 411 site, however, precluded us from obtaining relevant conclusions on the regulation of microtubule nucleation in mitosis through the three sites (and the three pathways) using the AAA and DDD NEDD1 mutants.

Phosphorylation at the 411 residue is responsible for the migration shift of NEDD1 in mitosis

NEDD1 is highly phosphorylated in mitosis at least on 42 sites (Gomez-Ferreria et al., 2012c). This correlates well with its slow migrating form in SDS-PAGE versus interphase as shown previously (Haren et al., 2006, 2009; Lüders et al., 2006).

We also detected this shift in mitosis for the endogenous protein and the exogenously expressed NEDD1-WT.

Interestingly, the shift was unaffected when interfering with S377 or S405 phosphorylation. Instead, NEDD1-S411A did not exhibit this behavior, suggesting that S411 is in large part responsible for the shift of migration of NEDD1 in mitotic cell lysates.

In agreement with this idea, exogenous NEDD1-S411D migrated both in asynchronous and mitotic conditions as a band that was higher than phosphorylated endogenous mitotic NEDD1 and similar to that of phosphorylated Flag-hNEDD1 WT.

Additional experiments using different NEDD1 phospho-variants supported this hypothesis: NEDD1-AAA did not shift and only showed a small smear whereas NEDD1-DDD had a slow migrating form even in interphase.

In summary, all the phosphorylation variants with substitutions at S411 do not shift like the WT protein while any mutant with endogenous S411 (S377A and S405A) shift similarly to endogenous mitotic NEDD1. These results strongly support the hypothesis that 411 phosphorylation is responsible for the mobility shift of NEDD1 in mitosis.

Since NEDD1-S377A and S405A shift in mitosis like the endogenous protein, this suggests that in these mutants S411 is phosphorylated, pointing that phosphorylation at 377, 405 and 411 sites could be occurring simultaneously in mitosis. This also suggests that NEDD1-411A may not be phosphorylated on S377 and S405. Ideally, we could have unraveled these questions by using the phospho-antibodies generated to specifically detect each phosphorylation during mitosis. The phospho-antibodies are in principle a very powerful tool as they give spatial information on the phosphorylation events within the cell but, unfortunately, they did not work. As an alternative approach, we planned to used mass spectrometry to detect NEDD1 phosphorylation at least at the residues S377, S405 and S411. However, we could only detect phosphorylation at 411 site in NEDD1-WT pull-down from mitotic cell lysates. We wondered if this could be due to an experimental problem or if the overexpressed protein was only partially phosphorylated, and therefore active. In this case this could explain why we had to express higher levels of the NEDD1 variants for rescue. As there is usually substantial variability in the results from mass spectrometry experiments, more replicas would be needed to test these two hypotheses.

The kinase AurA and the other two kinases Cdk1 and Nek9 (activated through Plk1) are activated and enriched at the centrosome before NEBD. This suggests that NEDD1 could indeed be phosphorylated on the three sites S377, S405 and S411 from the beginning of mitosis. Other mechanisms (apart from NEDD1 phosphorylation) should therefore control its role in the three pathways. This could be spatial and/or temporal events. For example, an essential player in the chromosomal pathway is TPX2, a protein that is nuclear and therefore only functions in microtubule nucleation after NEBD. Interestingly, the Augmin subunit FAM29A (Haus-6 human homologue) has been shown to have an important role in regulating NEDD1 partitioning between centrosomes and spindle microtubules (Zhu et al., 2009). This process is regulated by the kinase Plk1 that recruits FAM29A to spindle microtubules; FAM29A then targets NEDD1 to the spindle to promote microtubule-dependent amplification. Plk1 also recruits NEDD1 to the centrosomes although it does so through a FAM29A-independent mechanism. Altering intracellular levels of FAM29A changes NEDD1 distribution between centrosomes and the spindle, indicating that FAM29A controls the partition of NEDD1 between these two structures and thus, the relative contribution of the centrosomal and Augmin-dependent

pathways to microtubule nucleation during mitosis. The existence of such mechanisms suggests that the activity of different kinases is actively regulated during mitosis to control microtubule nucleation through the different pathways. As it occurs with Cdk1 activity in mitosis, different loops of activation between Plk1 and AurA could regulate the targeting of NEDD1 to the different sites of microtubule nucleation when needed.

Another question we wanted to answer was if phosphorylation at the three residues 377, 405 and 411 is necessary for NEDD1 interaction with important mitotic players. Our hypothesis was that the three of them are, indeed, necessary. First of all, the individual role of each phosphorylation event in every microtubule nucleation pathways has been described. Second, the existence of protein complexes specific to each of the pathways has also been shown. As mentioned before, a RHAMM-γ-TuRC-TPX2 complex that is related with NEDD1 phosphorylation at the S405 has been shown to be essential for the activation of the chromosomal microtubule nucleation pathway (Scrofani et al., 2015). In addition, the phosphorylation of NEDD1 at S411 has been shown to be necessary for its interaction with different members of the Augmin complex (Johmura et al., 2011; Uehara et al., 2009).

All these data suggest the existence of specificity among pathways although it is not known if these phosphorylation events drive specific interactions. To investigate this question, we aimed at performing Flag-hNEDD1 pulldowns to check if known NEDD1 interactions were maintained upon expression of selected phospho-variants. In parallel, we also performed a SILAC-based approach to detect putative NEDD1 interactors specific from each of the pathways. Unfortunately, we were not successful with these experimental approaches and we could not get relevant information.

IV- Haus-6 localization in Flag-hNEDD1 S411A/D phosphorylation mutants

Currently two models have been proposed for the mechanism of Augmin recruitment and activation of microtubule nucleation in spindle assembly.

One model suggests that phosphorylation of NEDD1 at S411 is necessary for NEDD1 interaction with Augmin complex trough the subunit Hice1; this phosphorylation may

induce a structural change in NEDD1 that, in turn, enables the NEDD1-γ-TuRC complex to associate with Augmin. A second NEDD1 phosphorylation at S460 recruits Plk1 to NEDD1-γ-TuRC complex, Plk1 then phosphorylates Hice1 promoting in this way the Augmin-spindle microtubule interaction (Johmura et al., 2011).

A second model supports the idea that the Augmin complex associates first with microtubules independently of NEDD1 as Haus-6 (an Augmin subunit) localized to both centrosomes and spindle microtubules in NEDD1 silenced cells. The recruitment of NEDD1 occurs in a second step to drive microtubule amplification (Zhu et al., 2008).

Then these two models illustrate the existing controversy in the literature about the molecular mechanism behind Augmin-dependent microtubule nucleation

As an additional way of investigating the role of S411 phosphorylation in regulating NEDD1 function, I looked at the localization of the Augmin complex in cells expressing either a phospho-null (S411A) or a phospho-mimicking mutant (S411E).

My data agree with the model proposed by Zhu and colleagues since I detected Augmin on the microtubules independently of NEDD1. In fact, Haus-6 localized to both centrosomes and spindle microtubules in control cells. Interestingly, it also localized to both structures in NEDD1 silenced cells. Moreover, Haus-6 strongly localized to the disorganized microtubules and to the poles of aberrant spindles in silenced cells expressing any of the mutants S411A/E.

These data then suggest that the Augmin complex associates with the microtubules upstream and independently of NEDD1 and later it recruits the γ-TuRC thus promoting the activation of microtubule nucleation.

In summary, the work presented in this thesis has provided new insights on the global understanding of the regulation of microtubule nucleation through NEDD1 phosphorylation. The use of a well-established experimental approach to systematically examine each of the three different microtubule nucleation pathways in parallel in a single system has provided novel data about the role of NEDD1 phosphorylation in spindle assembly. Moreover, our results have contributed to broaden the existing knowledge about at least two of the pathways by completing missing information on the phenotypical consequences of interfering with NEDD1 phosphorylation on S377 and S405. In addition,

we have detected a putative role of S411 phosphorylation in NEDD1 function that may be beyond its previously proposed role in microtubule amplification. S411 might possibly have a fundamental role in NEDD1 structure and/or activity that will have to be further explored. Our results highlight the importance of re-examining previously proposed hypothesis on the basis of novel data to provide an updated interpretation on some aspects of NEDD1 function in mitosis.

We manipulated NEDD1 phosphorylation at the S377, S405 and S411 as a tool to try to specifically address the role of each of the three microtubule nucleation pathways. However, it is important to keep in mind that NEDD1 is also phosphorylated on more than 40 residues in mitosis. It is striking that by interfering with the phosphorylation of only three sites (individually or in combination) the function of NEDD1 is fully or partially abrogated. These sites are not very distant from each other in the middle of the protein after the predicted WD40 domain. Therefore, a closer examination of the NEDD1 structure and the specific position of each amino acid in the core 3D structure of the protein may be useful in determining the consequences of phosphorylation on these amino acids for NEDD1 function.

CONCLUSIONS

I. We have established an inducible system in tissue culture cells to study the different microtubule nucleation pathways in mitosis by manipulating the activity of the γ-TuRC adaptor NEDD1 and unravel their contribution to spindle assembly.

II. Nek9-dependent phosphorylation of NEDD1 on S377 is important for spindle assembly and may need to be finely regulated.

III. AuroraA-dependent phosphorylation of NEDD1 on S405 is essential for spindle assembly and mitosis.

IV. S411 is a critical residue for NEDD1 function in spindle assembly: although its phosphorylation is not required for γ-tubulin recruitment to the centrosomes it is essential for spindle assembly beyond its previously proposed role in driving the microtubule amplification pathway.

V. The phosphorylation of NEDD1 on S411 is responsible for the large migration shift of NEDD1 in mitosis observed in SDS-PAGE.

VI. Augmin localizes to microtubules independently of NEDD1 during mitosis, suggesting that it recruits NEDD1 and the γ-TuRC on the lattice of pre-existing microtubules to drive amplification.

VII. Spindle assembly requires a very tight spatial and temporal control of microtubule nucleation that involves NEDD1 phosphorylation.

MATERIALS AND METHODS

Cell culture and protein induction

All cell lines were grown at 37ºC in a 5% CO_2 humid atmosphere. The culture medium was DMEM 4.5g/L Glucose, supplemented with ultraglutamine (BE12-604F/U1, Lonza), 10% fetal bovine serum without tetracycline (S181T-500, Biowest), 100 units/ml penicillin and 100 µg/ml streptomycin (15140-122, Gibco) and 0.2 mg/ml Hygromycin B (10687-010, Invitrogen). To induce protein expression from the inducible promoter, cells were incubated with tetracycline (T7660-5G, Sigma) at 0.05 µg/ml.

Stable inducible cell lines

To generate cell lines expressing the different NEDD1 phospho-variants, a siRNA-resistant ORF of NEDD1 was cloned in pcDNA5/FRT/TO (Invitrogen). Mutations of S377, S405 and S411 in A and in D/E were then generated by site directed mutagenesis. These plasmids were transfected into a HeLa-FRT/TR cell line (gift from J. Pines) and stable cell lines were generated using the FLIP-in system (K6500-01, Invitrogen). Plasmids were transfected with 3 µl of X-tremeGENE 9 (Roche, 6365809001) and 100 µl of Optimem (Invitrogen, 31985047) using 100 ng of DNA + 900 ng of pOG44 (Invitrogen, V6005-20) per well in a 6-well plate (400.000 cells/well at ≈ 85% confluence) of HeLa-FRT/TR cells. Positive clones were selected using Hygromycin B at 0.6 mg/ml (10687-010, Invitrogen) and picked up using cloning cylinders (C7983-50EA, Sigma) or cloning discs (Z374431, Sigma).

Immunofluorescence

Cells were grown on 20x20 mm coverslips and fixed in methanol at -20ºC for 10 minutes. Methanol was washed out by immersion in PBS1X and samples were immediately blocked and permeabilized for 15 minutes in IF buffer: PBS1X, 0.1% TritonX100 (T8787-250ML, Sigma), 0.5% BSA (A7906-100g, Sigma). Samples were incubated with primary antibodies diluted in IF buffer during 1 hour, washed 3 times with IF buffer (10 minutes/wash) and incubated again with secondary antibodies and Hoechst at 1 µg/ml (H3570, Invitrogen) diluted in IF buffer for another 45 minutes. Samples were then washed once with IF buffer and twice with PBS1X for 10 minutes each. Coverslips were mounted in 10% Mowiol (0.1M Tris-HCl pH 8.2; 25% glycerol (Merck)). Fixed cells

were visualized using 63X or 100X objectives on an inverted DMI-6000 Leica wide-field fluorescent microscope. Pictures were acquired with the Leica Application Suite software. Images were processed and mounted using Adobe Photoshop CS5.1 (Adobe) or Fiji program/ImageJ (Schindelin et al., 2012).

Quantifications of immunofluorescence in fixed cells

The quantification of γ-tubulin recruitment to the mitotic centrosomes in cells expressing Flag-hNEDD1 S411A/D was performed in ImageJ. I used a homemade macro (circle of a defined size) to measure the intensity of the fluorescence signal on the focused mitotic centrosomes, I then used the same macro to obtain two values of background fluorescence signal in different regions close to each centrosome and I subtracted the average of these two values to the initial signal.

Gene silencing using RNA interference

siRNA were transfected with Lipofectamine RNAiMAX (Invitrogen, 13778-150) using 100 pmols per well in 6-wells plates according to the manufacturer protocol.

The control siRNA is a scrambled sequence (5'- CGUACGCGGAAUACUUCGAUU-3').

The siRNA targeting human NEDD1 is (5'-GCAGACAUGUGUCAAUUUA-3') (Lüders et al., 2006). Both siRNA sequences have been purchased at Dharmacon.

Cell lysates preparation

Cells growing in 6-well plates were first washed with 1 ml PBS1X and then collected by scraping them in 1 ml of PBS1X. Cells were pelleted for 5 minutes at 3000 rpm at 4ºC in a 5415 R Eppendorf centrifuge. Supernatant was discarded and cells were resuspended in 30 µl of cell lysis buffer (20 mM Tris-HCl pH 7.5-8, 137 mM NaCl, 1mM EDTA, 1.5 mM $MgCl_2$, 10% glycerol, 1% TritonX100), vortexed and incubated 30 minutes on ice. Following incubation, tubes were centrifuged for 15 minutes at top speed (13200 rpm) at 4ºC. Supernatant was collected into a fresh tube and protein concentration was measured

using the Bradford protein assay (Bio-Rad). For western blot analysis, 30 to 40 µg of protein extract were loaded per lane for SDS-PAGE.

Cell lysis using the liquid N_2 bomb

To detect protein interactions in Flag pull-down experiments, cells were lysed by using the liquid N_2 bomb. Cells collected by shake off or scrapping were washed twice with PBS1X and then resuspended in liquid N_2 lysis buffer (20 mM HEPES pH 7.8, 175 mM NaCl, 2.5 mM $MgCl_2$, 10% glycerol + freshly added Protease inhibitor cocktail, 1 mM DTT, 5 mM NaF, 20 mM β-glycerolphosphate, 100 µM orthovanadate). Approximately 1 volume of liquid N_2 lysis buffer was added to 1 volume of cell pellet (minimal volume ≈ 300 µl). Cell lysate was then introduced in the previously cooled liquid N_2 bomb (PRAXAIR, GNI3X10) at 4ºC. The bomb was closed and a pressure of 1500-2000 PSI was applied for 15 minutes at 4ºC (bomb placed in a box with ice). After the incubation period, the valve of the liquid N_2 bomb was opened carefully and the cell extract was slowly collected. Cell lysate was then cleared at 13000 rpm for 15 minutes at 4ºC for further protein quantification.

Cell synchronization and anti-flag pull-downs

Cells expressing the different NEDD1 variants were synchronized in mitosis by incubating them for 16 hours in 0.33 µM nocodazole (Sigma). Cells were collected by shake-off and resuspended in lysis buffer (20 mM Tris-HCl pH 7.5-8, 137 mM NaCl, 1 mM EDTA,1.5 mM $MgCl_2$, 10% glycerol, 1% Triton) containing proteases and phosphatases inhibitors (5 mM NaF, 100 mM orthovanadate, 20 mM β-glycerophosphate) and incubated for 30 minutes on ice. The lysate was then cleared by centrifugation at 13200 rpm (4ºC). Anti-Flag M2 magnetic beads (M8823, Sigma) were incubated with the lysate for 2 hours at 4ºC following manufacturer's protocol. After incubation, beads were washed twice with 50 mM HEPES pH 7.4, 100 Mm NaCl, 1 mM $MgCl_2$, 1 Mm EDTA, 0.1% NP40, containing proteases and phosphatases inhibitors. Once washed, beads were then subjected to elution with 35 µl of SDS 5X. The eluted fraction was then loaded on SDS-PAGE before western-blot analysis.

SDS-PAGE, Coomassie, colloidal and Western blot

Proteins samples were analyzed by SDS-PAGE (8% acrylamide concentration). Protein gels were usually stained by incubation in Coomassie blue solution (Coomassie Brilliantblue R250 (C.I 42660), Merck) for 15 minutes and washed abundantly with distaining solution overnight. For mass spectrometry analysis protein gels were stained with colloidal blue solution (LC6025, Invitrogen) instead. In this case, gels were incubated in colloidal blue staining overnight and washed the next day by incubation in water.

For western-blotting, samples were run at 100V for 10 minutes and then at 180V until necessary. Protein transfer was performed by using either a semidry system (Amersham biosciences; 80-6211-86; TE 77 semi-dry transfer unit) or the iBlot dry blotting system (Thermofisher). In the semi-dry system proteins were transferred to nitrocellulose membranes (55cm^2 area) (10600002, GE Healthcare) adding transfer buffer containing 20% methanol for 90 minutes at 60 mA per membrane. In the iBlot dry system proteins were also transferred to nitrocellulose membranes already packed into the transfer stacks. Membranes were blocked in blocking solution (TBS1X-5% milk and 0.05% Tween) for at least 2 hours at room temperature. The primary and secondary antibodies were diluted in TBS1X-0,05% Tween and incubated overnight at 4ºC and 1 hour at room temperature, respectively. Three washes of 10 minutes in TBS1X-0.05% Tween were performed before and after incubation with Alexa Fluor 680 (Invitrogen) and/or IRdye 800 (Li-cor) labelled secondary antibodies.

Blots were developed using an Odyssey Infrared imaging system (Li-Cor).

Microtubule Regrowth Assays

Cells were grown on 20x20 mm sterilized coverslips placed at the bottom of 6-well plates. 52 hours after transfection, nocodazole (M1404, Sigma) was added to the media at a final concentration of 2 μM. After 3 hours of incubation at 37ºC, nocodazole was washed-out by three washes with 2 ml of pre-warmed PBS1X and once with 2 ml of pre-warmed medium. Cells were fixed in -20ºC methanol for 10 minutes immediately before nocodazole wash out (time 0) or 5 minutes later and samples were processed for immunofluorescence for posterior analysis.

Proteomics

For SILAC experiments, cells were grown in either heavy medium DMEM-R6K8 (DMEM-LM017, Dundee cell products) or light medium DMEM R0K0 (DMEM-LM014, Dundee cell products), supplemented with 10% of dialyzed fetal bovine serum (DS1002, Dundee cell products), 100 units/ml penicillin and 100 µg/ml streptomycin (15140-122, Gibco). Freshly prepared medium was sterilized with a 0.22 µM filter (SCGPT05RE, Millipore).

For cell lysis, cells were resuspended in liquid N_2 lysis buffer and lysed using the liquid N_2 bomb by applying 1500-2000 PSI for 15 minutes. Anti-flag immunoprecipitation was performed following the same procedure explained above. Proteins associated to the magnetic beads were either digested with trypsin and processed for mass spectrometry analysis or they were eluted from the beads by incubation in 5X SDS, separated by SDS-PAGE and processed in the proteomics facility for mass spectrometry analysis.

For the identification of phosphorylated residues in NEDD1-WT pull down from mitotic cell lysates, proteins were resolved in a SDS-PAGE gel and stained with colloidal Coomassie. Gel band containing NEDD1 was excised and reduced with dithiothreitol (10 mM), alkylated with iodoacetamide (55 mM), and digested with trypsin (Promega).

45% of the sample was analyzed using an Orbitrap Fusion Lumos with an EASY-Spray nanosource coupled to a nano-UPLC system (EASY-nanoLC 1000 liquid chromatograph) equipped with a 50-cm C18 column (EASY-Spray; 75 μm id, PepMap RSLC C18, 2 μm particles, 45 ºC). Chromatographic gradients started at 5% buffer B with a flow rate of 300 nL/min and gradually increased to 22% buffer B in 52 minutes and to 32% in 8 minutes. After each analysis, the column was washed for 10 minutes with 95% buffer B (Buffer A: 0.1% formic acid in water. Buffer B: 0.1% formic acid in acetonitrile). The mass spectrometer was operated in data-dependent acquisition mode, with full MS scans over a mass range of m/z 350–1500 with detection in the Orbitrap (120K resolution) and with auto gain control (AGC) set to 100,000. In each cycle of data-dependent acquisition analysis, following each survey scan, the most intense ions above a threshold ion count of 10,000 were selected for fragmentation with HCD and ETD. The number of selected precursor ions for fragmentation was determined by the "Top Speed" acquisition algorithm (maximum cycle time of 3 seconds), and a dynamic exclusion of

60 seconds was set. Fragment ion spectra were acquired in the Orbitrap (30k resolution) with an AGC of 100,000 and a maximum injection time of 300 ms.

Acquired data were analyzed using the Proteome Discoverer software suite (v2.0, Thermo Fisher Scientific), and the Mascot search engine (v2.5.1, Matrix Science) was used for peptide identification. Data were searched against a *Homo Sapiens* protein database derived from SwissProt plus the most common contaminants. A precursor ion mass tolerance of 7 ppm at the MS1 level was used, and up to three missed cleavages for trypsin were allowed. The fragment ion mass tolerance was set to 20 mmu. Oxidation of Methionine, N-terminal protein acetylation and phosphorylation in Serine, Threonine and Tyrosine were defined as variable modification and carbamidomethylation of Cysteines was set as fixed modification. The identified peptides were filtered by 5%FDR.

For the identification of NEDD1 interactors using SILAC, anti-Flag M2 magnetic beads (M8823, Sigma) were washed three times with 500 μL of 0.2 M NH_4HCO_3, resuspended in 60 μL of 6 M urea 0.2 M NH_4HCO_3, reduced with dithiothreitol (10 μL DTT 10 mM, 37ºC, 60 minutes), alkylated with iodoacetamide (10 μL IAM 20 mM, 25ºC, 30 minutes), diluted up to 1 M urea with 0.2M NH_4HCO_3 and digested overnight with trypsin (1 μg, 37ºC). Samples were desalted using a C18 column, evaporated to dryness and diluted to 10 μL with H_2O with 0.1% formic acid.

45% of each sample was analyzed using an Orbitrap Fusion Lumos with an EASY-Spray nanosource coupled to a nano-UPLC system (EASY-nanoLC 1000 liquid chromatograph) equipped with a 50-cm C18 column (EASY-Spray; 75 μm id, PepMap RSLC C18, 2 μm particles, 45 ºC). Chromatographic gradients started at 5% buffer B with a flow rate of 300 nL/min and gradually increased to 22% buffer B in 79 minutes and to 32% in 11 minutes. After each analysis, the column was washed for 10 minutes with 95% buffer B (Buffer A: 0.1% formic acid in water. Buffer B: 0.1% formic acid in acetonitrile). The mass spectrometer was operated in data-dependent acquisition mode, with full MS scans over a mass range of m/z 350–1500 with detection in the Orbitrap (120K resolution) and with auto gain control (AGC) set to 100,000. In each cycle of data-dependent acquisition analysis, following each survey scan, the most intense ions above a threshold ion count of 10,000 were selected for fragmentation with HCD at normalized collision energy of 28%. The number of selected precursor ions for fragmentation was

determined by the "Top Speed" acquisition algorithm (maximum cycle time of 3 seconds), and a dynamic exclusion of 60 seconds was set. Fragment ion spectra were acquired in the ion trap with an AGC of 10,000 and a maximum injection time of 200 ms.

Acquired data were analyzed using the Proteome Discoverer software suite (v2.0, Thermo Fisher Scientific), and the Mascot search engine (v2.5.1, Matrix Science) was used for peptide identification. Data were searched against a *Homo sapiens* protein database derived from SwissProt plus the most common contaminants. A precursor ion mass tolerance of 7 ppm at the MS1 level was used, and up to three missed cleavages for trypsin were allowed. The fragment ion mass tolerance was set to 0,5 Da Oxidation of Methionine, N-terminal protein acetylation, Lys ($^{13}C_6{}^{15}N_2$), Arg ($^{13}C_6{}^{15}N_4$) and phosphorylation in Serine, Threonine and Tyrosine were defined as variable modification and carbamidomethylation of Cysteines was set as fixed modification. The identified peptides were filtered by 5%FDR.

Phospho-antibodies production and purification

To obtain the phospho-antibodies, three different peptides were injected into rabbits for immunization. Each peptide was injected into two different rabbits to increase good immunization probabilities:

Peptide 1 with S377 phosphorylation: EKAGLPR**Sp**INTDTLC (15 aa).

Peptide 2 with S405 phosphorylation: DDTGKS**Sp**LGDMFC (13 aa).

Peptide 3 with S411 phosphorylation: GDMF**Sp**PIRDDAC (12 aa).

To purify phospho-antibodies, SulfoLink Resin Columns (Thermo Scientific, 20402) were prepared with the NEDD1 phospho-peptides following the instructions of the manufacturers.

Rabbit serums were thawed at room temperature, centrifuged at 4000 g for 10 minutes, and filtered using a low binding filter 0.45 µm (Millex, SLHP033RS). Purification was performed using the previously prepared columns either on FPLC-AKTA purifier or on peristaltic pumps. In both cases, columns were calibrated with 10 ml PBS pH 7.5 at the recommended flow (1ml/min). Serums were then pumped into the columns and possibly left circulating over night at 4ºC. Columns were washed with 10-30 ml of PBS. To elute

the antibodies, 100 mM Glycine pH 2.5 were passed through the column. 0.4 ml fractions were collected in tubes, each containing 100/150 µl of 1 M Tris pH 8. Protein peak was found by adding 5 µl of each fraction in 200 µl of Bradford protein assay. If using FPLC, UV absorbance can be followed online during the whole purification. Column was re-equilibrated with PBS pH 7.5 and stored at 4ºC in storage solution (Ethanol 20% or PBS 1X+Azide).

Peaked fractions were pooled and dialyzed overnight against PBS at 4ºC in stirring. Antibody concentration was determined by measuring the absorbance at 280 nm. IgG solution of 1 mg/ml gives the absorbance 1.35A at 280 nm.

Statistics

Statistical analyses were conducted by using the program Prism 6 (GraphPad Software, La Jolla, CA). All data followed normal distributions and we applied one-way or two-way analysis of variance (ANOVA) for the analysis of several replicas at once, followed by Tukey's post hoc test. The statistics applied in each experiment are specified within the text.

Venn diagrams

Venn diagrams have been produced using the online tool: Venny 2.1 (http://bioinfogp.cnb.csic.es/tools/venny/).

Antibodies

PROTEIN	RAISED IN	IF DILUTION	WB DILUTION	COMPANY+ REFERENCE
Flag	Mouse	1:1000	1:1000	Sigma, F1804
NEDD1 (M05)	Mouse	1:1500	1:600	Abnova, H00121441-M05
α-Tubulin (DM1A)	Mouse	1:1000	1:1000	Sigma, T6199
β-Tubulin	Rabbit	1:300	-	Abcam, ab6046
γ-Tubulin (GTU-488)	Mouse	1:1000	1:200	Sigma, T6557
Pericentrin	Rabbit	1:1000	-	Abcam, ab4448
Centrin (20H5)	Rabbit	1:1000	-	Millipore, 04-1624
Plk1 (208G4)	Rabbit	-	1:800	Cell signaling, 4513
Vinculin	Mouse	-	1:20000	Sigma, V9131-100UL
Haus-6	Rabbit	1:2000	1:500	Gift from Jens Lüders
h-TPX2	Rabbit	-	0.5 μg/ml	Home-made

Buffers

BUFFER	COMPOSITION
Coomassie solution	Coomassie Brillant Blue R250, 10% acetic acid, 50% methanol
Colloidal solution	22.5 ml H_2O, 10 ml methanol, 2.5 ml Stain B, and 10 ml Stain A. Stain A and B are from Invitrogen NOVEX Colloidal Blue Staining Kit
Distaining	10% methanol, 10% acetic acid
Lammeli buffer	2% w/v SDS, 10% glycerol, 50 mM Tris-HCl pH 6.8, 5% β-mercaptoethanol
Immunofluorescence buffer	PBS-0.1% TritonX100, 0.5% BSA
Mowiol	0.1 M Tris-HCl pH 8.2; 25% glycerol
PBS 10X	80.6 mM sodium phosphate, 19.4 mM potassium phosphate, 27 mM KCl and 1.37 M NaCl in high purity dH_2O pH 7.4
PBS-Tween	PBS-0.05% Tween-20
TBS 10X	100 ml 1M Tris-HCl pH 7.5 200 ml 5M NaCl
TBS-Tween	TBS-0.05% Tween-20
Blocking solution	TBS-5% milk, 0.05% Tween-20
Protease inhibitors solution	One tablet of complete, Mini EDTA-free Protease Inhibitor Cocktail (Sigma) in 10 ml of extraction solution
Running buffer	25 mM Tris-Base, 200 mM glycine, 0.1% SDS
SDS protein loading buffer	10% glycerol, 3% SDS, 10 mM Tris-HCl pH 6.8, 5 mM DTT 0.2% Bromophenolblue
Stacking gel	8% acrylamide (30% acrylamide BioRad), 125 mM Tris-HCl pH 6.8, 0.1 % SDS, 0.07% ammoniun persulfate, 0.1% TEMED
Semi-dry transfer buffer	25 mM Tris-Base, 192 mM glycine, 10%/20% methanol, 0.15% SDS
Cell lysis buffer	20 mM Tris-HCl pH 7.5-8, 137 mM NaCl, 1 mM EDTA, 1.5 mM $MgCl_2$, 10% glycerol, 1% TritonX100.
liquid N_2 lysis buffer	20 mM HEPES pH 7.8, 175 mM NaCl, 2.5 mM $MgCl_2$, 10% glycerol + freshly added protease inhibitor cocktail, 1 mM DTT, 5 mM NaF, 20 mM β-glycerolphosphate, 100 μM orthovanadate.
Beads wash buffer	50 mM HEPES pH 7.4, 100 Mm NaCl, 1 mM $MgCl_2$, 1 Mm EDTA, 0.1% NP40 + freshly added protease inhibitor cocktail, 1 mM DTT, 5 mM NaF, 20 mM β-glycerolphosphate, 100 μM orthovanadate.
Proteomics beads wash buffer	200 mM Ammonium bicarbonate (Sigma, 09830-500G)).

Drugs

DRUG	EFFECT	STOCK [ ]	WORKING [ ]	COMPANY
Nocodazole	MT destabilization	20 mM	2 μM for microtubule regrowth 0.33 μM for cell synchronization in mitosis	Sigma, M1404

BIBLIOGRAPHY

Akhmanova, A., and Steinmetz, M.O. (2008). Tracking the ends: A dynamic protein network controls the fate of microtubule tips. Nat. Rev. Mol. Cell Biol. *9*, 309–322.

Akhmanova, A., and Steinmetz, M.O. (2015). Control of microtubule organization and dynamics: Two ends in the limelight. Nat. Rev. Mol. Cell Biol. *16*, 711–726.

Al-Bassam, J., Kim, H., Brouhard, G., van Oijen, A., Harrison, S.C., and Chang, F. (2010). CLASP promotes microtubule rescue by recruiting tubulin dimers to the microtubule. Dev. Cell *19*, 245–258.

Alberts, B. (2007). Molecular Biology of the Cell.

Aldaz, H., Rice, L.M., Stearns, T., and Agard, D.A. (2005). Insights into microtubule nucleation from the crystal structure of human γ-tubulin. Nature *435*, 523–527.

Alushin, G.M., Lander, G.C., Kellogg, E.H., Zhang, R., Baker, D., and Nogales, E. (2014). High-Resolution microtubule structures reveal the structural transitions in αβ-tubulin upon GTP hydrolysis. Cell *157*, 1117–1129.

Alushin et al. (2013). NIH Public Access. *6*, 1117–1129.

Anders, A., and Sawin, K.E. (2011). Microtubule stabilization in vivo by nucleation-incompetent -tubulin complex. J. Cell Sci. *124*, 1207–1213.

Asenjo, A.B., Chatterjee, C., Tan, D., DePaoli, V., Rice, W.J., Diaz-Avalos, R., Silvestry, M., and Sosa, H. (2013). Structural model for tubulin recognition and deformation by kinesin-13 microtubule depolymerases. Cell Rep. *3*, 759–768.

Bakhoum, S.F., Thompson, S.L., Manning, A.L., and Compton, D.A. (2009). Genome stability is ensured by temporal control of kinetochore-microtubule dynamics. Nat. Cell Biol. *11*, 27–35.

Barr, F.A., Silljé, H.H.W., and Nigg, E.A. (2004). Polo-like kinases and the orchestration of cell division. Nat. Rev. Mol. Cell Biol. *5*, 429–440.

Basto, R., Lau, J., Vinogradova, T., Gardiol, A., Woods, C.G., Khodjakov, A., and Raff, J.W. (2006). Flies without Centrioles. Cell *125*, 1375–1386.

Becker, J., Melchior, F., Gerke, V., Bischoff, F.R., Ponstingl, H., and Wittinghofer, A. (1995). RNA1 encodes a GTPase-activating protein specific for Gsp1p, the Ran/TC4 homologue of Saccharomyces cerevisiae. J. Biol. Chem. *270*, 11860–11865.

Belham, C., Roig, J., Caldwell, J.A., Aoyama, Y., Kemp, B.E., Comb, M., and Avruch, J. (2003). A mitotic cascade of NIMA family kinases: Nercc1/Nek9 activates the Nek6 and Nek7 kinases. J. Biol. Chem. *278*, 34897–34909.

Bertran, M.T., Sdelci, S., Regué, L., Avruch, J., Caelles, C., and Roig, J. (2011). Nek9 is a Plk1-activated kinase that controls early centrosome separation through Nek6/7 and Eg5. EMBO J. *30*, 2634–2647.

Bettencourt-Dias, M., and Glover, D.M. (2007). Centrosome biogenesis and function: Centrosomics brings new understanding. Nat. Rev. Mol. Cell Biol. *8*, 451–463.

Bischoff, F.R., and Ponstingl, H. (1991a). Mitotic regulator protein RCC1 is complexed with a nuclear ras-related polypeptide. Proc. Natl. Acad. Sci. U. S. A. *88*, 10830–10834.

Bischoff, F.R., and Ponstingl, H. (1991b). Catalysis of guanine nucleotide exchange on Ran by the mitotic regulator RCC1. Nature *354*, 80–82.

Bischoff, F.R., Klebe, C., Kretschmer, J., Wittinghofer, A., and Ponstingl, H. (1994). RanGAP1 induces GTPase activity of nuclear Ras-related Ran. Proc. Natl. Acad. Sci. *91*, 2587–2591.

Bischoff, F.R., Krebber, H., Smirnova, E., Dong, W., and Ponstingl, H. (1995). Co-activation of RanGTPase and inhibition of GTP dissociation by Ran-GTP binding protein RanBP1. EMBO J. *14*, 705–715.

Bowers, A.J., and Boylan, J.F. (2004). Nek8, a NIMA family kinase member, is overexpressed in primary human breast tumors. Gene *328*, 135–142.

Brouhard, G.J., Stear, J.H., Noetzel, T.L., Al-Bassam, J., Kinoshita, K., Harrison, S.C., Howard, J., and Hyman, A.A. (2008). XMAP215 Is a Processive Microtubule Polymerase. Cell *132*, 79–88.

Cai, S., O'Connell, C.B., Khodjakov, A., and Walczak, C.E. (2009). Chromosome congression in the absence of kinetochore fibres. Nat. Cell Biol. *11*, 832–838.

Carazo-Salas, R.E., Guarguaglini, G., Gruss, O.J., Segref, A., Karsenti, E., and Mattaj, L.W. (1999). Generation of GTP-bound ran by RCC1 is required for chromatin-induced mitotic spindle formation. Nature *400*, 178–181.

Carazo-Salas, R.E., Gruss, O.J., Mattaj, I.W., and Karsenti, E. (2001). Ran-GTP coordinates regulation of microtubule nucleation and dynamics during mitotic-spindle assembly. Nat. Cell Biol. *3*, 228–234.

Carlier, M.F. (1989). Role of nucleotide hydrolysis in the dynamics of actin-filaments and microtubules. Int. Rev. Cytol. *115*, 139–170.

Carmena, M., and Earnshaw, W.C. (2003). The cellular geography of Aurora kinases. Nat. Rev. Mol. Cell Biol. *4*, 842–854.

Carvalho-Santos, Z., Machado, P., Branco, P., Tavares-Cadete, F., Rodrigues-Martins, A., Pereira-Leal, J.B., Bettencourt-Dias, M., Altschul, S.F., Gish, W., Miller, W., et al. (2010). Stepwise evolution of the centriole-assembly pathway. J. Cell Sci. *123*, 1414–1426.

Carvalho-Santos, Z., Azimzadeh, J., Pereira-Leal, J.B., and Bettencourt-Dias, M. (2011). Tracing the origins of centrioles, cilia, and flagella. J. Cell Biol. *194*, 165–175.

Caudron, M., Bunt, G., Bastiaens, P., and Karsenti, E. (2005). Cell Biology: Spatial coordination of spindle assembly by chromosome-mediated signaling gradients. Science (80-.). *309*, 1373–1376.

Cavazza, T., and Vernos, I. (2016). The RanGTP Pathway: From Nucleo-Cytoplasmic Transport to Spindle Assembly and Beyond. Front. Cell Dev. Biol. *3*.

Cavazza, T., Malgaretti, P., and Vernos, I. (2016). The sequential activation of the mitotic microtubule assembly pathways favors bipolar spindle formation. Mol. Biol. Cell *27*, 2935–2945.

Chan, J., Sambade, A., Calder, G., and Lloyd, C. (2009). Arabidopsis Cortical Microtubules Are Initiated along, as Well as Branching from, Existing Microtubules. PLANT CELL ONLINE *21*, 2298–2306.

Choi, Y.-K., Liu, P., Sze, S.K., Dai, C., and Qi, R.Z. (2010). CDK5RAP2 stimulates microtubule nucleation by the gamma-tubulin ring complex. J. Cell Biol. *191*, 1089–1095.

Chretien, D., Metoz, F., Verde, F., Karsenti, E., and Wade, R.H. (1992). Lattice defects in microtubules: Protofilament numbers vary within individual microtubules. J. Cell Biol. *117*, 1031–1040.

Chrétien, D., and Wade, R.H. (1991). New data on the microtubule surface lattice. Biol. Cell *71*, 161–174.

Chrétien, D., Buendia, B., Fuller, S.D., and Karsenti, E. (1997). Reconstruction of the centrosome cycle from cryoelectron micrographs. J. Struct. Biol. *120*, 117–133.

Clarke, P.R., and Zhang, C. (2008a). Spatial and temporal coordination of mitosis by Ran GTPase. Nat. Rev. Mol. Cell Biol. *9*, 464–477.

Clarke, P.R., and Zhang, C. (2008b). Spatial and temporal coordination of mitosis by Ran GTPase. Nat. Rev. Mol. Cell Biol. *9*, 464–477.

Cota, R.R., Teixidó-Travesa, N., Ezquerra, A., Eibes, S., Lacasa, C., Roig, J., and Lüders, J. (2017). MZT1 regulates microtubule nucleation by linking γTuRC assembly to adapter-mediated targeting and activation. J. Cell Sci. *130*, 406–419.

Coutavas, E., Ren, M., Oppenheim, J.D., D'Eustachio, P., and Rush, M.G. (1993). Characterization of proteins that interact with the cell-cycle regulatory protein Ran/TC4. Nature *366*, 585–587.

Desai, A., and Mitchison, T.J. (1997). Microtubule Polymerization Dynamics. Annu. Rev. Cell Dev. Biol. *13*, 83–117.

Desai, A., Verma, S., Mitchison, T.J., and Walczak, C.E. (1999). Kin I kinesins are microtubule-destabilizing enzymes. Cell *96*, 69–78.

Dhani, D.K., Goult, B.T., George, G.M., Rogerson, D.T., Bitton, D.A., Miller, C.J., Schwabe, J.W.R., and Tanaka, K. (2013). Mzt1/Tam4, a fission yeast MOZART1 homologue, is an essential component of the -tubulin complex and directly interacts with GCP3Alp6. Mol. Biol. Cell *24*, 3337–3349.

Downing, K.H., and Nogales, E. (1998). New insights into microtubule structure and function from the atomic model of tubulin. Eur. Biophys. J. *27*, 431–436.

Drewes, G., Ebneth, A., Preuss, U., Mandelkow, E.M., and Mandelkow, E. (1997). MARK, a novel family of protein kinases that phosphorylate microtubule-associated proteins and trigger microtubule disruption. Cell *89*, 297–308.

Drivas, G.T., Shih, A., Coutavas, E., Rush, M.G., and D'Eustachio, P. (1990). Characterization of four novel ras-like genes expressed in a human teratocarcinoma cell line. Mol. Cell. Biol. *10*, 1793–1798.

Dunphy, W.G., Brizuela, L., Beach, D., and Newport, J. (1988). The Xenopus cdc2 protein is a component of MPF, a cytoplasmic regulator of mitosis. Cell *54*, 423–431.

Eckerdt, F., Pascreau, G., Phistry, M., Lewellyn, A.L., DePaoli-Roach, A.A., and Maller, J.L. (2009). Phosphorylation of TPX2 by Plx1 enhances activation of Aurora A. Cell Cycle *8*, 2413–2419.

Erickson, H.P., and Stoffler, D. (1996). Protofilaments and rings, two conformations of the tubulin family conserved from bacterial FtsZ to α/β and γ tubulin. J. Cell Biol. *135*, 5–8.

Evans, T., Rosenthal, E.T., Youngblom, J., Distel, D., and Hunt, T. (1983). Cyclin: A protein specified by maternal mRNA in sea urchin eggs that is destroyed at each cleavage division. Cell *33*, 389–396.

Fawcett, D.W., and Porter, K.R. (1954). A study of the fine structure of ciliated epithelia. J. Morphol. *94*, 221–281.

Fischer, U., Huber, J., Boelens, W.C., Mattajt, L.W., and Lührmann, R. (1995). The HIV-1 Rev Activation Domain is a nuclear export signal that accesses an export pathway used by specific cellular RNAs. Cell *82*, 475–483.

Gable, A., Qiu, M., Titus, J., Balchand, S., Ferenz, N.P., Ma, N., Collins, E.S., Fagerstrom, C., Ross, J.L., Yang, G., et al. (2012). Dynamic reorganization of Eg5 in the mammalian spindle throughout mitosis requires dynein and TPX2. Mol. Biol. Cell *23*, 1254–1266.

Gard, D.L., and Kirschner, M.W. (1987). Microtubule assembly in cytoplasmic extracts of Xenopus oocytes and eggs. J. Cell Biol. *105*, 2091–2201.

Gibbons, and Rowe (1965). Dynein : A Protein with Adenosine Triphosphatase Activity from Cilia Author (s): I . R . Gibbons and A . J . Rowe Published by : American Association for the Advancement of Science Stable. *149*, 424–426.

Goldstein, L.S.B., and Philp, A.V. (1999). THE ROAD LESS TRAVELED 1 : Emerging Principles of Kinesin Motor Utilization. Annu. Rev. Cell Dev. Biol *15*, 141–183.

Gomez-Ferreria, M., Bashkurov, M., Helbig, A., Larsen, B., Pawson, T., Gingras, A.C., and Pelletier, L. (2012a). Novel NEDD1 phosphorylation sites regulate γ-tubulin bindingand mitotic spindle assembly. J. Cell Sci.

Gomez-Ferreria, M.A., Bashkurov, M., Helbig, A.O., Larsen, B., Pawson, T., Gingras, A.-C., and Pelletier, L. (2012b). Novel NEDD1 phosphorylation sites regulate γ-tubulin binding and mitotic spindle assembly. J. Cell Sci. *125*, 3745–3751.

Gomez-Ferreria, M.A., Bashkurov, M., Helbig, A.O., Larsen, B., Pawson, T., Gingras, A.-C., and Pelletier, L. (2012c). Novel NEDD1 phosphorylation sites regulate -tubulin binding and mitotic spindle assembly. J. Cell Sci. *125*, 3745–3751.

Gorlich, D., Pante, N., Kutay, U., Aebi, U., and Bischoff, F.R. (1996). Identification of different roles for RanGTP and RanGTP In nuclear protein import. EMBO J. *15*, 5584–5594.

Goshima, G., Wollman, R., Goodwin, S.S., Zhang, N., Scholey, J.M., Vale, R.D., and Stuurman, N. (2007). Genes required for mitotic spindle assembly in Drosophila S2 cells. Science *316*, 417–421.

Goshima, G., Mayer, M., Zhang, N., Stuurman, N., and Vale, R.D. (2008). Augmin: A protein complex required for centrosome-independent microtubule generation within the spindle. J. Cell Biol. *181*, 421–429.

Gruss, O.J., Carazo-Salas, R.E., Schatz, C.A., Guarguaglini, G., Kast, J., Wilm, M., Le Bot, N., Vernos, I., Karsenti, E., and Mattaj, I.W. (2001). Ran induces spindle

assembly by reversing the inhibitory effect of importin α on TPX2 activity. Cell *104*, 83–93.

Gruss, O.J., Wittmann, M., Yokoyama, H., Pepperkok, R., Kufer, T., Silljé, H., Karsenti, E., Mattaj, I.W., and Vernos, I. (2002). Chromosome-induced microtubule assembly mediated by TPX2 is required for spindle formation in HeLa cells. Nat. Cell Biol. *4*, 871–879.

Guarguaglini, G., Renzi, L., D'Ottavio, F., Di Fiore, B., Casenghi, M., Cundari, E., and Lavia, P. (2000). Regulated Ran-binding protein 1 activity is required for organization and function of the mitotic spindle in mammalian cells in vivo. Cell Growth Differ. *11*, 455–465.

Guillet, V., Knibiehler, M., Gregory-Pauron, L., Remy, M., Chemin, C., Raynaud-Messina, B., Bon, C., Kollman, J.M., Agard, D. a, Merdes, A., et al. (2011). Crystal structure of γ-tubulin complex protein GCP4 provides insight into microtubule nucleation. Nat. Struct. Mol. Biol. *18*, 915–919.

Haren, L., Remy, M.H., Bazin, I., Callebaut, I., Wright, M., and Merdes, A. (2006). NEDD1-dependent recruitment of the γ-tubulin ring complex to the centrosome is necessary for centriole duplication and spindle assembly. J. Cell Biol. *172*, 505–515.

Haren, L., Stearns, T., and Lüders, J. (2009). Plk1-dependent recruitment of γ-tubulin complexes to mitotic centrosomes involves multiple PCM components. PLoS One *4*.

Hayward, D., Metz, J., Pellacani, C., and Wakefield, J.G. (2014). Synergy between Multiple Microtubule-Generating Pathways Confers Robustness to Centrosome-Driven Mitotic Spindle Formation. Dev. Cell *28*, 81–93.

Hayward, D.G., Clarke, R.B., Faragher, A.J., Pillai, M.R., Hagan, I.M., and Fry, A.M. (2004). The centrosomal kinase Nek2 displays elevated levels of protein expression in human breast cancer. Cancer Res. *64*, 7370–7376.

Heald, R., Tournebize, R., Blank, T., Sandaltzopoulos, R., Becker, P., Hyman, A., and Karsenti, E. (1996). Self-organization of microtubules into bipolar spindles around artificial chromosomes in Xenopus egg extracts. Nature *382*, 420–425.

Hendershott, M.C., and Vale, R.D. (2014). Regulation of microtubule minus-end dynamics by CAMSAPs and Patronin. Proc. Natl. Acad. Sci. *111*, 5860–5865.

Hirokawa, N., Noda, Y., Tanaka, Y., and Niwa, S. (2009). Kinesin superfamily motor proteins and intracellular transport. Nat. Rev. Mol. Cell Biol. *10*, 682–696.

Hsia, K.C., Wilson-Kubalek, E.M., Dottore, A., Hao, Q., Tsai, K.L., Forth, S., Shimamoto, Y., Milligan, R.A., and Kapoor, T.M. (2014). Reconstitution of the augmin complex provides insights into its architecture and function. Nat. Cell Biol. *16*, 852–863.

Hunter, A.W., Caplow, M., Coy, D.L., Hancock, W.O., Diez, S., Wordeman, L., and Howard, J. (2003). The kinesin-related protein MCAK is a microtubule depolymerase that forms an ATP-hydrolyzing complex at microtubule ends. Mol. Cell *11*, 445–457.

Hutchins, J.R.A., Toyoda, Y., Hegemann, B., Poser, I., Hériché, J.-K., Sykora, M.M.,

Augsburg, M., Hudecz, O., Buschhorn, B.A., Bulkescher, J., et al. (2010). Systematic analysis of human protein complexes identifies chromosome segregation proteins. Sci. (New York, NY) *328*, 593–599.

Ibrahim, R., Messaoudi, C., Chichon, F.J., Celati, C., and Marco, S. (2009). Electron tomography study of isolated human centrioles. Microsc. Res. Tech. *72*, 42–48.

Janski, N., Masoud, K., Batzenschlager, M., Herzog, E., Evrard, J.-L., Houlne, G., Bourge, M., Chaboute, M.-E., and Schmit, A.-C. (2012). The GCP3-Interacting Proteins GIP1 and GIP2 Are Required for -Tubulin Complex Protein Localization, Spindle Integrity, and Chromosomal Stability. Plant Cell *24*, 1171–1187.

Jiang, K., Hua, S., Mohan, R., Grigoriev, I., Yau, K.W., Liu, Q., Katrukha, E.A., Altelaar, A.F.M., Heck, A.J.R., Hoogenraad, C.C., et al. (2014). Microtubule Minus-End Stabilization by Polymerization-Driven CAMSAP Deposition. Dev. Cell *28*, 295–309.

Johmura, Y., Soung, N.-K., Park, J.-E., Yu, L.-R., Zhou, M., Bang, J.K., Kim, B.-Y., Veenstra, T.D., Erikson, R.L., and Lee, K.S. (2011). Regulation of microtubule-based microtubule nucleation by mammalian polo-like kinase 1. Proc. Natl. Acad. Sci. U. S. A. *108*, 11446–11451.

Joshi, H.C. (1994). Microtubule organizing centers and γ-tubulin. Curr. Opin. Cell Biol. *6*, 55–62.

Kalab, P., Pu, R.T., and Dasso, M. (1999). The Ran GTPase regulates mitotic spindle assembly. Curr. Biol. *9*, 481–484.

Kalab, P., Weis, K., and Heald, R. (2002). Visualization of a Ran-GTP gradient in interphase and mitotic Xenopus egg extracts. Science (80-.). *295*, 2452–2456.

Kaláb, P., Pralle, A., Isacoff, E.Y., Heald, R., and Weis, K. (2006). Analysis of a RanGTP-regulated gradient in mitotic somatic cells. Nature *440*, 697–701.

Kalderon, D., Roberts, B.L., Richardson, W.D., and Smith, A.E. (1984). A short amino acid sequence able to specify nuclear location. Cell *39*, 499–509.

Kamasaki, T., O'Toole, E., Kita, S., Osumi, M., Usukura, J., McIntosh, R.R., and Goshima, G. (2013). Augmin-dependent microtubule nucleation at microtubule walls in the spindle. J. Cell Biol. *202*, 25–32.

Kardon, J.R., and Vale, R.D. (2009). Regulators of the cytoplasmic dynein motor. Nat. Rev. Mol. Cell Biol. *10*, 854–865.

Karsenti, E., Newport, J., Hubble, R., and Kirschner, M. (1984). Interconversion of metaphase and interphase microtubule arrays, as studied by the injection of centrosomes and nuclei into Xenopus eggs. J. Cell Biol. *98*, 1730–1745.

Katayama, H., Brinkley, W.R., and Sen, S. (2003). The Aurora kinases: Role in cell transformation and tumorigenesis. Cancer Metastasis Rev. *22*, 451–464.

Khodjakov, A., and Rieder, C.L. (1999). The sudden recruitment of γ-tubulin to the centrosome at the onset of mitosis and its dynamic exchange throughout the cell cycle, do not require microtubules. J. Cell Biol. *146*, 585–596.

Khodjakov, A., Cole, R.W., Oakley, B.R., and Rieder, C.L. (2000a). Centrosome-independent mitotic spindle formation in vertebrates. Curr. Biol. *10*, 59–67.

Khodjakov, A., Copenagle, L., Gordon, M.B., Compton, D.A., and Kapoor, T.M. (2003). Minus-end capture of preformed kinetochore fibers contributes to spindle morphogenesis. J. Cell Biol. *160*, 671–683.

Khodjakov, a, Cole, R.W., Oakley, B.R., and Rieder, C.L. (2000b). Centrosome-independent mitotic spindle formation in vertebrates. Curr. Biol. *10*, 59–67.

Kimmy Ho, C.-M., Hotta, T., Kong, Z., Tracy Zeng, C.J., Sun, J., Julie Lee, Y.-R., and Liu, B. (2011). Augmin Plays a Critical Role in Organizing the Spindle and Phragmoplast Microtubule Arrays in Arabidopsis. Plant Cell *23*, 2606–2618.

Kirschner, M., and Mitchison, T. (1986). Beyond self-assembly: From microtubules to morphogenesis. Cell *45*, 329–342.

Kitagawa, D., Vakonakis, I., Olieric, N., Hilbert, M., Keller, D., Olieric, V., Bortfeld, M., Erat, M.C., Flückiger, I., Gönczy, P., et al. (2011). Structural basis of the 9-fold symmetry of centrioles. Cell *144*, 364–375.

Knoblich, J.A. (2010). Asymmetric cell division: Recent developments and their implications for tumour biology. Nat. Rev. Mol. Cell Biol. *11*, 849–860.

Kollman, J.M., Zelter, A., Muller, E.G.D., Fox, B., Rice, L.M., Davis, T.N., and Agard, D.A. (2008). The Structure of the -Tubulin Small Complex: Implications of Its Architecture and Flexibility for Microtubule Nucleation. Mol. Biol. Cell *19*, 207–215.

Kollman, J.M., Polka, J.K., Zelter, A., Davis, T.N., and Agard, D.A. (2010a). Microtubule nucleating γ 3-TuSC assembles structures with 13-fold microtubule-like symmetry. Nature *466*, 879–882.

Kollman, J.M., Polka, J.K., Zelter, A., Davis, T.N., and Agard, D.A. (2010b). Microtubule nucleating γ-TuSC assembles structures with 13-fold microtubule-like symmetry. Nature *466*, 879–882.

Kollman, J.M., Merdes, A., Mourey, L., and Agard, D.A. (2011). Microtubule nucleation by γ-tubulin complexes. Nat. Rev. Mol. Cell Biol. *12*, 709–721.

Kollman, J.M., Greenberg, C.H., Li, S., Moritz, M., Zelter, A., Fong, K.K., Fernandez, J.-J., Sali, A., Kilmartin, J., Davis, T.N., et al. (2015). Ring closure activates yeast γTuRC for species-specific microtubule nucleation. Nat. Struct. Mol. Biol. *22*, 132–137.

Komarova, Y.A., Akhmanova, A.S., Kojima, S.I., Galjart, N., and Borisy, G.G. (2002). Cytoplasmic linker proteins promote microtubule rescue in vivo. J. Cell Biol. *159*, 589–599.

Kumar, S., Tomooka, Y., and Noda, M. (1992). Identification of a set of genes with developmentally down-regulated expression in the mouse brain. Biochem. Biophys. Res. Commun. *185*, 1155–1161.

Kumar, S., Matsuzaki, T., Yoshida, Y., and Noda, M. (1994). Molecular cloning and biological activity of a novel developmentally regulated gene encoding a protein with beta-transducin-like structure. J. Biol. Chem. *269*, 11318–11326.

Labbe, J.C., Picard, A., Peaucellier, G., Cavadore, J.C., Nurse, P., and Doree, M. (1989). Purification of MPF from starfish: Identification as the H1 histone kinase

p34cdc2and a possible mechanism for its periodic activation. Cell *57*, 253–263.

Lambrus, B.G., Uetake, Y., Clutario, K.M., Daggubati, V., Snyder, M., Sluder, G., and Holland, A.J. (2015). P53 protects against genome instability following centriole duplication failure. J. Cell Biol. *210*, 63–77.

Lane, H.A., and Nigg, E.A. (1996). Antibody microinjection reveals an essential role for human polo-like kinase 1 (Plk1) in the functional maturation of mitotic centrosomes. J. Cell Biol. *135*, 1701–1713.

Lanford, R.E., Kanda, P., and Kennedy, R.C. (1986). Induction of nuclear transport with a synthetic peptide homologous to the SV40 T antigen transport signal. Cell *46*, 575–582.

Lawo, S., Bashkurov, M., Mullin, M., Ferreria, M.G., Kittler, R., Habermann, B., Tagliaferro, A., Poser, I., Hutchins, J.R.A., Hegemann, B., et al. (2009). HAUS, the 8-Subunit Human Augmin Complex, Regulates Centrosome and Spindle Integrity. Curr. Biol. *19*, 816–826.

Lawo, S., Hasegan, M., Gupta, G.D., and Pelletier, L. (2012). Subdiffraction imaging of centrosomes reveals higher-order organizational features of pericentriolar material. Nat. Cell Biol. *14*, 1148–1158.

Lawrence, C.J., Dawe, R.K., Christie, K.R., Cleveland, D.W., Dawson, S.C., Endow, S.A., Goldstein, L.S.B., Goodson, H. V., Hirokawa, N., Howard, J., et al. (2004). A standardized kinesin nomenclature. J. Cell Biol. *167*, 19–22.

Lecland, N., and Lüders, J. (2014). The dynamics of microtubule minus ends in the human mitotic spindle. Nat. Cell Biol. *16*, 770–778.

Ledbetter, M.C., and Porter, K.R. (1963). A "microtubule" in plant cell fine structure. J. Cell Biol. *19*, 239–250.

Lindqvist, A., Rodríguez-Bravo, V., and Medema, R.H. (2009). The decision to enter mitosis: feedback and redundancy in the mitotic entry network. J. Cell Biol. *185*, 193–202.

Liu, L., and Wiese, C. (2008). Xenopus NEDD1 is required for microtubule organization in Xenopus egg extracts. J. Cell Sci. *121*, 578–589.

Liu, T., Tian, J., Wang, G., Yu, Y., Wang, C., Ma, Y., Zhang, X., Xia, G., Liu, B., and Kong, Z. (2014). Augmin triggers microtubule-dependent microtubule nucleation in interphase plant cells. Curr. Biol. *24*, 2708–2713.

Lüders, J., Patel, U.K., and Stearns, T. (2006). GCP-WD is a γ-tubulin targeting factor required for centrosomal and chromatin-mediated microtubule nucleation. Nat. Cell Biol. *8*, 137–147.

Ma, N., Titus, J., Gable, A., Ross, J.L., and Wadsworth, P. (2011). TPX2 regulates the localization and activity of Eg5 in the mammalian mitotic spindle. J. Cell Biol. *195*, 87–98.

Magidson, V., O'Connell, C.B., Lončarek, J., Paul, R., Mogilner, A., and Khodjakov, A. (2011). The spatial arrangement of chromosomes during prometaphase facilitates spindle assembly. Cell *146*, 555–567.

Mahoney, N.M., Goshima, G., Douglass, A.D., and Vale, R.D. (2006). Making

microtubules and mitotic spindles in cells without functional centrosomes. Curr. Biol. *16*, 564–569.

Maiato, H., Rieder, C.L., and Khodjakov, A. (2004). Kinetochore-driven formation of kinetochore fibers contributes to spindle assembly during animal mitosis. J. Cell Biol. *167*, 831–840.

Manandhar, G., Schatten, H., and Sutovsky, P. (2005). Centrosome Reduction During Gametogenesis and Its Significance1. Biol. Reprod. *72*, 2–13.

Manning, J.A., Shalini, S., Risk, J.M., Day, C.L., and Kumar, S. (2010). A direct interaction with NEDD1 regulates γ-tubulin recruitment to the centrosome. PLoS One *5*.

Manton, I., and Clarke, B. (1952). An electron microscope study of the spermatozoid of sphagnum. J. Exp. Bot. *3*, 265–275.

Mastronarde, D.N., McDonald, K.L., Ding, R., and McIntosh, J.R. (1993). Interpolar spindle microtubules in PTK cells. J. Cell Biol. *123*, 1475–1489.

Masuda, H., Mori, R., Yukawa, M., and Toda, T. (2013). Fission yeast MOZART1/Mzt1 is an essential -tubulin complex component required for complex recruitment to the microtubule organizing center, but not its assembly. Mol. Biol. Cell *24*, 2894–2906.

Masui, and Markert (1971). Cytoplasmic control of nuclear behavior during meiotic maturation of frog oocytes. J. Exp. Zool. 177(2), 129–145. doi10.1002/jez.1401770202 *177*, 129–145.

McEwen, B.F., Heagle, A.B., Cassels, G.O., Buttle, K.F., and Rieder, C.L. (1997). Kinetochore fiber maturation in PtK1 cells and its implications for the mechanisms of chromosome congression and anaphase onset. J. Cell Biol. *137*, 1567–1580.

McIntosh, J.R., Morphew, M.K., Grissom, P.M., Gilbert, S.P., and Hoenger, A. (2009). Lattice Structure of Cytoplasmic Microtubules in a Cultured Mammalian Cell. J. Mol. Biol. *394*, 177–182.

Meads, T., and Schroer, T.A. (1995). Polarity and nucleation of microtubules in polarized epithelial cells. Cell Motil. Cytoskeleton *32*, 273–288.

Megraw, T.L., Li, K., Kao, L.R., and Kaufman, T.C. (1999). The centrosomin protein is required for centrosome assembly and function during cleavage in Drosophila. Development *126*, 2829–2839.

Megraw, T.L., Kao, L.R., and Kaufman, T.C. (2001). Zygotic development without functional mitotic centrosomes. Curr. Biol. *11*, 116–120.

Melchior, F., Paschal, B., Evans, J., and Gerace, L. (1993). Inhibition of nuclear protein import by nonhydrolyzable analogues of GTP and identification of the small GTPase Ran/TC4 as an essential transport factor. J. Cell Biol. *123*, 1649–1659.

Mennella, V., Keszthelyi, B., Mcdonald, K.L., Chhun, B., Kan, F., Rogers, G.C., Huang, B., and Agard, D.A. (2012). Subdiffraction-resolution fluorescence microscopy reveals a domain of the centrosome critical for pericentriolar material organization. Nat. Cell Biol. *14*, 1159–1168.

Meunier, S., and Vernos, I. (2011). K-fibre minus ends are stabilized by a RanGTP-

dependent mechanism essential for functional spindle assembly. Nat. Cell Biol. *13*, 1406–1414.

Meunier, S., and Vernos, I. (2012). Microtubule assembly during mitosis – from distinct origins to distinct functions? J. Cell Sci. *125*, 2805–2814.

Meunier, S., and Vernos, I. (2016). Acentrosomal Microtubule Assembly in Mitosis: The Where, When, and How. Trends Cell Biol. *26*, 80–87.

Meunier, S., Shvedunova, M., Van Nguyen, N., Avila, L., Vernos, I., and Akhtar, A. (2015). An epigenetic regulator emerges as microtubule minus-end binding and stabilizing factor in mitosis. Nat. Commun. *6*.

Meunier, S., Timón, K., and Vernos, I. (2016). Aurora-A regulates MCRS1 function during mitosis. Cell Cycle *4101*, 00–00.

Mey, J. De, Lambert, A.M., Bajer, A.S., Moeremans, M., and Brabander, M. De (1982). Visualization of microtubules in interphase and mitotic plant cells of Haemanthus endosperm with the immuno-gold staining method. Proc. Natl. Acad. Sci. *79*, 1898–1902.

Mitchison, T., and Kirschner, M. (1984). Dynamic instability of microtubule growth. Nature *312*, 237–242.

Mitchison, T., Evans, L., Schulze, E., and Kirschner, M. (1986). Sites of microtubule assembly and disassembly in the mitotic spindle. Cell *45*, 515–527.

Moore, M.S., and Blobel, G. (1993). The GTP-binding protein Ran/TC4 is required for protein import into the nucleus. Nature *365*, 661–663.

Moritz, M., Braunfeld, M.B., Sedat, J.W., Alberts, B., and Agard, D. a (1995). Microtubule nucleation by gamma-tubulin-containing rings in the centrosome. Nature *378*, 638–640.

Moritz, M., Braunfeld, M.B., Guénebaut, V., Heuser, J., Agard, D.A., Guenebaut, V., Heuser, J., and Agard, D.A. (2000). Structure of the gamma-tubulin ring complex: a template for microtubule nucleation. Nat Cell Biol *2*, 365–370.

Moudjou, M., Bordes, N., Paintrand, M., and Bornens, M. (1996). gamma-Tubulin in mammalian cells: the centrosomal and the cytosolic forms. J. Cell Sci. *109 (Pt 4*, 875–887.

Murata, T., Sonobe, S., Baskin, T.I., Hyodo, S., Hasezawa, S., Nagata, T., Horio, T., and Hasebe, M. (2005). Microtubule-dependent microtubule nucleation based on recruitment of gamma-tubulin in higher plants. Nat. Cell Biol. *7*, 961–968.

Murphy, S.M., Urbani, L., and Stearns, T. (1998). The mammalian γ-tubulin complex contains homologues of the yeast spindle pole body components Spc97p and Spc98p. J. Cell Biol. *141*, 663–674.

Nachury, M. V., Maresca, T.J., Salmon, W.C., Waterman-Storer, C.M., Heald, R., and Weis, K. (2001). Importin β is a mitotic target of the small GTPase ran in spindle assembly. Cell *104*, 95–106.

Nakamura, M., Ehrhardt, D.W., and Hashimoto, T. (2010). Microtubule and katanin-dependent dynamics of microtubule nucleation complexes in the acentrosomal Arabidopsis cortical array. Nat. Cell Biol. *12*, 1064–1070.

Nakamura, M., Yagi, N., Kato, T., Fujita, S., Kawashima, N., Ehrhardt, D.W., and Hashimoto, T. (2012). Arabidopsis GCP3-interacting protein 1/MOZART 1 is an integral component of the γ-tubulin-containing microtubule nucleating complex. Plant J. *71*, 216–225.

Nakaoka, Y., Kimura, A., Tani, T., and Goshima, G. (2015). Cytoplasmic Nucleation and Atypical Branching Nucleation Generate Endoplasmic Microtubules in *Physcomitrella patens*. Plant Cell Online *27*, 228–242.

Nigg, E.A. (2001). Mitotic kinases as regulators of cell division and its checkpoints. Nat. Rev. Mol. Cell Biol. *2*, 21–32.

Nigg, E.A., and Stearns, T. (2011). The centrosome cycle: Centriole biogenesis, duplication and inherent asymmetries. Nat. Cell Biol. *13*, 1154–1160.

Nogales, E., Wolf, S.G., and Downing, K.H. (1998). Electron Crystallography. Nature *391*, 199–204.

Nogales, E., Whittaker, M., Milligan, R.A., and Downing, K.H. (1999). High-resolution model of the microtubule. Cell *96*, 79–88.

O'Regan, L., Blot, J., and Fry, A.M. (2007). Mitotic regulation by NIMA-related kinases. Cell Div. *2*, 25.

Oakley, C.E., and Oakley, B.R. (1989). Identification of γ-tubulin, a new member of the tubulin superfamily encoded by mipA gene of Aspergillus nidulans. Nature *338*, 662–664.

Oegema, K., Wiese, C., Martin, O.C., Milligan, R.A., Iwamatsu, A., Mitchison, T.J., and Zheng, Y. (1999). Characterization of two related Drosophila γ-tubulin complexes that differ in their ability to nucleate microtubules. J. Cell Biol. *144*, 721–733.

Ohba, T., Nakamura, M., Nishitani, H., and Nishimoto, T. (1999). Self-organization of microtubule asters induced in Xenopus egg extracts by GTP-bound ran. Science (80-.). *284*, 1356–1358.

Ohtsubo, M., Kai, R., Furuno, N., Sekiguchi, T., Sekiguchi, M., Hayashida, H., Kuma, K., Miyata, T., Fukushige, S., and Murotsu, T. (1987). Isolation and characterization of the active cDNA of the human cell cycle gene (RCC1) involved in the regulation of onset of chromosome condensation. Genes Dev. *1*, 585–593.

Ohtsubo, M., Okazaki, H., and Nishimoto, T. (1989). The RCC1 protein, a regulator for the onset of chromosome condensation locates in the nucleus and binds to DNA. J. Cell Biol. *109*, 1389–1397.

Paintrand, M., Moudjou, M., Delacroix, H., and Bornens, M. (1992). Centrosome organization and centriole architecture: Their sensitivity to divalent cations. J. Struct. Biol. *108*, 107–128.

Pereira, G., and Schiebel, E. (1997). Centrosome-microtubule nucleation. J. Cell Sci. *110 (Pt 3*, 295–300.

Petry, S., Pugieux, C., Nedelec, F.J., and Vale, R.D. (2011). Augmin promotes meiotic spindle formation and bipolarity in Xenopus egg extracts. Proc. Natl. Acad. Sci. *108*, 14473–14478.

Petry, S., Groen, A.C., Ishihara, K., Mitchison, T.J., and Vale, R.D. (2013). Branching

microtubule nucleation in xenopus egg extracts mediated by augmin and TPX2. Cell *152*, 768–777.

Piehl, M., Tulu, U.S., Wadsworth, P., and Cassimeris, L. (2004). Centrosome maturation: Measurement of microtubule nucleation throughout the cell cycle by using GFP-tagged EB1. Proc. Natl. Acad. Sci. *101*, 1584–1588.

Pinyol, R., Scrofani, J., and Vernos, I. (2013). The role of NEDD1 phosphorylation by aurora a in chromosomal microtubule nucleation and spindle function. Curr. Biol. *23*, 143–149.

Qian, Y.W., Erikson, E., Taieb, F.E., and Maller, J.L. (2001). The polo-like kinase Plx1 is required for activation of the phosphatase Cdc25C and cyclin B-Cdc2 in Xenopus oocytes. Mol. Biol. Cell *12*, 1791–1799.

Quarmby, L.M., and Mahjoub, M.R. (2005). Caught Nek-ing: cilia and centrioles. J. Cell Sci. *118*, 5161–5169.

Ramkumar, A., Jong, B.Y., and Ori-McKenney, K.M. (2018). ReMAPping the microtubule landscape: How phosphorylation dictates the activities of microtubule-associated proteins. Dev. Dyn. *247*, 138–155.

Renault, L., Kuhlmann, J., Henkel, A., and Wittinghofer, A. (2001). Structural basis for guanine nucleotide exchange on Ran by the regulator of chromosome condensation (RCC1). Cell *105*, 245–255.

Reyes-Lamothe, R., Nicolas, E., and Sherratt, D.J. (2012). Chromosome Replication and Segregation in Bacteria. Annu. Rev. Genet. *46*, 121–143.

Rice, L.M., Montabana, E.A., and Agard, D.A. (2008). The lattice as allosteric effector: structural studies of alphabeta- and gamma-tubulin clarify the role of GTP in microtubule assembly. Proc. Natl. Acad. Sci. U. S. A. *105*, 5378–5383.

Rieder, C.L. (1981). The structure of the cold-stable kinetochore fiber in metaphase PtK1cells. Chromosoma *84*, 145–158.

Robbins, J., Dilwortht, S.M., Laskey, R.A., and Dingwall, C. (1991). Two interdependent basic domains in nucleoplasmin nuclear targeting sequence: Identification of a class of bipartite nuclear targeting sequence. Cell *64*, 615–623.

Roig, J., Mikhailov, A., Belham, C., and Avruch, J. (2002). Nercc1, a mammalian NIMA-family kinase, binds the Ran GTPase and regulates mitotic progression. Genes Dev. *16*, 1640–1658.

Roig, J., Groen, A., Caldwell, J., and Avruch, J. (2005). Active Nercc1 Protein Kinase Concentrates at Centrosomes Early in Mitosis and Is Necessary for Proper Spindle Assembly. Mol. Biol. Cell *16*, 4827–4840.

Rosenblatt, J. (2005). Spindle assembly: Asters part their separate ways. Nat. Cell Biol. *7*, 219–222.

Sánchez-Huertas, C., and Lüders, J. (2015). The augmin connection in the geometry of microtubule networks. Curr. Biol. *25*, R294–R299.

Sánchez-Huertas, C., Freixo, F., Viais, R., Lacasa, C., Soriano, E., and Lüders, J. (2016). Non-centrosomal nucleation mediated by augmin organizes microtubules in post-mitotic neurons and controls axonal microtubule polarity. Nat. Commun. *7*.

Sardon, T., Peset, I., Petrova, B., and Vernos, I. (2008). Dissecting the role of Aurora A during spindle assembly. EMBO J. *27*, 2567–2579.

Sawin, K.E., and Mitchison, T.J. (1991). Poleward microtubule flux in mitotic spindles assembled in vitro. J. Cell Biol. *112*, 941–954.

Scheer, U. (2014). Historical roots of centrosome research: Discovery of Boveri's microscope slides in Würzburg. Philos. Trans. R. Soc. B Biol. Sci. *369*.

Schindelin, J., Arganda-Carreras, I., Frise, E., Kaynig, V., Longair, M., Pietzsch, T., Preibisch, S., Rueden, C., Saalfeld, S., Schmid, B., et al. (2012). Fiji: An open-source platform for biological-image analysis. Nat. Methods *9*, 676–682.

Schorderet-Slatkine, S., and Drury, K.C. (1973). Progesterone induced maturation in oocytes of Xenopus laevis. Appearance of a "maturation promoting factor" in enucleated oocytes. Cell Differ. *2*, 247–254.

Scrofani, J., Sardon, T., Meunier, S., and Vernos, I. (2015). Microtubule nucleation in mitosis by a RanGTP-dependent protein complex. Curr. Biol. *25*, 131–140.

Sdelci, S., Schütz, M., Pinyol, R., Bertran, M.T., Regué, L., Caelles, C., Vernos, I., and Roig, J. (2012). Nek9 phosphorylation of NEDD1/GCP-WD contributes to Plk1 control of γ-tubulin recruitment to the mitotic centrosome. Curr. Biol. *22*, 1516–1523.

Seewald, M.J., Körner, C., Wittinghofer, A., and Vetter, I.R. (2002). RanGAP mediates GTP hydrolysis without an arginine finger. Nature *415*, 662–666.

Sharp, D.J., and Ross, J.L. (2012). Microtubule-severing enzymes at the cutting edge. J. Cell Sci. *125*, 2561–2569.

Stearns, T., and Kirschner, M. (1994). In vitro reconstitution of centrosome assembly and function: the central role of gamma-tubulin. Cell *76*, 623–637.

Stenoien, D.L., Sen, S., Mancini, M.A., and Brinkley, B.R. (2003). Dynamic association of a tumor amplified kinase, Aurora-A, with the centrosome and mitotic spindle. Cell Motil. Cytoskeleton *55*, 134–146.

Takai, N., Hamanaka, R., Yoshimatsu, J., and Miyakawa, I. (2005). Polo-like kinases (Plks) and cancer. Oncogene *24*, 287–291.

Teixido-Travesa, N., Villen, J., Lacasa, C., Bertran, M.T., Archinti, M., Gygi, S.P., Caelles, C., Roig, J., and Luders, J. (2010). The γTuRC Revisited: A Comparative Analysis of Interphase and Mitotic Human TuRC Redefines the Set of Core Components and Identifies the Novel Subunit GCP8. Mol. Biol. Cell *21*, 3963–3972.

Tournebize, R., Popov, A., Kinoshita, K., Ashford, A.J., Rybina, S., Pozniakovsky, A., Mayer, T.U., Walczak, C.E., Karsenti, E., and Hyman, A.A. (2000). Control of microtubule dynamics by the antagonistic activities of XMAP215 and XKCM1 in Xenopus egg extracts. Nat. Cell Biol. *2*, 13–19.

Tsai, C.Y., Ngo, B., Tapadia, A., Hsu, P.H., Wu, G., and Lee, W.H. (2011). Aurora-A phosphorylates augmin complex component hice1 protein at an N-terminal serine/threonine cluster to modulate its microtubule binding activity during spindle assembly. J. Biol. Chem. *286*, 30097–30106.

Tsou, M.F.B., Wang, W.J., George, K.A., Uryu, K., Stearns, T., and Jallepalli, P. V. (2009). Polo Kinase and Separase Regulate the Mitotic Licensing of Centriole Duplication in Human Cells. Dev. Cell *17*, 344–354.

Tulu, U.S., Fagerstrom, C., Ferenz, N.P., and Wadsworth, P. (2006). Molecular requirements for kinetochore-associated microtubule formation in mammalian cells. Curr. Biol. *16*, 536–541.

Uehara, R., Nozawa, R., Tomioka, A., Petry, S., Vale, R.D., Obuse, C., and Goshima, G. (2009). The augmin complex plays a critical role in spindle microtubule generation for mitotic progression and cytokinesis in human cells. Proc. Natl. Acad. Sci. U. S. A. *106*, 6998–7003.

Uhlmann, F., Wernic, D., Poupart, M.A., Koonin, E. V., and Nasmyth, K. (2000). Cleavage of cohesin by the CD clan protease separin triggers anaphase in yeast. Cell *103*, 375–386.

Vale, R.D., Reese, T.S., and Sheetz, M.P. (1985). Identification of a novel force-generating protein, kinesin, involved in microtubule-based motility. Cell *42*, 39–50.

Vale, R.D., Coppin, C.M., Malik, F., Kull, F.J., and Milligan, R.A. (1994). Tubulin GTP hydrolysis influences the structure, mechanical properties, and kinesin-driven transport of microtubules. J. Biol. Chem. *269*, 23769–23775.

Vallee, R.B., Wall, J.S., Paschal, B.M., and Shpetner, H.S. (1988). Microtubule-associated protein 1c from brain is a two-headed cytosolic dynein. Nature *332*, 561–563.

Vanneste, D., Ferreira, V., and Vernos, I. (2011). Chromokinesins: localization-dependent functions and regulation during cell division. Biochem. Soc. Trans. *39*, 1154–1160.

Varga, V., Helenius, J., Tanaka, K., Hyman, A.A., Tanaka, T.U., and Howard, J. (2006). Yeast kinesin-8 depolymerizes microtubules in a length-dependent manner. Nat. Cell Biol. *8*, 957–962.

Varga, V., Leduc, C., Bormuth, V., Diez, S., and Howard, J. (2009). Kinesin-8 Motors Act Cooperatively to Mediate Length-Dependent Microtubule Depolymerization. Cell *138*, 1174–1183.

Verde, F., Dogterom, M., Stelzer, E., Karsenti, E., and Leibler, S. (1992). Control of Microtubule Dynamics and Length by Cyclin A- and Cyclin B-dependant Kinases in Xenophobus Egg Extracts. J. Cell Biol. *118*, 1097–1108.

Vérollet, C., Colombié, N., Daubon, T., Bourbon, H.M., Wright, M., and Raynaud-Messina, B. (2006). Drosophila melanogaster γ-TuRC is dispensable for targeting γ-tubulin to the centrosome and microtubule nucleation. J. Cell Biol. *172*, 517–528.

Vicente, J.J., and Wordeman, L. (2015). Mitosis, microtubule dynamics and the evolution of kinesins. Exp. Cell Res. *334*, 61–69.

Vorobjev, I.A., and Chentsov, Y.S. (1982). Centrioles in the cell cycle. I. Epithelial cells. J. Cell Biol. *93*, 938–949.

Wainman, A., Buster, D.W., Duncan, T., Metz, J., Ma, A., Sharp, D., and Wakefield, J.G.

(2009). A new Augmin subunit, Msd1, demonstrates the importance of mitotic spindle-templated microtubule nucleation in the absence of functioning centrosomes. Genes Dev. *23*, 1876–1881.

Weil, C.F., Oakley, C.E., and Oakley, B.R. (1986). Isolation of mip (microtubule-interacting protein) mutations of Aspergillus nidulans. Mol. Cell. Biol. *6*, 2963–2968.

Wen, W., Meinkotht, J.L., Tsien, R.Y., and Taylor, S.S. (1995). Identification of a signal for rapid export of proteins from the nucleus. Cell *82*, 463–473.

Wiese, C., and Zheng, Y. (2000). A new function for the gamma-tubulin ring complex as a microtubule minus-end cap. Nat. Cell Biol. *2*, 358–364.

Wiese, C., and Zheng, Y. (2006). Microtubule nucleation: gamma-tubulin and beyond. J. Cell Sci. *119*, 4143–4153.

Wignall, S.M., and Villeneuve, A.M. (2009). Lateral microtubule bundles promote chromosome alignment during acentrosomal oocyte meiosis. Nat. Cell Biol. *11*, 839–844.

Wilde, A., and Zheng, Y. (1999). Stimulation of microtubule aster formation and spindle assembly by the small GTPase ran. Science (80-.). *284*, 1359–1362.

Winey, and O'Toole (2014). Centriole structure. Philos. Trans. R. Soc. Lond. B. Biol. Sci. *369*.

Wittmann, T., Wilm, M., Karsenti, E., and Vernos, I. (2000). TPX2, a novel Xenopus MAP involved in spindle pole organization. J. Cell Biol. *149*, 1405–1418.

Wollman, R., Cytrynbaum, E.N., Jones, J.T., Meyer, T., Scholey, J.M., and Mogilner, A. (2005). Efficient chromosome capture requires a bias in the "search-and-capture" process during mitotic-spindle assembly. Curr. Biol. *15*, 828–832.

Wong, Y.L., Anzola, J. V, Davis, R.L., Yoon, M., Motamedi, A., Kroll, A., Seo, C.P., Hsia, J.E., Kim, S.K., Mitchell, J.W., et al. (2015). Cell biology. Reversible centriole depletion with an inhibitor of Polo-like kinase 4. Science (80-.). *348*, 1155–1160.

Wunderlich, V. (2002). JMM - Past and present. Chromosomes and cancer: Theodor Boveri's predictions 100 years later. J. Mol. Med. *80*, 545–548.

Yokoyama, N., Hayashi, N., Seki, T., Panté, N., Ohba, T., Nishii, K., Kuma, K., Hayashida, T., Miyata, T., Aebi, U., et al. (1995). A giant nucleopore protein that binds Ran/TC4. Nature *376*, 184–188.

Zhai, Y., Kronebusch, P.J., and Borisy, G.G. (1995). Kinetochore microtubule dynamics and the metaphase-anaphase transition. J. Cell Biol. *131*, 721–734.

Zhang, C., Hughes, M., and Clarke, P.R. (1999). Ran-GTP stabilises microtubule asters and inhibits nuclear assembly in Xenopus egg extracts. J. Cell Sci. *112 (Pt 1*, 2453–2461.

Zhang, X., Chen, Q., Feng, J., Hou, J., Yang, F., Liu, J., Jiang, Q., and Zhang, C. (2009). Sequential phosphorylation of Nedd1 by Cdk1 and Plk1 is required for targeting of the gammaTuRC to the centrosome. J. Cell Sci. *122*, 2240–2251.

Zheng, Y., Wong, M.L., Alberts, B., and Mitchison, T. (1995). Nucleation of microtubule assembly by a γ-tubulin-containing ring complex. Nature *378*, 578–583.

Zhu, H., Coppinger, J.A., Jang, C.Y., Yates, J.R., and Fang, G. (2008). MFAM29A promotes microtubule amplification via recruitment of the NEDDI-??-tubuIin complex to the mitotic spindle. J. Cell Biol. *183*, 835–848.

Zhu, H., Fang, K., and Fang, G. (2009). FAM29A, a target of Plk1 regulation, controls the partitioning of NEDD1 between the mitotic spindle and the centrosomes. J. Cell Sci. *122*, 2750–2759.

ANNEX

Meunier S, Timón K, Vernos I. Aurora-A regulates MCRS1 function during mitosis. Cell Cycle. 2016 Jul 2;15(13):1779–86. DOI: 10.1080/15384101.2016.1187342